FU JEN STUDIES

NATURAL SCIENCES

NO. 6 1973

FU JEN UNIVERSITY
TAIPEI, TAIWAN, REPUBLIC OF CHINA

FU JEN STUDIES

is published annually by the College of Natural Sciences of Fu Jen University

EDITORIAL BOARD

All correspondence regarding contributions, subscriptions and exchanges should be addressed to:

Dr. H. Hesselfeld, SVD
College of Natural Sciences
Fu Jen University
242 Hsin Chuang, Taipei,
Taiwan, R. O. C.

關于所有投稿、訂閱或交換之函件請寄：
郝思漢　物理系系主任　臺北縣新莊鎮輔仁大學

Price: US$ 1.50

FU JEN STUDIES

NATURAL SCIENCES

NO. 6 1973

CONTENTS

FU JEN UNIVERSITY

TAIPEI, TAIWAN, REPUBLIC OF CHINA

STAND, SUN, DO NOT MOVE

(Marking the 500th Anniversary of Copernicus' Birth)

M. RICHARTZ, S. V. D.

INTRODUCTION

NICHOLAS COPERNICUS (1473–1543), the famous German ecclesiastic, became the founder of a new astronomy. In his pioneer work, "On the Revolutions of the Celestial Spheres" he succeeded in proving that the Earth is not the center of the universe, but the Sun stands and does not move. On a monument erected to his memory in Saint Anne's church at Cracow, you find the inscription: "Sta, sol, ne moveare" (Stand, Sun, do not move). This word, taken from the Bible (Josue 10, 12), expressed his ardent desire to prove that the Sun does not move. And the more he studied "the godlike circular movements of the world, the course of the stars, their magnitudes, distances, risings and settings", the more he was convinced that "the Sun stood still in the midst of heaven" (Josue 10, 13).

COPERNICUS' LIFE

Copernicus was the son of a merchant of Cracow. While he was still a child, his father died and his uncle, a Catholic bishop, looked after the education of the boy. After studying mathematics and science at the University of Cracow, he went to Italy to continue his studies at the University of Bologna: Greek, medicine, philosophy and astronomy. In 1512 he became a member of the Cathedral Chapter at Frauenburg in East Prussia. There he led a busy life, as an active administrator, a practising physician, and a writer on economics and astronomy. His reputation of being a great astronomer was such that in 1514, the Lateran Council, convoked by Pope Leo X, asked for his opinion on the reform of the ecclesiastical calendar. His answer was that the length of the year and of the months as well as the motions of the Sun and Moon were not yet

sufficiently known to attempt a reform. The incident, however, spurred him on as he himself wrote to Pope Paul III, to make more observations, and these actually served seventy years later as a basis for the working out of the Gregorian Calendar. Copernicus laid the groundwork for his heliocentric theory between 1506 and 1512, and brought it to completion in "De Revolutionibus Orbium Coelestium" (1543).

At the time that Copernicus studied astronomy the science was in about the same state in which Ptolemy had left it. In his astronomical treatise "Almagest" Ptolemy described the accomplishments of his predecessors and explained the system which bears his name. Copernicus wrote De Revolutionibus as a careful parallel to the Almagest, with the mathematical and computational methods revised for a different concept of planetary motion. Thus before explaining the Copernican system it may be profitable to describe the Ptolemaic system in order to appreciate Copernicus' great contribution to astronomy.

PTOLEMAIC SYSTEM

For thousands of years astronomers and laymen had agreed that the evidence of the senses was a reliable guide even to the heavens; and the evidence of the senses confirmed what mathematical and philosophical argument deduced, that all heavenly motion was truly circular. Plato, who had first suggested the search for a mathematical device that would interpret the observed planetary motions in terms of precise mathematical law, had also insisted that the law when found must express such motions in terms of uniform circular motion about a unique center. Eudoxus, a pupil of Plato and one of the foremost Greek mathematicians gave the first major astronomical theory. He employed a series of concentric spheres whose center is the immovable Earth. Hipparchus (born about 150 B. C.) recognized that the scheme of Eudoxus did not account for many observed facts; especially it contained significant errors in the motions of Mars and Venus. His mathematical system of planetary motion was perfected by Ptolemy 300 years later. In utilizing a great number of subsidiary

geometrical devices such as epicycles, the Ptolemaic system represented the movements and positions of the Sun, Moon, planets, and stars in such a way that they fitted recorded observations with a considerable degree of accuracy. The center was the Earth; fixed immovably in its place, it was subject to the influences of the ever-widening spheres which surrounded it (Fig. 1). First in the terrestrial region, below the Moon, came the spheres of the four elements, earth, water, air and fire, the region of generation, corruption and

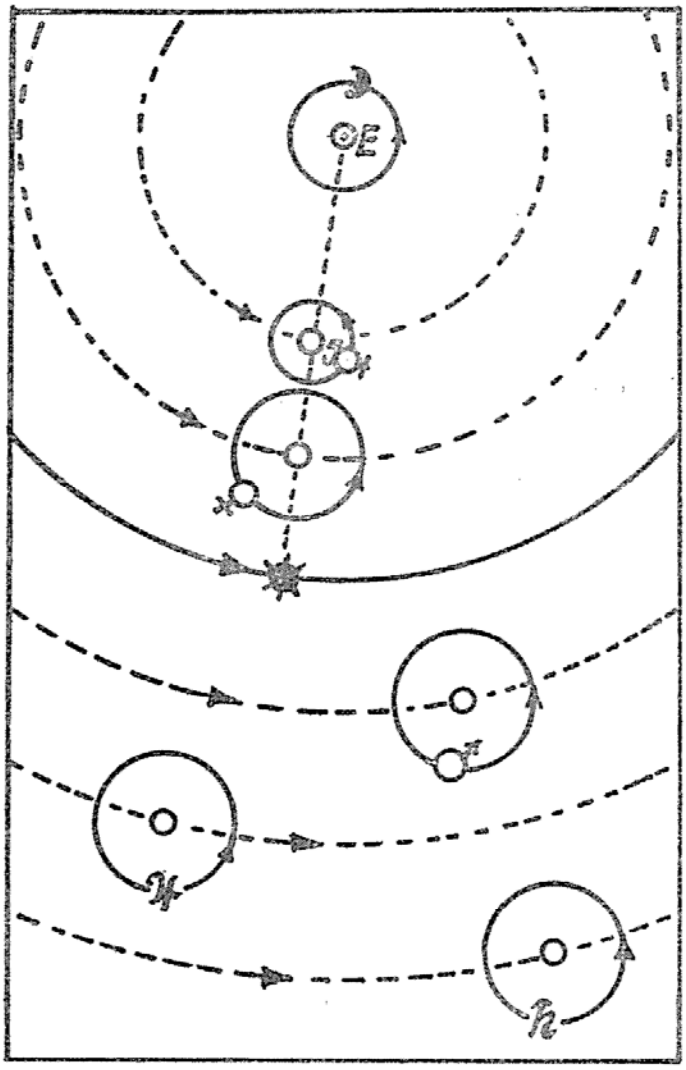

Fig. 1. The Ptolemaic System.
E, the Earth, center of the universe; Moon and Sun move on concentric spheres around the Earth; the inner planets, Mercury and Venus, as well as the outer planets, Mars, Jupiter and Saturn move on epicycles the centers of which move on concentric spheres around the Earth.

change. Then, in the celestial region, the eternal and unchanging heavens, came the crystalline spheres of the Moon, Mercury, Venus, the Sun, Mars, Jupiter, Saturn; hollow spheres nesting one within the other, so that although their radii were large, the outer surface of one touched the inner surface of the next bigger one. Beyond the planetary spheres lay the sphere of the fixed stars; and beyond that again the ninth sphere of the Primum Mobile.

COPERNICAN SYSTEM

Copernicus himself said that he had kept his work in abeyance for over thirty years. He presumably had constructed at least the outlines some time before he wrote his first sketch, the "Commentariolus" (Little Commentary), in 1512. This brief synopsis circulated among his friends; and it had reached Rome by 1533 and was discussed enough there to cause ecclesiastical pressure to be exerted on Copernicus to publish further. The Church, with an eye on calendar reform, was eager at this period to encourage mathematical astronomy.

In 1539 a young professor from the Protestant University of Wittenberg, Georg Joachim Rheticus arrived at Frauenburg and begged for astronomical enlightenment. Copernicus did not scruple to let the young man, Protestant though he was, have full access to his astronomical papers. Two months later he permitted Rheticus to prepare for publication a brief account of the system, the "Narratio Prima", published in 1540. This paper reached a wider audience than the Little Commentary. Rheticus never named Copernicus, though he dated his work from Frauenburg; he merely referred to "my teacher." No doubt Copernicus had stipulated anonymity.

Rheticus also urged the publication of the years of work accumulated by Copernicus. Finally the book appeared in 1543 under the title "De Revolutionibus Orbium Coelestium Libri Sex" (Six Books on the Revolution of the Celestial Orbs). Tradition has it that Copernicus saw his great work only on his death-bed; he was certainly ill in the months immediately preceding its publication, and died soon afterwards.

De Revolutionibus is the Almagest rewritten to incorporate the new Copernican theory, but otherwise altered as little as might be. Copernicus saw no higher aim than to explain by his own system the appearances of the heaven as known to Ptolemy. The Copernican would replace the Ptolemaic system, he believed, because it was simpler, more harmonious, more ingenious. Copernicus himself explained it:

> In the first book I describe all the positions of the spheres together with such movements as I ascribe to the Earth; so that this book contains, as it were, the general system of the universe. Afterwards, in the remaining books, I relate the motions of the other planets and all the spheres to the mobility of the Earth, so that we may thus comprehend how far the motions and appearances of the remainder of the planets and spheres may be preserved, if they are related to the motions of the Earth.

But the rearrangement of the Ptolemaic system to form the Copernican required more than the assignation of motion to the Earth. In the outline sketched in the Little Commentary, Copernicus listed seven assumptions required before serious considerations of the system could begin.

1. There was no one center of motion for all the heavenly bodies. Although he was to postulate that the planets all revolved about the Sun, the Moon still clearly revolved about the Earth. That seemed to be a disadvantage, for one of the niceties of the Ptolemaic system was that all the heavenly bodies revolved around the same point.

2. The Earth as the center of the lunar sphere brought about another disadvantage. According to the Aristotelian physics heavy bodies fell to the Earth because it was the center of the universe; when Copernicus made this explanation impossible, he left gravity as a mysterious force.

3. The center of motion of the planetary system was the Sun, which was therefore the true center of the universe. Copernicus emphatically wrote:

> In the middle of all sits the Sun enthroned. How could we place this luminary in any better position in this most beautiful temple from which to illuminate the whole at once? He is rightly called

the Lamp, the Mind, the Ruler of the universe. So the Sun sits as upon a royal throne ruling his children the planets which circle around him.

4. The size of the universe must be very large, so large that the distance from the Earth to the Sun is negligibly small compared with the distance of the Sun from the sphere of fixed stars. This postulate alone could account for the fact that the motion of the Earth is not reflected in an apparent motion of the fixed stars, as it would otherwise be. The fixed stars in the Copernican system ought to exhibit the phenomenon of parallax. Copernicus could only insist that the parallax was there but was too small, owing to the immense distance of the stars from the Earth to be detectable.

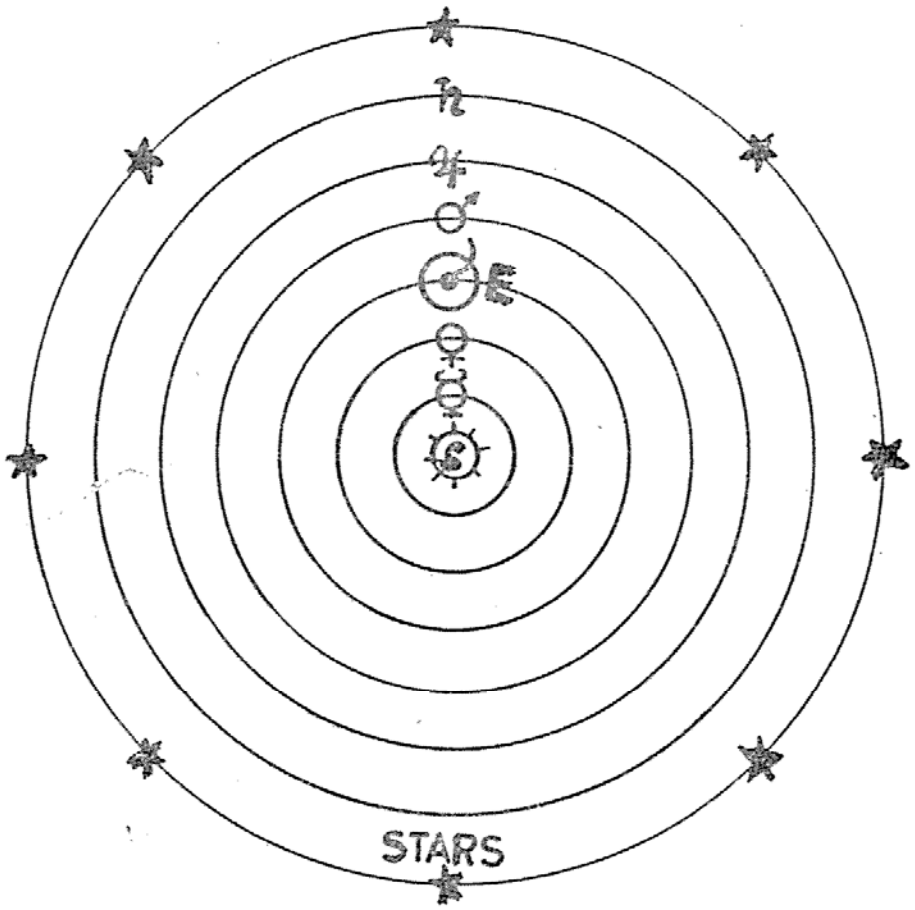

Fig. 2. The Copernican Universe.
S, the Sun, center of the universe; all planets move on concentric orbits around the Sun; the Moon moves around the Earth; the sphere of fixed stars forms the boundary of the universe.

Assumptions 5 to 7 were concerned with the motion of the Earth. Copernicus assumed that the Earth's diurnal rotation produced the apparent rising and setting of the Sun, planets and fixed stars, and the Earth's annual revolution about the Sun produced the apparent annual motion of the Sun, and the apparent retrogradations of some planets.

The general arrangement of the solar system as conceived by Copernicus is shown in his well-known diagram (Fig. 2), where Mercury, Venus, the Earth, Mars, Jupiter, and Saturn describe concentric orbits about the Sun. The stationary sphere of the fixed stars is forming a boundary and limit to the universe as a whole. He still had to use eccentrics and epicycles, but these refinements are not shown in his diagram.

From the theories set forth on the De Revolutionibus, Copernicus constructed numerical planetary tables as accurate as any based on the geocentric hypothesis. These tables, which form an essential feature of his book, were an improvement upon those in current use, and this circumstance helped indirectly to make the new doctrine acceptable among astronomers.

COPERNICUS' CONTRIBUTION TO ASTRONOMY

A few years before Copernicus' work was published, in 1538 there appeared a book, entitled "Homocentrics," dedicated, like De Revolutionibus, to Pope Paul III. The author, Girolamo Fracastoro, an Italian humanist and astronomer, proposed an anti-Ptolemaic system, which was to replace Ptolemaic epicycles and eccentrics with the homocentric spheres originated by Eudoxus and elaborated by Aristotle. But he did not offer a replacement to the computational methods of Ptolemy.

Copernicus, on the other hand, knowing that Eudoxus' theory would never fit to serve as the basis of planetary tables, realized that no progress was possible along those lines. The Ptolemaic system, however, was eminently suited to serve as the basis of tables. Copernicus then turned to the classical writers to see what

alternative theories they had to offer. He wrote in the preface to De Revolutionibus:

> I began to reflect upon the Earth's capacity for motion. And though the idea appeared absurd, yet I knew that others before me had been allowed freedom to imagine what circles they pleased in order to represent the phenomena of the heavenly bodies.

He quotes several classical writers to this effect. We cannot be certain whether Copernicus really derived his ideas, in the first instance, from these writers.

From whatever source he derived his fundamental ideas, Copernicus' unquestionable contribution to astronomy must be held to lie in his elaboration of those ideas into a coherent planetary theory capable of furnishing tables of an accuracy not before attained. Copernicus had found a simpler mathematical account of the motions of the heavens. To him the heliocentric theory represented the most symmetrical arrangement of the planets, and the simplest manner of accounting for their observed motions. Although it was a matter of scientific reasoning rather than of direct observations, it marked the beginning of a series of epochmaking discoveries. Two outstanding achievements served to make the triumph of the Copernican system over the Ptolemaic theory completely possible. One was the perfection of the telescope and its use by Galileo; the other was the discovery by Kepler of the laws of planetary motion, the keynote of which was the substitution of elliptical for circular orbits as an explanation of the movement of the planets around the Sun.

APPRECIATION OF THE HELIOCENTRIC THEORY

There can be little doubt that Copernicus was convinced of the truth of his theory. Opposition was first raised against the Copernican system by Protestant theologians for Biblical reasons. On the Catholic side a clear statement about the interpretation of Biblical texts was already made by Nicolas Oresme in the 14th century. The scriptures speak according to a common mode of speech. For nearly three quarters of a century no difficulties were raised; neither Pope Paul III,

nor any of the nine Popes who followed him, nor the Roman Congregations raised any alarm. Trouble arose when Galilei proclaimed the truth of the Copernican doctrine with stubborn persistence. Although there was as yet no sufficient proof of the system, no objection was made to its being taught as a hypothesis which explained all phenomena in a simpler manner than the Ptolemaic, and might for all practical purposes be adopted by astronomers. What was objected to was the assertion that Copernicanism "appears to contradict Scripture."

On March 5, 1616, the work of Copernicus was forbidden by the Congregation of the Index "until corrected," and in 1620 these corrections were made known. Nine sentences, by which the heliocentric system was represented as "certain," had to be either omitted or changed. This done, the reading of the book was allowed. In 1758 the book disappeared from the revised Index.

The heliocentric theory owed its final acceptance in scientific circles chiefly to the authority of Galilei, Kepler, Descartes, and Newton.

REFERENCES

(1) E. J. DIJKSTERHUIS: "Die Mechanisierung des Weltbildes" (German Translation by Helga Habicht) Springer-Verlag, 1956.
(2) MARIE BOS: "The Scientific Renaissance 1450-1630 (Harper Torchbooks 1962).
(3) A. WOLF: "A History of Science, Technology, and Philosophy in the 16th & 17th Centuries" (London: George Allen & Unwin LTD 1950).
(4) J. MAYER: "The Seven Seals of Science" (New York: D. Appleton-Century Co., 1937).
(5) MORRIS KLINE: "Mathematics in Western Culture" (New York: Oxford University Press 1953).
(6) STEPHEN P. MIZWA: "Nicholas Copernicus" (New York: The Kosciuszko Foundation 1943).

"There is no perfect measure of continuous quantity except by means of indivisible continuous quantity, for example by means of a point, and no quantity can be perfectly measured unless it is known how many individual points it contains. And since these are infinite, therefore their number cannot be known by a creature but by God alone, who disposes everything in number, weight, and measure."

ROBERT GROSSETESTE
13th century A. D.

ON THE DIFFERENTIAL GEOMETRY OF SPACE CURVES

YI-CHING YEN

Abstract: It is shown by the explicit relation between the curvature and the torsion of a spherical curve that the congruence of two space curves can be expressed as the equality of the curvature function of their spherical images.

It is well known in the differential geometry that a space curve is spherical if and only if its curvature function $k = 1/\rho$ (>0) and torsion function $\tau = 1/\sigma$ $(\neq 0)$ satisfy the differential equation

$$(1) \qquad [\sigma(s)\,\rho'(s)]' + \rho(s)/\sigma(s) = 0\,.$$

Recently Breuer and Gottlieb have deduced from the result of their former paper[1] that a curve is spherical if and only if $\rho(s)$ and $\tau(s)$ satisfy the explicit relation

$$(2) \qquad \rho(s) = A\cos\Big[\int\tau(s)\,ds\Big] + A\sin\Big[\int\tau(s)\,ds\Big]\,[2]\,.$$

In this note we get the same result by simply solving the differential equation (1), and by the way, we obtain some consequences about the congruence of spherical curves and space curves. We discuss the problems as follows.

Multiplying the differential equation (1) by $2\sigma(s)$, we have

$$\rho'(s)\frac{d}{ds}[\sigma(s)]^2 + 2\rho''(s)[\sigma(s)]^2 = -2\rho(s)\,.$$

This is a 1st order linear differential equation of $[\sigma(s)]^2$ and hence

$$(3) \qquad [\sigma(s)]^2 = \frac{1}{[\rho'(s)]^2}[C_1^2 - (\rho(s))^2]\,,$$

i. e.,

$$\int\tau(s)\,ds + C_2 = \pm\int\frac{d\rho}{\sqrt{C_1^2-\rho^2}}$$

which implies that

$$(4) \qquad \rho(s) = C_1 \cos\left[\int \tau(s)\, ds + C_2\right],$$

where C_1, C_2 are arbitrary constants. Therefore, we have

THEOREM 1. A space curve with curvature $k = 1/\rho > 0$ and torsion $\tau = 1/\sigma$ $(\neq 0)$ is spherical if and only if

$$\rho(s) = C_1 \cos\left[\int \tau(s)\, ds + C_2\right],$$

where C_1 and C_2 are arbitrary constants.

THEOREM 2. Two spherical curves $\alpha, \beta : I \to E^3$ are congruent if and only if the two curves have the same curvature function, and at a pair of corresponding points their absolute values of torsions are equal.

PROOF. Since every spherical curve satisfies (3), the absolute value of the torsion of a spherical curve is uniquely determined by the given curvature function and the boundary condition of the torsion. Thus the absolute values of the torsions of α, β are equal when the curvature functions and the boundary conditions of the torsions of the two curves are respectively equal. Hence at every pair of corresponding points the two spherical curves have equal curvatures and equal absolute values of torsion, which are necessary and sufficient conditions for the congruence of two space curves[3]. q. e. d.

It is an exercise of differential geometry[4] that the arbitrary constant C_1 of (3) is equal to the radius of the sphere on which the spherical curve lies. Thus we have the following corollary:

COROLLARY. Two spherical curves on the spheres of equal radius are congruent if and only if they have the same curvature function.

From differential geometry one can also easily obtain the computational results that the curvature and torsion of the tangent indicatrix α and binormal indicatrix β of a curve γ are respectively given by

$$(5) \qquad k_\alpha^2 = 1 + \left(\frac{\tau_\gamma}{k_\gamma}\right)^2, \qquad \tau_\alpha = \frac{\left(\frac{\tau_\gamma}{k_\gamma}\right)'}{k_\gamma\left[1 + \left(\frac{\tau_\gamma}{k_\gamma}\right)^2\right]},$$

$$(6) \qquad k_\beta^2 = 1 + \left(\frac{k_\tau}{\tau_\tau}\right)^2, \qquad \tau_\beta = \frac{\left(\frac{k_\tau}{\tau_\tau}\right)'}{\tau_\tau\left[1 + \left(\frac{k_\tau}{\tau_\tau}\right)^2\right]}.$$

Since a space curve is uniquely determined up to the Euclidean motion when its curvature and absolute value of torsion are given, from (3), (5) and (6), we have the following lemma:

LEMMA. A space curve with $(k, \tau) \neq 0$ is uniquely determined if and only if its tangent indicatrix or binormal indicatrix has a known curvature function.

Thus we obtain

THEOREM 3. Two space curves $\alpha, \beta : I \to E^3$ with $(k, \tau) \neq 0$ are congruent if and only if their spherical images of tangents or binormals have the same curvature function.

REFERENCES

(1) S. BREUER & D. GOTTLIEB: The reduction of linear ordinary differential equations to equations with constant coefficients, *J. Math. Anal. Appl.* 31 (1970).

(2) ———: Explicit characterization of spherical curves, *Proc. of the Amer. Math. Soc.* 27 (1971).

(3) B. O'NEILL: "Elementary differential geometry", Academic Press, New York, 1966.

(4) T. J. WILLMORE: "Introduction to Differential Geometry", Oxford Univ. Press, 1959.

Simplicio: "Concerning natural things we need not always seek the necessity of mathematical demonstrations."

Sagredo: "Of course, when you cannot reach it. But if you can, why not?"

GALILEO GALILEI, Dialogue
on the Two Major Systems
of the World

CONSEQUENCES OF DISTENDED WAVE FUNCTIONS AND FINITE-PRECISION OPERATORS

E. E. FITCHARD

Part One

I. INTRODUCTION

The value and its attendant error are two numbers associated with any measurement. Of interest here is the latter quantity which typifies the degree of confidence accorded the former.

The three terms, uncertainty, accuracy, and precision, are germane to the jargon of experimental errors. To establish a definite, distinct meaning for each term they are related to the basic experimental quantities, the "least count error", and the "r. m. s. deviations", which are respectively one half the smallest distinguishable scale division of the measurement apparatus and the root mean square deviation in the set of measurements. To this end the following three definitions are given.

The PRECISION of a measurement apparatus is the inverse of its least count error.

The ACCURACY of an ensemble of α-measurements is the inverse of the r. m. s. deviation of these measurements.

The UNCERTAINTY in the measurement of a pair of observables α and β is the inverse product of their respective accuracies.

In a theoretical discussion of a physical system it is generally assumed for simplicity that the precision and accuracy are as large and the uncertainties as small as possible. Such measurements are here referred to as ideal measurements. That classical and quantal ideal measurements are disjunctive is pointed out by the following comparison:

1. Ideal Limit for Classical Measurements

Precision	——→	Infinity
Accuracy	——→	Infinity
Uncertainty	——→	Zero

2. Ideal Limit for Quantal Measurements

Precision	——→	Infinity
Accuracy	——→	Finite
Uncertainty	——→	Finite

The objection can be raised here that a quantum system prepared in the eigenstate ψ_k of observable a will always yield the measurement result a_k. However, it is not possible to prepare a quantum system in a state that is simultaneously an eigenstate of all observables. Thus (1) can be satisfied for all observables of a classical system and (2) can be met for some observables of a quantum system.

Only precision has the same ideal limit in both theories. The disagreements are of course a result of Heisenberg's uncertainty principle. The single accordance is subject to question by the following consideration. Let M be a meter stick with scale divisions separated by a distance $2L$ and least count error L. The precision of the meter stick can be increased by placing an additional scale division between each adjacent pair. Can this procedure be continued indefinitely? Classically there is no difficulty. One merely locates the position of two continuous scale divisions and constructs the bisector of the joining line segment. In quantum mechanics the idea of position becomes meaningless at atomic dimensions which requires the termination of the sequence.

A system composed of two masses connected by a spring may be approximated by a single mass joined to an immovable wall with a spring if one mass is very large relative to the other. These two systems are compared in the remainder of part one. As expected in the large mass limit these two systems give identical results according to classical mechanics. The quite unexpected result is that there exists a quantum mechanical disagreement between the two systems in this same limit.

Part two is concerned with the replacement of quantal operators corresponding to infinitely-precise measurement devices with operators corresponding to finite-precision measurement devices. It is also concerned with alternative forms for these operators.

II. THE HEISENBERG PICTURE

By specifying a complete orthonormal set (CONS) of eigenfunctions which span the Hilbert space of the system under consideration a representation has been singled out. This selection is certainly not unique; in fact the choices are nondenumerably infinite.

Consider two distinct CONS $\{\psi_i\}$ and $\{\phi_j\}$ which span the same Hilbert space. If x is any state of the system then

$$x=\sum_i c_i\psi_i \qquad \text{and} \qquad x=\sum_j d_j\phi_j \tag{1}$$

The c's and d's are the coordinates of x in the respective representations.

Since $\{\psi_i\}$ is a CONS any vector can be expressed in terms of it. In particular:

$$\phi_j=\sum_\lambda U_{\lambda j}\psi_\lambda \tag{2}$$

the $U_{\lambda j}$ are the coordinates of ϕ_j in the ψ-representation. Using this result in the proceeding equations gives:

$$x=\sum_\lambda c_\lambda\psi_\lambda=\sum_j d_j\sum_\lambda U_{\lambda j}\psi_\lambda$$

From which it follows that:

$$c_\lambda=\sum_j d_j U_{\lambda j}$$

From Eq. (1) and the definition of the scalar product on a Hilbert space:

$$(\psi_i,\ \phi_j)=\sum_\lambda U_{\lambda j}(\psi_i,\ \psi_\lambda)=\sum_\lambda U_{\lambda j}\delta_{i\lambda}=U_{ij}$$

Now consider:

$$\begin{aligned}(U^+U)_{nm}&=\sum_l U^*_{lm}U_{lm}=\sum_l(\psi_l,\ \phi_n)^*(\psi_l,\ \phi_m)\\&=\sum_l(\phi_m,\ \psi_l)(\psi_l,\ \phi_m)=(\phi_n,\ \phi_m)=\delta_{nm}\\&=(UU^+)_{nm}\end{aligned}$$

which implies that U is unitary.

Thus at least for Hilbert spaces with countable dimensionality the representations are related by unitary transformations. This conclusion can be extended to Hilbert spaces with nondenumerable dimensionality. To show that all representations connected by a unitary transformation give the same measurement results it is necessary first to note that the theory answers the following two types of questions.

a) What is the arithmetic mean of the measurement of observable A on an ensemble of identically prepared systems?

b)[1] What is the probability that a measurement of the observable A will result in the eigenvalue a_k?

The mathematical form taken by the answer to both of these questions is that of the magnitude of a scalar product. It is one of the fundamental properties of the unitary operator that it leaves a scalar product invariant. Therefore all representations connected by unitary[2] transformations are physically equivalent, i. e., they predict identical measurement results.

Of particular importance in wave mechanics is the unitary operator $U(t, t_0)$ which transforms a state given by $|a, t_0\rangle$ at time t_0 into the corresponding state at time t, $|a, t_0, t\rangle$. This operator called the propagator is also used to transform the Schrodinger representation into the Heisenberg representation.

By definition:

$$U^+(t, t_0)\,|a, t_0\rangle_s \equiv |c, t_0, t\rangle_H$$

and

$$A_H \equiv U^+(t, t_0) A_s U(t, t_0)$$

where the subscript s indicates the Schrodinger representation and H that of Heisenberg's. For an isolated system the Hamiltonian is time independent, $t_0=0$:

$$U(t, 0) = e^{-iHt/\hbar} \Rightarrow A_H(t) = e^{-iHt/\hbar} A e^{-iHt/\hbar} \qquad (3)$$

---

(1) b) is actually a special case of a).

(2) The term unitary transformation does not exclude antiunitary transformations which are at the same time both unitary and antilinear.

From Eq. (3) $A_H(0)=A_s$ thus the Heisenberg operators are initially the Schrodinger operators and evolve according to Eq. (3). The equation of motion follows from differentiation. The result is:

$$i\hbar\frac{dA_H(t)}{dt}=[A_H(t),\ H] \tag{4}$$

which is the counterpart of Schrodingers equation. The resemblance to the classical equations of motion is most striking. However, it must be born in mind that classical observables are functions which obey the rules of ordinary algebra whereas quantum observables are functionals (functions of operator) which obey the rules of noncommutative algebra. With this distinction clearly in mind the basic commutation relations for momentum and position are used to find one further analogy between the Heisenberg representation and Hamilton's formulation of classical mechanics.

The following commutator relations are the consequence of quantum mechanics and certain assumptions about the nature of space.

$$\begin{aligned} &[x,\ f(x)]=0, && [p,\ h(p)]=0 \\ &[x,\ g(p)]=i\hbar\frac{\partial g}{\partial p}, && [p,\ \Omega(x)]=\frac{\hbar}{i}\frac{\partial\Omega}{\partial x} \end{aligned} \tag{5}$$

From Eq. (4):

$$\dot{x}(t)=\frac{1}{i\hbar}[x(t),\ H]=\frac{\partial H}{\partial p}$$

$$\dot{p}(t)=\frac{1}{i\hbar}[p(t),\ H]=-\frac{\partial H}{\partial x}$$

These are Hamilton's equations of motion in terms of Heisenberg operators. Thus the operators in the Heisenberg representation of quantum mechanics satisfy equations identical in form to those of the corresponding equations in classical mechanics. Therefore, if the most general classical solution, i. e., that solution in terms of arbitrary initial position and momentum, are known, the appropriate quantum equations for the system are obtained immediately by replacing the position and momentum by the corresponding operators, the initial position and momentum going over to the Schrodinger operators as indicated earlier.

In the sequel this technique will be used to solve two mechanics problems. It is worth noting that there exist only a few mechanical systems in which the complete solution for position and momentum is a simple function of time.

III. LARGE MASS APPROXIMATION WITH A GAUSSIAN WAVE FUNCTION[3]

In this section a comparison is made of the classical and quantal calculations for the two systems of Fig. 1. It is common practice both in classical and quantum mechanics to approximate the system depicted in Model II by that of Model I for the case $m_2 \gg m_1$. That such a supplantation is not in general valid follows from the ensuing calculation.

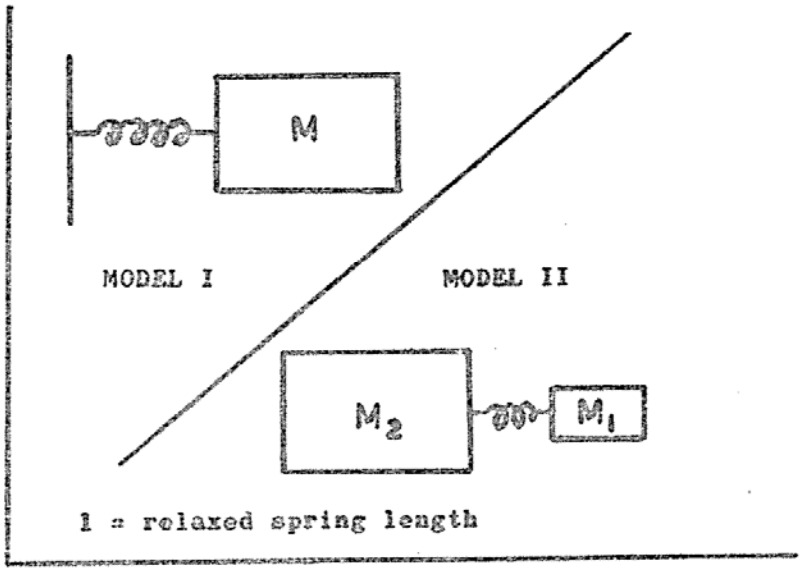

Fig 1. Two models of harmonic oscillators. It is common practice to approximate model II by model I if $M_2 \gg M_1$.

As outlined in section II it is necessary to determine the complete classical solution.

First for Model I:

$$\bar{H}=\frac{\bar{p}^2}{2m}+\frac{1}{2}k(\bar{x}-l)^2$$

(3) Portions of sections III and IV are taken from Dr. James Park's research notes.

which through Hamilton's equations gives:

$$\dot{\bar{x}}=\bar{p}/m$$
$$\dot{\bar{p}}=-k(\bar{x}-l)$$

The resulting equation of motion is:

$$\ddot{\bar{x}}=-\frac{k}{m}(\bar{x}-l)$$

which has the solution:

$$\bar{x}=l+\frac{\bar{p}_0}{\bar{\omega}m}\sin\bar{\omega}t+(\bar{x}_0-l)\cos\bar{\omega}t$$
$$\bar{\omega}=\sqrt{\frac{k}{m}} \qquad (6)$$

$\bar{x}_0$, $\bar{p}_0$ are the initial position and momentum, respectively.

For Model II:

$$H=\frac{p_1^2}{2m_1}+\frac{p_2^2}{2m_2}+\frac{1}{2}k(x_1-x_2-l)^2$$

from which:

$$\dot{x}_1=p_1/m_1, \qquad \dot{p}_1=-k(x_1-x_2-l)$$
$$\dot{x}_2=p_2/m_2, \qquad \dot{p}_2=k(x_1-x_2-l)$$

The resulting equations of motion are:

$$\ddot{x}_1+\frac{k}{m_1}(x_1-x_2-l)=0$$
$$\ddot{x}_2-\frac{k}{m_2}(x_1-x_2-l)=0$$

To decouple these equations, a transformation to center of mass (C.M.) coordinates is convenient. C.M. coordinates are defined by:

$$R=\frac{m_1x_1+m_2x_2}{M},\ \Omega=x_1-x_2,\ M=m_1+m_2$$

The inverse equations are:

$$x_1=R+\frac{m_2}{M}\Omega,\ x_2=R-\frac{m_1}{M}\Omega$$

This transformation yields the equations of motion:

$$M\ddot{R}=0,\ \ddot{\Omega}+\frac{k}{\mu}(\Omega-l)=0,\ \text{where}\ \frac{1}{\mu}=\frac{1}{m_1}+\frac{1}{m_2}$$

with the solutions:

$$\Omega=l+\frac{\dot{\Omega}_0}{\omega}\sin\omega t+(\Omega_0-l)\cos\omega t$$

$$R=\dot{R}_0 t+R,\ \omega=\sqrt{\frac{k}{\mu}}$$

Ω_0, R_0 are initial values.

The inverse transformation results in the solutions:

$$x_1=\frac{m_1x_{10}+m_2x_{20}}{M}+\frac{p_{10}+p_{20}}{M}t+\frac{m_2}{M}\left[l+\frac{1}{\omega}\left(\frac{p_{10}}{m_1}-\frac{p_{20}}{m_2}\right)\cos\omega t\right.$$

$$\left.+(x_1-x_2'-l)\sin\omega t\right]$$

$$p_1=\frac{m_1}{M}(p_{10}+p_{20})+\mu\left[\left(\frac{p_{10}}{m_1}-\frac{p_{20}}{m_2}\right)\cos\omega t-(x_1-x_2-l)\omega\sin\omega t\right]$$

$$x_2=\frac{m_1x_{10}+m_2x_2}{M}+\frac{p_{10}+p_{20}}{M}t-\frac{m_1}{M}\left[l+\frac{1}{\omega}\left(\frac{p_{10}}{m_1}-\frac{p_{20}}{m_2}\right)\sin\omega t\right.$$

$$\left.+(x_1-x_2-l)\cos\omega t\right]$$

$$p_2=\frac{m_2}{M}(p_{10}+p_{20})-\mu\left[\left(\frac{p_{10}}{m_1}-\frac{p_{20}}{m_2}\right)\cos\omega t-\omega(x_1-x_2-l)\sin\omega t\right]$$

x_{10}, x_{20}, etc. are initial values.

In the classical case the large mass approximation is obtained by the substitution

$$m_2\gg m_1,\ x_2=p_2=0. \tag{7}$$

In this limit the equation for x_1 reduces to:

$$x_1=\frac{m_1}{m_2}x_{10}+\frac{p_{10}}{m_2}t+l+\frac{p_{10}}{m_1\omega}\sin\omega t+(x_{10}-l)\cos\omega t$$

$$\xrightarrow[m_2\to\infty]{} l+\frac{p_{10}}{m_1\omega}\sin\omega t+(x_{10}-l)\cos\omega t \tag{8}$$

The second term on the right of (8) will be negligible if the time is not large. With the relabeling $m_1\to m$, $x_1\to\bar{x}$, $p_1\to\bar{p}$, it follows that in classical mechanics as $m_2\to\infty$, the model I solution Eq. (6) is

identical to the model II solution Eq. (8). This of course is the expected result. Since model I is the simpler system it is the natural choice for a large mass calculation.

In the quantum mechanical case the particular substitution of Eq. (7) is no longer valid. The distinction between classical functions and quantal operators attains paramount importance at this point. The quantum theory can predict only the arithmetic mean of an ensemble of position or momentum measurements. Thus it is possible only to specify and verify through measurement, that the arithmetic mean of position or momentum measurements on an ensemble of identically prepared systems will be zero. This is written:

$$\langle x_2 \rangle = 0, \ \langle p_2 \rangle = 0$$

These conditions along with $m_2 \gg m_1$, give the closest possible quantal analogy to the former classical situation.

From the proof of the Heisenberg uncertainty principle it can be shown that the minimum uncertainty in x_2 and p_2 is obtained when the wave function describing mass two has the form:

$$\psi_2(x_2) = \frac{(2\pi)^{-1/4}}{\sqrt{\Delta}} e^{-x_2^2/4\Delta^2} \qquad (9)$$

Δ is a length characteristic of the width of $\psi_2(x_2)$ as show in fig. 2.

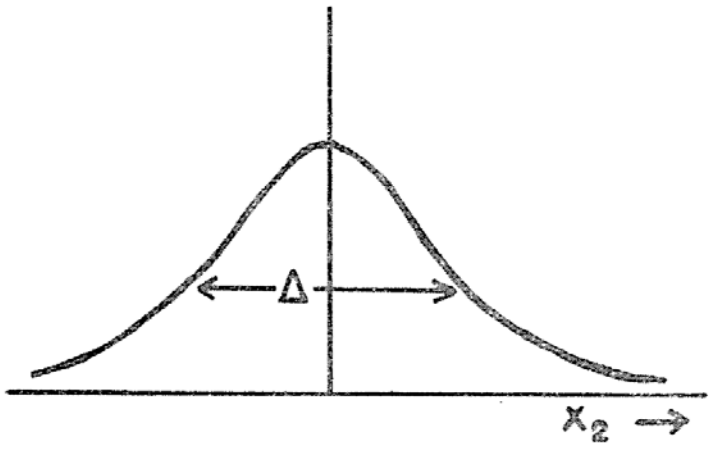

Fig. 2. The width of a wave function.

The model II Heisenberg operator x_1, for $m_2 \gg m_1$, is

$$x_1=\frac{m_1}{m_2}x_{10}+x_{20}+\frac{p_{10}+p_{20}}{m_2}t+l+\frac{1}{\omega}\left(\frac{p_{10}}{m_1}+\frac{p_{20}}{m_2}\right)\sin\omega t$$

$$+(x_1-x_2-l)\cos\omega t\xrightarrow[m_2\to\infty]{}\left[l+\frac{p_{10}}{m_1\omega}\sin\omega t\right.$$

$$\left.+(x_{10}-l)\cos\omega t\right]+(1-\cos\omega t)x_2 \tag{10}$$

Note that $p_2=\frac{\hbar}{i}\frac{\partial}{\partial x_2}$ is independent of m_2 so $\frac{p_2}{m_2}\to 0$. The square brackets correspond to the model I solution $\bar{x}$ of Eq. (6) with the replacement:

$$x_1\to\bar{x},\ p_1\to\bar{p},\ m_1\to m.$$

As mentioned previously only expectation values of x and p are observable. For x this is:

$$\langle x_1\rangle=\langle\psi_1\psi_2|\psi_1\psi_2\rangle$$

$$\langle x_1\rangle=\langle\psi_1|\bar{x}|\psi_1\rangle+(1-\cos\omega t)\langle\psi_2|x_2|\psi_2\rangle \tag{11}$$

From the symmetry of the wave function the second term on the right is zero so $\langle x_1\rangle$ is the same in both models. Next consider:

$$\langle x_1^2\rangle=\langle\bar{x}^2\rangle+2\langle\bar{x}\rangle\langle x_2\rangle(1-\cos\omega t)+\langle x_2^2\rangle(1-\cos\omega t)^2$$

$$=\langle\bar{x}^2\rangle+(1-\cos\omega t\rangle^2\Delta^2 \tag{12}$$

For this moment the expectation values of x is different in the two models. For the n^{th} moment:

$$\langle x_1^n\rangle=\langle\bar{x}^n\rangle+\sqrt{n!}\,\Delta^n(1-\cos\omega t)^n+\text{other terms}$$

If n is even, the "other terms" will all be positive. The second term on the right for large n is approximated by:

$$\exp\left[n\left(\frac{1}{2}\ln n+\ln\delta\right)\right]$$

If Δ is small then $\ln\delta$ is a large negative number which gives a negligible difference in the two models except for very large n.

For the Gaussian wave of this section the uncertainty in position and momentum is the smallest possible value:

$$\Delta x\Delta p=\hbar/2$$

In the following two sections the effect of increasing this uncertainty is explored.

IV. DISTENDED WAVE FUNCTION

The calculation of section III hints that a wave function with more than a minimum uncertainty would result in a greater quantal disparity between the two models. To support this assertion it is interesting to consider a wave function which has a macroscopic spread in the position and momentum uncertainty. In search of such a function consider the harmonic oscillator eigenkets $\{|n\rangle\}$ with associated Hamiltonian:

$$H=\frac{p^2}{2m}+\frac{m\omega^2}{2}x^2$$

These kets have the following eigenvalues and properties:

$$E_n=(x+1/2)\hbar\omega,\ n=0,\ 1,\ 2,\cdots$$

$$\langle x\rangle=\langle n|x|n\rangle=\langle p\rangle=\langle n|p|n\rangle=0$$

$$(\Delta x)^2=\langle n|x^2|n\rangle=E_n/m\omega^2,\ (\Delta p)^2=\langle n|p^2|n\rangle=mE_n$$

$$\Delta x\Delta p=\frac{E_n}{\omega}=(n+1/2)\hbar$$

Consider the transformed kets:

$$|n;\ a,b\rangle=e^{ipb/\hbar}e^{-ipa/\hbar}|n\rangle$$

where the two exponential operators are respectively the momentum and position translation operators. The expectation values for these eigenfunctions are:

$$\langle n;\ a,b|x|n;\ a,b\rangle=\langle n|e^{ipa/\hbar}e^{-ixb/\hbar}xe^{-ixb/\hbar}e^{-ipa/\hbar}|n\rangle$$

Using the commutability of x with any function of itself

$$=\langle n|e^{ipa/\hbar}xe^{-ipa/\hbar}|n\rangle=\langle n|x+a|n\rangle=a$$

$$\langle n;\ a,b|p|n;\ a,b\rangle=b$$

$$\langle n;\ a,b|x^2|n;\ a,b\rangle=\langle n|e^{ipa/\hbar}x^2e^{-ipa/\hbar}|n\rangle$$

$$=\langle n|e^{ipa/\hbar}xe^{-ipa/\hbar}e^{ipa/\hbar}xe^{-ipa/\hbar}|n\rangle \qquad (13)$$

$$=\langle n|(x+a)^2|n\rangle=\langle x^2\rangle+a^2$$

$$=\frac{E_n}{m\omega}+a^2$$

$$\langle n;\, a, b|p^2|n;\, a, b\rangle=mE_n+b^2$$

Thus,

$$\Delta x\Delta p=\sqrt{mE_n\frac{E_n}{m\omega^2}}=\frac{E_n}{\omega}(n+1/2)\hbar$$

The uncertainty in x and p can be adjusted by varying n. For large enough values of n, $\Delta x\Delta p$ is comparable to the least count error of a physical ruler. In the next section this wave function will be used to calculate the expectation values of section III corresponding to a distended wave function. It is important to note that $\{|n\rangle\}$ are stationary states, but $|n;\, a,\, b\rangle$ are not.

V. LARGE MASS APPROXIMATION WITH DISTENDED WAVE FUNCTION

In section III it was shown that the model I and model II mechanical systems depicted in Fig. 1 yield identical results for the large mass approximation in the classical case but not in the quantum mechanical case. In this section a completely similar calculation is performed employing the distended wave functions of section IV.

Recalling that the distended wave function is centered at $x_2=a_2$, the equations which replace equations (11) and (12) are:

$$\langle x_1\rangle=\langle\bar{x}\rangle+(\langle x_2\rangle-a_2)(1-\cos\omega t)$$

$$=\langle\bar{x}\rangle$$

This is the model I result.

$$\langle\bar{x}_1^2\rangle=\langle\bar{x}^2\rangle+2\langle\bar{x}\rangle(\langle x_2\rangle-a_2)(1-\cos\omega t)$$

$$+(\langle x_2^2\rangle-2a_2\langle x_2\rangle-a_2^2)(1-\cos\omega t)^2 \qquad (14)$$

$$=\langle\bar{x}^2\rangle+(E_n/m_2\omega^2)(1-\cos\omega t)^2$$

The factor $E_n/m_2\omega^2$ can be adjusted by changing n. For large n it is comparable to the least count error in x. The third and fourth moments give even greater discrepancies between the two models as indicated by:

$$\langle x_1^3\rangle=\langle\bar{x}^3\rangle+\frac{3E_n}{m_2\omega^2}\langle\bar{x}\rangle(1-\cos\omega t)^2$$
$$\langle x_1^4\rangle=\langle\bar{x}^4\rangle+\frac{6E_n}{m_2\omega^2}\langle\bar{x}^2\rangle(1-\cos\omega t)^2+\left(\frac{E_n}{m_2\omega^2}\right)^2(1-\cos\omega t)^4 \tag{15}$$

Thus it is apparent that as the distention of the wave function increases so does the quantal disparity between the two models.

Part Two

I. FINITE-PRECISION OPERATORS

It is a fundamental axiom of quantum mechanics that to each observable there corresponds an operator on Hilbert space. Two such operators, momentum and position, are endowed with a continuous spectrum of eigenvalues. Such operators correspond to measurement apparatus with zero least count errors. It is tacitly assumed that such devices which are called infinitely precise exist. Since this is not the case, operators incorporating finite precision are desirable. Candidates for the finite-precision position and momentum operators are defined as follows.

$$x_I=\sum_{n=-\infty}^{\infty}n\Delta_x\int_{I_n}|x\rangle dx\langle x|,\ I_n=[(n-1/2)\Delta_x,\ (n+1/2)\Delta_x]$$
$$p_J=\sum_{n=-\infty}^{\infty}n\Delta_p\int_{J_m}|p\rangle dp\langle p|,\ J_n=[(n-1/2)\Delta_p,\ (n+1/2)\Delta_p] \tag{16}$$

These operators are nondenumerably degenerate in that the continuum of eigenvalues corresponding to an interval of length Δ_x for position and Δ_p for momentum are equal. The graph of eigenvalues associated with x_I is illustrated in Fig. 3. A similar graph for the eigenvalues of p_J obtains. From this definition it is possible, given a wavefunction, to compute the moments of x_I and p_J. First consider:

$$\langle x_I\rangle=\langle\psi|x_I|\psi\rangle=\langle\psi|\sum_{n=-\infty}^{\infty}n\Delta_x\int_{I_n}|x\rangle dx\langle x|\psi\rangle$$
$$=\sum_{n=-\infty}^{\infty}n\Delta_x\int_{I_n}|\psi(x)|^2dx \tag{17}$$

If $\psi(x)$ has a definite parity x_I can be simplified as follows:

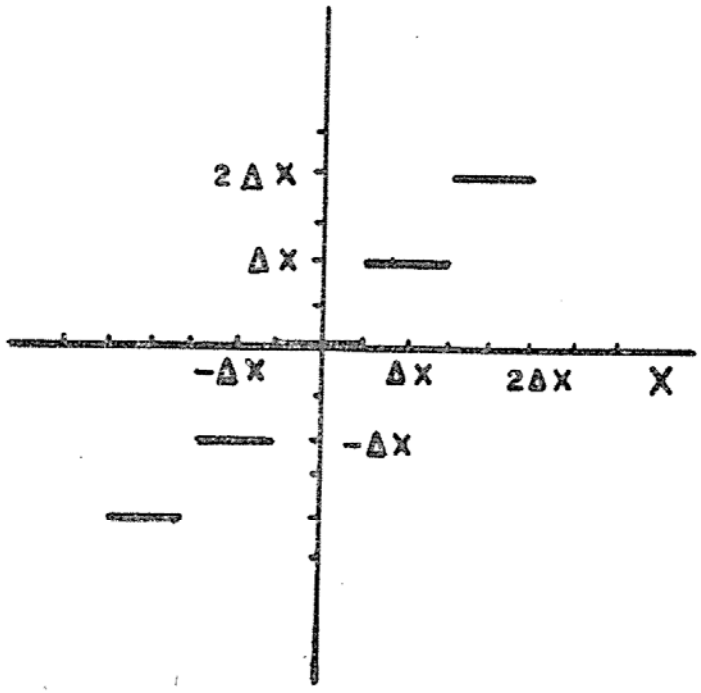

Fig. 3. Eigenvalues corresponding to an interval Δx for position are equal.

$$\langle x_I\rangle=\sum_{n=1}^{\infty} n\Delta_x\Big[\int_{I_n}\psi^*(x)\psi(x)dx-\int_{I_{(-n)}}\psi^*(x)\psi(x)dx\Big]$$

Since $|\psi(x)|^2$ is symmetric, $I_{(-n)}\rightarrow I_n$ when $x\rightarrow -x$, so:

$$\langle x_I\rangle=\sum_{n=1}^{\infty}\Delta_x(n-n)\int_{I_n}|\psi(x)|^2dx=0$$

For the second moment:

$$\langle x_I^2\rangle=\langle\psi|\sum_{n=-\infty}^{\infty} n\Delta_x\int_{I_n}|x\rangle dx\langle x|\sum_{m=-\infty}^{\infty} m\Delta_x\int_{I_m}|x'\rangle dx'\langle x'|\psi\rangle$$

$$=\sum_{n=-\infty}^{\infty}\sum_{m=-\infty}^{\infty} nm\Delta_x^2\int_{I_n}dx\int_{I_m}dx'\psi^*(x)\delta(x-x')\psi(x')$$

The δ-function gives a nonzero result only when x and x' are in the same interval which implies that $I_n=I_m$, since all intervals are assumed disjoint. This gives:

$$\langle x_I^2\rangle=\sum_{n=-\infty}^{\infty} n^2\Delta_x^2\int_{I_n}dx|\psi(x)|^2$$

Continuing to the k^{th} moment:

$$\langle x_I^k\rangle=\langle\psi|\sum_{n_1=-\infty}^{\infty} n_1\Delta_x\int_{I_{n_1}}dx_1|x_1\rangle dx_1\langle x_1|\cdots$$

$$\sum_{n_k=-\infty}^{\infty} n_k\Delta_x\int_{I_{n_k}}dx_k|x_k\rangle dx_k\langle x_k|\psi\rangle$$

Using linearity this reduces to:

$$\langle x_I^k\rangle = \sum_{n_1=-\infty}^{\infty}\cdots\sum_{n_k=-\infty}^{\infty}(n_1\cdots n_k)\Delta_x^k\int_{I_{n_1}}dx_1\cdots\int_{I_{n_k}}dx_k$$
$$\psi(x)\delta(x_1-x_2)\cdots\delta(x_{k-1}-x_k)\psi(x_k)$$

Note that

$$\int_{I_{n_1}}dx_1\int_{I_{n_2}}dx_2\int_{I_{n_3}}dx_3\delta(x_1-x_2)\delta(x_2-x_3)$$
$$=\int_{I_{n_1}}dx_1\int_{I_{n_3}}dx_3\delta(x_1-x_3)$$

if x_1 and x_3 are in I_2 and zero otherwise.

Therefore

$$I_{n_1}=I_{n_2}=I_{n_3}$$

The effect of the product of delta functions is to insure that

$$n_1=n_2=\cdots\cdots=n_k=n$$

Thus:

$$\langle x_I^k\rangle=\sum_{n=-\infty}^{\infty}n^k\Delta_x^k\int_{I_n}dx|\psi(x)|^2$$

As an example let $\psi(x)=ae^{-\alpha|x|}$

$$|\psi(x)|^2=|a|^2e^{-2\alpha|x|}\Rightarrow\int_{I_n}dx|\psi(x)|^2=|a|^2\int_{I_n}e^{-2\alpha|x|}dx$$

For $n>0$ the absolute value signs on x may be removed after integration:

$$|a|^2\left.\frac{e^{-2\alpha x}}{-2\alpha}\right|_{(n-1/2)\Delta x}^{(n+1/2)\Delta x}=\frac{|a|^2}{\alpha}e^{-2n\Delta_x\alpha}\sinh\Delta_x\alpha$$

Eq. (18) may be rewritten to exclude all $n<0$ by noting

$$\sum_{n=-\infty}^{\infty}n^k\Delta_x^k\int_{I_n}dx|\psi(x)|^2=\sum_{n=-\infty}^{-1}n^k\Delta_x^k\int_{I_n}|\psi(x)|dx$$
$$+\sum_{n=1}^{\infty}n^k\Delta_x^k\int_{I_n}|\psi(x)|^2dx$$
$$=\sum_{n=1}^{\infty}n^k\Delta_x^k\left\{\int_{I_n}|\psi(x)|^2dx+(-1)^k\int_{I_{(-n)}}|\psi(x)\right.$$

If $\psi(x)$ has a definite parity then

Using linearity this reduces to:

$$\langle x_I^k\rangle = \sum_{n_1=-\infty}^{\infty}\cdots\sum_{n_k=-\infty}^{\infty}(n_1\cdots n_k)\Delta_x^k\int_{I_{n_1}}dx_1\cdots\int_{I_{n_k}}dx_k$$
$$\psi(x)\delta(x_1-x_2)\cdots\delta(x_{k-1}-x_k)\psi(x_k)$$

Note that

$$\int_{I_{n_1}}dx_1\int_{I_{n_2}}dx_2\int_{I_{n_3}}dx_3\delta(x_1-x_2)\delta(x_2-x_3)$$
$$=\int_{I_{n_1}}dx_1\int_{I_{n_3}}dx_3\delta(x_1-x_3)$$

if x_1 and x_3 are in I_2 and zero otherwise.

Therefore

$$I_{n_1}=I_{n_2}=I_{n_3}$$

The effect of the product of delta functions is to insure that

$$n_1=n_2=\cdots\cdots=n_k=n$$

Thus:

$$\langle x_I^k\rangle=\sum_{n=-\infty}^{\infty}n^k\Delta_x^k\int_{I_n}dx|\psi(x)|^2 \tag{18}$$

As an example let $\psi(x)=ae^{-\alpha|x|}$

$$|\psi(x)|^2=|a|^2e^{-2\alpha|x|}\Rightarrow\int_{I_n}dx|\psi(x)|^2=|a|^2\int_{I_n}e^{-2\alpha|x|}dx$$

For $n>0$ the absolute value signs on x may be removed to obtain after integration:

$$|a|^2\frac{e^{-2\alpha x}}{-2\alpha}\Bigg|_{(n-1/2)\Delta x}^{(n+1/2)\Delta x}=\frac{|a|^2}{\alpha}e^{-2n\Delta_x\alpha}\sinh\Delta_x\alpha$$

Eq. (18) may be rewritten to exclude all $n<0$ by noting:

$$\sum_{n=-\infty}^{\infty}n^k\Delta_x^k\int_{I_n}dx|\psi(x)|^2=\sum_{n=-\infty}^{-1}n^k\Delta_x^k\int_{I_n}|\psi(x)|dx$$
$$+\sum_{n=1}^{\infty}n^k\Delta_x^k\int_{I_n}|\psi(x)|^2dx$$
$$=\sum_{n=1}^{\infty}n^k\Delta_x^k\left\{\int_{I_n}|\psi(x)|^2dx+(-1)^k\int_{I_{(-n)}}|\psi(x)|^2dx\right\}$$

If $\psi(x)$ has a definite parity then

$$\langle x_I^k\rangle=\sum_{n=1}^{\infty} n^k\Delta_x^k[1+(-1)^k]\int_{In}|\psi(x)|^2dx$$

Obviously, only even powers of k give nonzero results. For the particular ψ-function under consideration,

$$\langle x_I^k\rangle=\sum_{n=1}^{\infty} n^k\Delta_x^k[1+(-1)^k]\frac{|a|^2}{\alpha}e^{-2n\Delta_x\alpha}\sinh\Delta_x\alpha$$

$$=\left(\frac{-1}{2}\right)^k\frac{|a|^2}{\alpha}\sinh\Delta_x\alpha\frac{\partial^k}{\partial\alpha^k}\sum_{n=1}^{\infty}e^{-2n\Delta_x\alpha}[1+(-1)^k]$$

$$=2^{-k}[1+(-1)^k]\frac{|a|^2}{\alpha}\sinh\Delta_x\alpha\frac{\partial^k}{\partial\alpha^k}(1-e^{-2\Delta_x\alpha})^{-1}$$

In the special case, $k=2$ the expectation value of x_I is:

$$\langle x_I^2\rangle=2\frac{|a|^2}{\alpha}\Delta_x^2e^{-2\Delta_x\alpha}\frac{\cosh\Delta_x\alpha}{\sinh\Delta_x\alpha} \tag{19}$$

For the traditional position operator the corresponding calculation proceeds along the following lines,

$$\langle x^2\rangle=|a|^2\int_{-\infty}^{\infty}x^2e^{-\alpha|x|}dx=2|a|^2\int_0^{\infty}x^2e^{-2\alpha x}dx$$

$$=|a|^2\frac{\partial^2}{\partial\alpha^2}\left(\frac{1}{\alpha}\right)=\frac{2|a|^2}{\alpha^3}$$

Using this result the finite precision position operator can be written

$$\langle x_I^2\rangle=\langle x^2\rangle\alpha^2\Delta_x^2e^{-2\Delta_x\alpha}\frac{\cosh\Delta_x\alpha}{\sinh^2\Delta_x\alpha}=\langle x^2\rangle[1-2\Delta_x\alpha+\cdots]$$

II. ALTERNATIVE FORMS FOR FINITE-PRECISION OPERATORS

To determine alternatives forms for these operators consider first the expectation value of p_J:

$$\langle\phi|p_J|\phi\rangle=\langle\phi|\sum_{n=-\infty}^{\infty}n\Delta_p\int_{Jn}|p\rangle dp\langle p|\phi\rangle$$

$$=\sum_{n=-\infty}^{\infty}n\Delta_p\int_{Jn}\langle\phi|p\rangle dp\langle p|\phi\rangle=\sum_{n=-\infty}^{\infty}n\Delta_p\int_{Jn}|\phi(p)|^2dp$$

The function $\phi(p)$ in momentum space is the Fourier transform of the corresponding function in coordinate space, so:

$$\phi(p)=\frac{1}{\sqrt{2\pi\hbar}}\int_{-\infty}^{\infty}\psi(x)e^{-ipx/\hbar}dx$$

where $\psi(x)$ is the coordinate representation of $\phi(p)$. From this:

$$\langle\phi|p_J|\phi\rangle=\sum_{n=-\infty}^{\infty}\frac{n\Delta_p}{2\pi\hbar}\int_{J_n}dp\int_{-\infty}^{\infty}dxdx'\psi^*(x')\psi(x)e^{-ip(x-x')/\hbar} \qquad (20)$$

It is straightforward to show that:

$$\sum_{n=-\infty}^{\infty}n\int_{J_n}dpe^{-ip(x-x')/\hbar}=\frac{2\hbar}{x-x'}\sin\frac{\alpha}{2}\sum_{n=-\infty}^{\infty}ne^{-i\alpha n}$$

$$=\frac{-\hbar}{x-x'}\frac{1/2}{\sin\alpha/2},\quad \alpha=\frac{\Delta_p(x-x')}{\hbar}$$

On substituting this result, Eq. (20) becomes:

$$\langle\phi|p_J|\phi\rangle=-\frac{\Delta_p}{4\pi}\int_{-\infty}^{\infty}dxdx'\frac{\psi^*(x)\psi(x')}{x-x'}\frac{1}{\sin\alpha/2} \qquad (21)$$

Taking the limit as $\Delta_p\to 0$ and using the Cauchy integral formula, p_J reduces in coordinate space to $\frac{\hbar}{i}\frac{\partial}{\partial x}$ which is the usual continuous momentum operator. Further integration of (21) can be done by analytically continuing x into the complex z-plane.

Let:

$$I(x)=-\frac{\Delta_p}{4\pi}\int_{-\infty}^{\infty}\frac{\psi(x)dx}{(x-x')\sin\beta(x-x')},\quad \beta=\frac{\Delta_p}{2\hbar}$$

and

$$z_0\equiv x'+i\varepsilon,\quad I(z)=-\frac{\Delta_p}{4\pi}\int_c dz\frac{\psi(z)}{(z-z_0)\sin\beta(z-z_0)}$$

The contour C is shown in Fig. 4. If $\psi(z)$ is sufficiently well behaved that the integrand of $I(z)$ vanishes as $|z|\to\infty$ in the upper-half z-plane, then

$$I(x)=\lim_{\varepsilon\to 0}I(z)$$

This restriction on $\psi(z)$ is quite severe. In fact it can be easily shown that the Gaussian wave function does not satisfy it. The resulting animadversion will be mitigated by a forthcoming observation. Since the choice of z_0 has moved the poles below the real axis, this axis can be used as part of the contour. It is advantageous to make a Mittag-Leffler expansion of csc z, as follows:

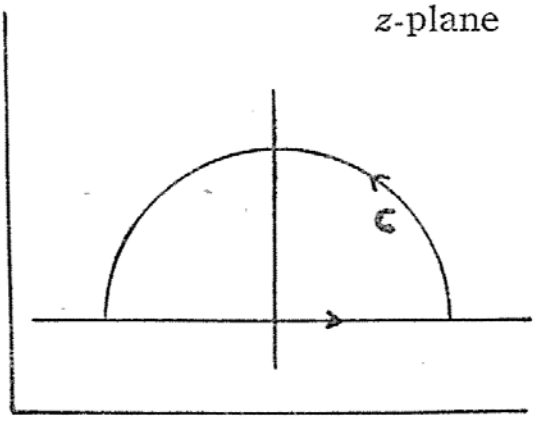

Fig. 4. The contour C of the complex integral $I(z)$.

$$\csc z=\frac{1}{z}-2z\sum_{n=1}^{\infty}\frac{(-1)^n}{n^2\pi^2-z^2}$$

From which, through the application of partial fractions it follows:

$$\frac{\csc\beta(z-z_0)}{z-z_0}=\frac{1}{\beta(z-z_0)^2}-\beta\sum_{n=1}^{\infty}\frac{(-1)^n}{n\pi}\left\{\frac{1}{n\pi+\beta(z-z_0)}+\frac{1}{n\pi-\beta(z-z_0)}\right\}$$

Substituting this in the integral and applying the generalized Cauchy integral formula

$$f^{[n]}(z)=\frac{n!}{2\pi i}\int_c\frac{f(z)dz}{(z-z_0)^{n+1}}$$

provided $f(z)$ is analytic within and on the contour C. Assuming $\psi(z)$ is analytic in the upper-half plane and on the real axis:

$$I(z)=-\frac{\Delta_p}{4\pi}\int_{-\infty}^{\infty}\frac{\psi(z)dz}{\beta(z-z_0)^2}+\frac{\Delta_p}{4\pi^2}\sum_{n=1}^{\infty}\frac{(-1)^n}{n}\left\{\int_{-\infty}^{\infty}\frac{\psi(z)dz}{z-z_0+n\pi/\beta}+\int_{-\infty}^{\infty}\frac{\psi(z)dz}{z-z_0-n\pi/\beta}\right\}$$

$$=\frac{\Delta_p}{2\beta i}\left.\frac{d\psi(z)}{dz}\right|_{z=z_0}+\frac{\Delta_p i}{2\pi}\sum_{n=1}^{\infty}\frac{(-1)^n}{n}\{\psi(z_0+n\pi/\beta)-\psi(z_0-n\pi/\beta)\}$$

Letting $\varepsilon\to 0$ the result is:

$$I(x)=\left\{\frac{\hbar}{i}\frac{\partial}{\partial x}+\frac{\Delta_p i}{2\pi}\sum_{n=1}^{\infty}\frac{(-1)^n}{n}[e^{2in\pi\hbar p/\Delta_p}-e^{-2in\pi\hbar p/\Delta_p}]\right\}\psi(x)$$

This in turn implies:

$$p_I = p + \frac{\Delta_p}{2\pi i} \sum_{n=1}^{\infty} \frac{(-1)^n}{n} (e^{-2in\pi p/\Delta_p} - e^{2in\pi p/\Delta_p}) \tag{22}$$

Following nearly an identical derivation it can be shown that:

$$x_I = + \frac{\Delta_x}{4\pi} \int_{-\infty}^{\infty} dp dp' \frac{|p'\rangle\langle p|}{(p-p') \sin \tau(p-p')}, \quad \tau = \frac{\Delta_x}{2\hbar}$$

$$x_I = x + \frac{\Delta_x}{2\pi i} \sum_{n=1}^{\infty} \frac{(-1)^n}{n} (e^{-2in\pi x/\Delta_x} - e^{2in\pi x/\Delta_x})$$

The preceding equations are actually operator equations and as such are not subject to all of the manipulation of real or complex variables. Operators in quantum mechanics satisfy:

$$f(x_{0p}) = \int_{-\infty}^{\infty} f(x_c) |x\rangle dx \langle x| \tag{23}$$

where $f(x_{0p})$ is a function of an operator and $f(x_c)$ is the same function of the eigenvalues of the operator and as such is amenable to ordinary functional analysis. In particular the eigenvalues of x_I are subject to the methods of Fourier analysis. Thus:

$$x_I = x + \frac{\Delta_x}{\pi} \sum_{n=1}^{\infty} \frac{(-1)^n}{n} \sin \frac{2n\pi x}{\Delta_x}$$

$$= x - \Delta_x \left(\frac{x}{\Delta_x} - k \right), \quad 2k-1 < \frac{x}{\Delta_x} \leq 2k+1$$

k is an integer given by:

$$k = \left[\frac{x}{\Delta_x} + \frac{1}{2} \right]$$

where the brackets mean the largest integer less than or equal to the argument. Thus a further form for the physical position operator is:

$$x_I = \Delta_x \left[\frac{x}{\Delta_x} + \frac{1}{2} \right] \tag{24}$$

where the operator derives its meaning from Eq. (23).

It is apparent that this operator is equivalent to the originally defined physical operator of Eq. (16) which indicates that its range of validity is greater than that implied by the derivation. These four forms along with a fifth involving the Heaviside step function defined by:

$$H(\theta)=\begin{cases}0 & \theta<0\\ 1 & \theta\geq 0\end{cases}$$

are recorded in Table 1.

Table 1.

$x_I=$	$p_J=$
$\Delta_x\left[\frac{x}{\Delta_x}+\frac{1}{2}\right]$	$\Delta_p\left[\frac{p}{\Delta_p}+\frac{1}{2}\right]$
$\sum_{n=-\infty}^{\infty} n\Delta_x\int_{I_n}\|x\rangle dx\langle x\|$ $I_n=[(n-1/2)\Delta_x,\ (n+1/2)\Delta_x]$	$\sum_{n=-\infty}^{\infty} n\Delta_p\int_{J_n}\|p\rangle dp\langle p\|$ $J_n=[(n-1/2)\Delta_p,\ (n+1/2)\Delta_p]$
$x+\frac{\Delta_x}{2\pi}\sum_{n=1}^{\infty}\frac{(-1)^n}{n}\sin\frac{2\pi nx}{\Delta_x}$	$p+\frac{\Delta_p}{2\pi}\sum_{n=1}^{\infty}\frac{(-1)^n}{n}\sin\frac{2\pi np}{\Delta_p}$
$+\frac{\Delta_x}{4\pi}\int_{-\infty}^{\infty}dp\,dp'\frac{\|p\rangle\langle p'\|}{(p-p')\sin\gamma(p-p')}$ $\gamma=\frac{\Delta_x}{2\hbar}$	$-\frac{\Delta_p}{4\pi}\int_{-\infty}^{\infty}dx\,dx'\frac{\|x\rangle\langle x'\|}{(x-x')\sin\beta(x-x')}$ $\beta=\frac{\Delta_p}{2\hbar}$
$\Delta_x\sum_{n=1}\left\{H\left(\frac{x}{\Delta_x}+\frac{1}{2}+n\right)\right.$ $\left.+H\left(\frac{x}{\Delta_x}-\frac{1}{2}+n\right)-1\right\}$	$\Delta_p\sum_{n=1}^{\infty}\left\{H\left(\frac{p}{\Delta_p}+\frac{1}{2}+n\right)\right.$ $\left.+H\left(\frac{p}{\Delta_p}-\frac{1}{2}+n\right)-1\right\}$

III. CONCLUSION

In part one it has been shown that the large mass approximation defined in section III which has general validity in classical physics, fails for at least one instance in quantum mechanics. In section V the disparity between the two theories is shown to be quite marked for a system of uncertainty on the order of the measuring devices least count error. Such a large disagreement should result in measurable discrepancies between the two theories, however they have apparently not been observed. Two possible explanations of this are:

1) The proper experiment has not yet been performed.
2) The traditional position operator does not correspond to the actual measurement apparatus used in the laboratory.

In connection with (1) it should be pointed out that measurements on atomic systems generally involve energy differences between states and not position probability distributions.

Part two of this paper is directed at the second possibility. In this part the initial development of alternative position and momentum operators is attempted.

"Symmetry, as wide or as narrow as you may define its meaning, is one idea by which man through the ages has tried to comprehend and create order, beauty, and perfection."

H. WEYL

THE THEORY OF UNIVERSALITY IN THE LEPTON NON-CONSERVING WEAK INTERACTION*

PHILIP KWO-LUNG CHANG

Abstract: A theory for the non-conservation of the leptonic changes in the weak interaction is proposed. The interaction Hamiltonian preserves the current-current coupling form with one weak coupling constant G. The universality is saved and its domain is extended.

The conservation of the leptonic charges in the weak interaction has been studied by numerous experiments both in the nucleus double β decay[1] and in the high energy neutrino reaction.[2] All the experimental results are in favor of the lepton conservation. The weak process which violates the lepton conservation can be, at most, a few percent of the corresponding lepton conserving process. Recently a solar neutrino experiment has shown that the neutrino flux reaching the surface of the earth from the ^8B decay in the sun is unexpectedly smaller than the theoretical prediction[3,4]. Therefore doubts against the strict conservation of the leptonic charges were raised again. Theories have been proposed by Pontecorvo[5] and Gribov[6] in an attempt to describe the lepton non-conservation in the weak interaction. A new mechanism in the weak processes with coupling constant F, characterizing the strength of lepton non-conservation, is suggested. With an approach analogous to the CP violation in K^0 and $\bar{K}^0$ weak decays, it is also suggested that if the neutrino masses are different from zero, there will be oscillations in vacuum between the neutrino states and their charge conjugate states as well as between the *el*-neutrino state and *mu*-neutrino state. In other words, there will be some kinds of eigenstates which are linear combinations of the *el*-neutrino state, *mu*-neutrino state and

* Work supported by Accademia Nazionale dei Lincei and Scuola Normale Superiore, Pisa, Italy.

their charge conjugate partners. The mixing properties in the leptonic system are much more complicated than in the neutral K-meson system. It is because there are more leptonic particles than the neutral K-mesons for one reason, but also because the knowledge about the neutrino masses is so primitive and inconclusive for another. Therefore the diagonal and the off-diagonal leptonic mass matrix elements can be regarded as the free parameters. In the author's opinion, it would be more fruitful to make a theoretical analysis on the neutrino masses with the scheme of mixing leptonic states if the reliable data on all the possible channels of the lepton non-conserving weak processes are available in the future. Apart from the complications in the mixing properties of the neutrino states, there is a "topological inequivalence" between the mixing of the neutrino case and the mixing of the neutral K-meson case. In the $K^0 - \bar{K}^0$ system, the transition is in between the particle state and its antiparticle state which is obtained by a discrete transformation from the former one, namely, a CP-operation. The mixing between the ν_e state and ν_μ state on the other hand, can be pictured as a continuous transformation in the leptonic spin space; i.e. a pure rotation[7].

In order to avoid the unnecessary complication by introducing the new kind of weak F-coupling, and the practical difficulties of the mixing properties in the leptonic system, a theory is proposed as an alternative for the investigation of the lepton non-conservation in weak interaction. This theory is able to describe both the lepton conserving and the lepton non-conserving weak processes with the same universal weak coupling constant G. The phenomenological weak interaction Hamiltonian takes the conventional current-current coupling form, i.e.

$$(1) \qquad H^W_{\text{int}}(x) = \frac{G}{\sqrt{2}} \tfrac{1}{2} [J_\lambda(x) J^+_\lambda(x) + \text{h.c.})$$

where $J_\lambda(x)$ is the weak current which contains the leptonic weak current $I^{(+)}_\lambda(x)$ and the Cabibbo's weak hadronic current $h_\lambda(x)$,

$$(2)\qquad h_\lambda(x) = \cos\vartheta\,\{[j_\lambda^{(1)}(x) + ij_\lambda^{(2)}(x)] + [j_{5\lambda}^{(1)}(x) + ij_{5\lambda}^{(2)}(x)]\} + \sin\vartheta\,\{[j_\lambda^{(4)}(x) + ij_\lambda^{(5)}(x)] + [j_{5\lambda}^{(4)}(x) + ij_{5\lambda}^{(5)}(x)]\},$$

the superscript in the parentheses is the SU(3) index, the subscript 5 stands for the axial vector current and ϑ is the Cabibbo angle.

Similar to the structure of the weak hadronic current $h_\lambda(x)$, we will build up the leptonic current $I_\lambda^{(+)}(x)$ with two pieces, $l_\lambda(x)$ and $l'_\lambda(x)$, i. e.

$$(3)\qquad I_\lambda^{(+)}(x) = \alpha\, l_\lambda(x) + \beta\, l'_\lambda(x),$$

where α and β in general are complex parameters. $l_\lambda(x)$ is the usual lepton conserving weak current,

$$(4)\qquad l_\lambda(x) = i\,[\bar{e}\,\gamma_\lambda\,\tfrac{1}{2}\,(1+\gamma_5)\,\nu_e + \bar{\mu}\,\gamma_\lambda\,\tfrac{1}{2}\,(1+\gamma_5)\,\nu_\mu],$$

and $l'_\lambda(x)$ is the piece that is responsible for the violation of the conservation of the leptonic charges, or the lepton changing weak current,

$$(5)\qquad l'_\lambda(x) = \bar{e}\,\gamma_\lambda\,\tfrac{1}{2}\,(1+\gamma_5)\,\nu_\mu + \bar{\mu}\,\gamma_\lambda\,\tfrac{1}{2}\,(1+\gamma_5)\,\nu_e.$$

If we take the conventional assignment of the leptonic number[8]

$$L_e = \begin{cases} +1 & \text{for} \quad e^- \quad \nu_e \\ -1 & \text{for} \quad e^+ \quad \tilde{\nu}_e \end{cases},$$

and

$$L_\mu = \begin{cases} +1 & \text{for} \quad \mu^- \quad \nu_\mu \\ -1 & \text{for} \quad \mu^+ \quad \tilde{\nu}_\mu \end{cases},$$

where ν_e and ν_μ stand for the anti-*el*-neutrino and anti-*mu*-neutrino respectively, then the first term on the right hand side of eq. (5) is responsible for the weak processes with $\Delta L_e = +1$ and $\Delta L_\mu = -1$, the second term of the eq. (5) is responsible for $\Delta L_e = -1$ and $\Delta L_\mu = +1$.

Let us define another current $I_\lambda^{(-)}(x)$, the hermitian conjugate of the leptonic current in eq. (3), i. e.

$$(6)\qquad I_\lambda^{(-)}(x) = [I_\lambda^{(+)}(x)]^+ = \alpha^*\, l_\lambda^+(x) + \beta^*\, l'^+_\lambda(x),$$

and consider the equal time commutation relation between the time

components of the two currents $I_\lambda^{(+)}(x)$ and $I_\lambda^{(-)}(x)$. With the canonical quantization rules, one finds

$$
\begin{aligned}
(7)\qquad [I_0^{(+)}(\vec{x},t), I_0^{(-)}(\vec{y},t)] = \{&(|\alpha|^2+|\beta|^2)\,[e^+\tfrac{1}{2}(1+\gamma_5)\,e \\
&+\mu^+\tfrac{1}{2}(1+\gamma_5)\,\mu-\nu_e^+\tfrac{1}{2}(1+\gamma_5)\,\nu_e-\nu_\mu^+\tfrac{1}{2}(1+\gamma_5)\,\nu_\mu] \\
&+i(\alpha\beta^*-\alpha^*\beta)\,[e^+\tfrac{1}{2}(1+\gamma_5)\,\mu+\mu^+\tfrac{1}{2}(1+\gamma_5)\,e \\
&-\nu_e^+\tfrac{1}{2}(1+\gamma_5)\,\nu_\mu-\nu_\mu^+\tfrac{1}{2}(1+\gamma_5)\,\nu_e]\}\,\delta(\vec{x}-\vec{y})\,.
\end{aligned}
$$

Let us denote the quantity inside the bracket on the right hand side of eq. (7) by $2I_0^{(0)}(x)$, which is the time component of the neutral leptonic current $I_\lambda^{(0)}(x)$, and consider the commutation relations between $I_0^{(0)}(x)$ and $I_0^{(\pm)}(y)$. One can easily verify that

$$
\begin{aligned}
(8)\qquad [I_0^{(0)}(\vec{x},t),\, I_0^{(+)}(\vec{y},t)] = \{&(|\alpha|^2+|\beta|^2)\,I_0^{(+)} \\
&+i(\alpha\beta^*-\alpha^*\beta)\,(i\alpha l_0'-i\beta l_0)\}\,\delta(\vec{x}-\vec{y})\,,
\end{aligned}
$$

$$
\begin{aligned}
(9)\qquad [I_0^{(0)}(\vec{x},t),\, I_0^{(-)}(\vec{y},t)] = -\{&(|\alpha|^2+|\beta|^2)\,I_0^{(-)} \\
&-i(\alpha\beta^*-\alpha^*\beta)\,(i\alpha^* l_0'^{+}-i\beta^* l_0^+)\}\,\delta(\vec{x}-\vec{y})\,.
\end{aligned}
$$

Examining the commutators in the above two equations, one finds that the Lie algebra of the time components of the leptonic currents $I_\lambda^{(\pm)}(x)$ and $I_\lambda^{(0)}(x)$ closes, and the corresponding charges $L^\pm$ and L^0, defined as the spatial integral of $I_0^{(\pm)}(x)$ and $I_0^{(0)}(x)$ respectively, obey the SU(2) algebra provided that the following two conditions are satisfied.

$$(10)\qquad |\alpha|^2+|\beta|^2=1\,,$$

$$(11)\qquad \alpha\beta^*-\alpha^*\beta=0\,.$$

The solutions of the above two equations can be easily obtained[9],

$$(12)\qquad \alpha=\cos\varphi\,,\qquad \beta=\sin\varphi\,.$$

Therefore the leptonic current which enters the weak interaction Hamiltonian can be written as

$$
\begin{aligned}
(13)\qquad I_\lambda^{(+)}(x) = i\cos\varphi\,&[\bar{e}\gamma_\lambda\tfrac{1}{2}(1+\gamma_5)\,\nu_e+\bar{\mu}\gamma_\lambda\tfrac{1}{2}(1+\gamma_5)\,\nu_\mu] \\
&+\sin\varphi\,(\bar{e}\gamma_\lambda\tfrac{1}{2}(1+\gamma_5)\,\nu_\mu+\bar{\mu}\gamma_\lambda\tfrac{1}{2}(1+\gamma_5)\,\nu_e]\,.
\end{aligned}
$$

The above expression of the leptonic weak current $I_\lambda^{(+)}(x)$ has the similar structure as the weak hadronic current $h_\lambda(x)$. The angle

φ, characterizing the leptonic charges non-conservation, plays the equivalent role as the Cabibbo angle ϑ, which is responsible for the strangeness non-conservation in the strange hadrons weak decay. The value of the angle φ can be determined experimentally whenever more precise data on the lepton non-conservation are available[10].

Assuming that the weak hadronic current contains no field derivatives, the lepton field operators commute with the hadron field operators. Hence the spatial integral of the time component of the total weak interaction currents, i. e.

$$W^+ = \int J_0(x)\, d^3\vec{x},$$

$$W^- = \int J_0^+(x)\, d^3\vec{x} = (W^+)^+$$

together with $W^0 = \frac{1}{2}[W^+, W^-]$ also satisfy the SU(2) algebra. The same weak coupling constant G appearing in the weak interaction Hamiltonian enables us to extend the validity of the universality of weak interaction, which we are so reluctant to give up, to the domain of the lepton non-conserving weak processes.

The similarity between the leptonic weak current and hadronic weak current reminds us of a previous investigation in the internal symmetries of the hadrons and leptons by Radicati[11]. If we give up the two components neutrino theory, and combine the *el*-neutrino and anti-*mu*-neutrino as a four components Dirac field[7]; then the leptonic system will only involve three Dirac fields. The relations between the three leptonic Dirac fields in the leptonic system and the three quark fields in the hadronic system is now under investigation.

This work was stimulated by a conversation with Professor Radicati who informed the author about the recent solar neutrino experiment showing a possible violation of the lepton conservation. The author would like to thank Professor Radicati for the useful discussion and for the hospitality extended to him during his stay in Pisa. The conversation with Dr. Pham Tri Nang is also appreciated.

REFERENCES

(1) B. P. LAZARENKO and S. YU. LIKANOV: *Zurn. Exp. Teor.*, Fiz., **49**, 751 (1965).
E. DER MATEOSIAN and M. GOLDHABER: *Phys. Rev.*, **146**, 810 (1966).
R. K. BARDIN, P. J. GOLLON, J. D. ULLMAN and C. S. WU: *Phys. Letters* **26B**, 112 (1967).
The earlier data can be found in the review papers by H. Primakoff and S. P. Rosen: *Rept. Progr. Phys.*, **22**, 121 (1969); *Proc. Phys. Soc.* (London), **18**, 464 (1961).
α, β and γ-ray spectroscopy, P. 1449 (North-Holland, Amsterdam, 1965).

(2) R. DAVIS: *Int. Conf. on Radioisotopes in Scientific Research* (Paris, 1957).
J. K. BIENLEIN, A. BÖHM, G. VON DARDEL, H. FAISSNER, F. FERRERO, J. M. BAILLARD, H. J. GERBER, B. HAHN, V. KAFTANOV, F. KRIENNEN, M. REIHARZ, R. A. SALMERON, P. G. SEILER, A. STAUDE, J. STEIN and H. J. STEINER: *Phys. Letters*, **13**, 80 (1964).
M. BARDON, P. NORTON, J. PEOPLES, A. SACHS and J. LEE-FRANZINI: *Phys. Rev. Letters*, **14**, 449 (1965).
G. BERNARDINI: *Int. Conf. on High Energy Physics* (Dubna, 1964).

(3) R. DAVIS, D. HARMER and K. HOFFMAN: *Phys. Rev. Letters*, **20**, 1205 (1868).

(4) W. FOWLER: *Astrophys. J.*, **127**, 551 (1958).
J. N. BAHCALL, W. FOWLER, I. IBEN and R. SEARS: *Astrophys. J.*, **137**, 344 (1963).
J. N. BAHCALL, N. A. BAHCALL and R. K. ULRICH: *Astrophys. J.*, **156**, 599 (1969).

(5) B. PONTECORVO: *Soviet Physics JETP*, **26**, 984 (1968).
B. PONTECORVO: *Old and New Problems in Elementary Particles*, p. 251 (Academic Press, New York, 1968).

(6) V. GRIBOV and B. PONTECORVO: *Phys. Letters*, **28B**, 493 (1969).

(7) G. FEINBERG and F. GÜRSEY: *Phys. Rev.*, **128**, 378 (1962).

(8) A weaker assignment of the leptonic number is also possible.
G. FEINBERG and S. WEINBERG: *Phys. Rev.*, **123**, 439 (1961).

(9) The general solution allows α and β to have a common phase factor. It is put to zero without loss of generality.

(10) Sin $\varphi \simeq \varphi \sim F/G \sim 10^{-3}$ according to the present experimental data.

(11) L. A. RADICATI: *Strong and Weak Interaction-Present Problems*, p. 129 (Academic Press, New York, 1966).

THE ISOBARIC SPIN IN NUCLEAR STRIPPING REACTIONS

G. BREUER

Abstract

In this review article some data are collected as evidence for the conservation of isobaric spin in direct nuclear stripping reactions and its influence upon the absolute cross section.

§1. THE CONCEPT OF ISOBARIC SPIN

There are strong reasons to assume that protons and neutrons are two possible states of an elementary particle called a "nucleon". The physical facts which support this assumption are:

The masses of the proton and neutron are approximately the same. The spins of both particles are equal. The free neutron converts to a proton by β-decay:

$$n \rightarrow p + e^- + \bar{\nu} + 0.755 \text{ MeV}$$

The transmutation of protons into neutrons and neutrons into protons in nuclear reactions and in nucleon-nucleon interaction:

$$n + p \rightarrow p + n + \pi^+$$
$$p + n \rightarrow p + p + \pi^-,$$

and the charge exchange reactions in which a proton collides with a stationary neutron and exchanges charge with it, leaving an almost stationary proton and a fast moving neutron, and vice versa:

$$p + n \rightarrow n' + p'$$
$$n + p \rightarrow p' + n'.$$

The analysis of (p,p), (p,n), and (n,n) scattering experiments leads to the conclusion that the $n-n$, $n-p$, and $p-p$ internucleon forces are approximately the same. This is usually expressed as the "charge independence" of nuclear forces. If one imposes the weaker condition of equal $n-n$ and $p-p$ forces only, the forces are called

"charge symmetric". Another fact indicating the charge independence of nuclear forces is the existence of multiplets of nuclear energy states among the level systems of stable nuclei, as will be described in the following.

Usually the isobaric spin (abbreviated "i-spin") will be introduced as analogous to the ordinary spin of a particle. For a spin 1/2 particle, the component of the spin in a specified direction takes two possible values $+1/2$, $-1/2$, which are the eigenvalues of the third component of the spin operator $\vec{s}=\{\sigma_x, \sigma_y, \sigma_z\}$, where the σ's denote the well known Pauli spin-matrices.

Similarly the charge state of a nucleon will be described as the eigenvalue t_z of the third component of the i-spin operator $\vec{t}=\{\tau_x, \tau_y, \tau_z\}$ the components of which are represented as quite analogous to the spin operator by the Pauli-matrices

$$\tau_x=\frac{1}{2}\begin{pmatrix}0 & 1\\ 1 & 0\end{pmatrix}, \quad \tau_y=\frac{1}{2}\begin{pmatrix}0 & -i\\ i & 0\end{pmatrix}, \quad \tau_z=\frac{1}{2}\begin{pmatrix}1 & 0\\ 0 & -1\end{pmatrix}$$

The wave functions of the neutron and proton with eigenvalue $+1/2$ and $-1/2$ of the operator $\vec{t}$ are represented by the two-component vectors

$$x_+=\begin{pmatrix}1\\ 0\end{pmatrix} \qquad x_-=\begin{pmatrix}0\\ 1\end{pmatrix}$$

for neutron and proton respectively.

The three operators τ_x, τ_y, τ_z are considered to be the three components of the i-spin vector $\vec{t}$ in an hypothetical isobaric spin space. They satisfy the commutation relations $[\tau_i\tau_j]=i\tau_k$, (the indices $i,j,k=1,2,3$ replacing x,y,z in cyclic permutation). This corresponds to the relations satisfied by the three components of the angular momentum. Therefore the i-spin theory follows the same formalism as that of the angular momentum. For a nucleus with A nucleons the total i-spin is given by $\vec{T}=\sum_{i=1}^{A}\vec{t}_i$. The components of $\vec{T}$ satisfy the same commutation relation mentioned before. The eigenvalues of $\vec{T}^2$ are found to be $T(T+1)$, where T can assume the value zero or a positive half-integer or integer. The eigenvalues T_3 associated with an eigenstate of $\vec{T}^2$ are the components of an isobaric

spin multiplet. For a given eigenstate of $\vec{T}^2$ the eigenvalues of T_3 are T, $T-1$, ... $-T+1$, $-T$. These values have a direct significance. For if N is the number of neutrons, and Z is the number of protons, the eigenvalue of T_3 of the total nucleon system is $\frac{1}{2}(N-Z)$.

Considering a quantum-mechanical system of protons and neutrons the Pauli principle has to be applied to the total set of quantum numbers for each particle including the new quantum number of i-spin. This means that, regardles of i-spin, the Pauli principle in its conventional form has to be applied to neutrons and protons separately. In the following we will see in which way the energy level system of a nucleus containing four nucleons can in principle be constructed while taking into account the generalized Pauli principle. (See Schintlmeister[1]).

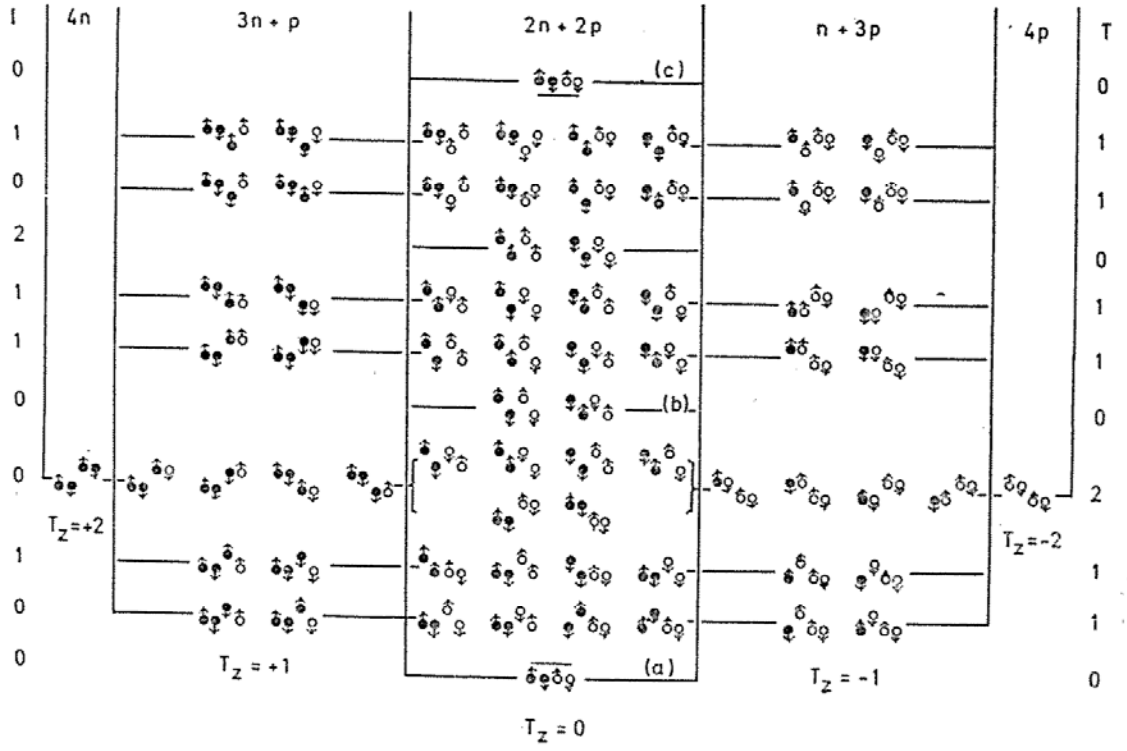

Fig. 1. Distribution of four nucleons over two levels (after Schintlmeister[1])

Fig. 1 represents a schematic diagram of the possible configurations of four nucleons distributed over two levels. The columns headed by $4p$, $3p+n$, etc. distinguish the cases of nuclei made up of 4 protons, 3 protons and one neutron, etc. The protons and neutrons

are designated by open and full circles respectively. The spin states (up and down) are indicated by arrows.

First we consider four identical particles which can be distributed over two levels. The only possible distribution is that with two particles in the lower state and two particles in the upper state. In each of these states the two particles differ by the z-components of their spin.

Also indicated in the first column of the diagram is the total spin I of each configuration. In the latter case the individual spins add up to $I=0$. The T_z value is $+2$ for $4n$ and -2 for $4p$ and, because $T_z \leqq T$, we have $T=2$.

Next we consider the four-nucleon systems $3p-n$ and $3n+p$. The possible configurations are found in the corresponding columns. Obviously, the group of levels with 3 nucleons in the lower state and 1 nucleon in the upper state is energetically lower than that with 2 nucleons in each of both states, and the group of levels with 3 nucleons in the upper state and 1 nucleon in the lower state is energetically higher. Each of these level groups consists of two different kinds: One kind has spin 0, the other kind has spin 1. In the construction of the level scheme it has always been assumed that levels with spin-saturated nucleons are energetically lower than those with unsaturated spins. Altogether we find 7 different energy states for the systems $3p+n$, $3n+p$. In quite a similar way the level system for the $2n+2p$ system can be found. It has many more possible nucleon configurations, some of them corresponding to the levels of the $3p+n$ system. But besides these levels there occur three new types of configuration: (i) Four nucleons in one level, with total spin $I=0$ and $T=0$. (ii) One level with $I=2$, and $T=0$. (iii) One level with $I=0$ and $T=0$. In Fig. 1 these three levels are labeled with a, b, c respectively. We see that level (a) is lower than the lowest one of the neighbouring $T_z=\pm 1$ level systems. The level diagram described so far corresponds to nuclei with a total number of 4 nucleons. This consideration can similarly be extended to a set of nuclei with a total number of more than 4 nucleons, without changing the main features:

i) Under the assumption of charge-independent nuclear forces we expect that isobaric nuclei have similar energy states, that means levels having the same energy, the same spin I, and the same i-spin T, but corresponding to different values of T_z. Levels of this kind are said to form an "i-spin multiplet".

ii) The lowest energy state (ground state) of a T_z-nucleus has lower energy than the ground states of the $\pm(|T_z|+1)$ nuclei.

iii) From ii) it follows that the ground state with the lowest energy is formed by the $T_z = 0$ nucleus, that is the nucleus which has an equal number ot protons and neutrons (self-conjugate).

In the example discussed above it is easily verified that the multiplicity of a configuration with i-spin T is $2T+1$, where $T<2$. The level diagram described so far concerns the ideal case, neglecting any distortion effects. Actually however, the effect of coulomb forces and the proton-neutron mass difference must be taken into account. The effect of the latter is to lower the energy of the levels as T_z is increased. The effect of the Coulomb forces is just opposite; they lift up the levels to higher energy as T_z is increased. (For $N+Z>4$ the effect of Coulomb forces is larger than the mass effect). In fact, the level diagrams of isobaric nuclei are no longer symmetric as in the schematic diagram of Fig. 1, but are found to be unsymmetric with respect to the nucleus with $T_z=0$. Fig. 2 shows a typical example.

It is possible to account for the disturbing effects quantitatively, because the level shift due to Coulomb- and mass-effects are calculable. (See, e. g. Preston[3], or Meyerhof[4]). Of course, a precise calculation of the Coulomb energy due to the repulsive electrostatic forces between the protons within the nucleus requires the knowledge of the wave functions of the protons. But fortunately a rather good result can be obtained by a classical model. Under the assumption of a uniform charge distribution over a spherical shaped nucleus of radius R the electrostatic potential is

$$E_c = \frac{3}{5} \frac{Z^2 e^2}{R}$$

But this expression still contains the "self-energy" $\frac{3}{5}\frac{e^2}{R}$ for each proton (setting $Z=1$ in the above formula). Subtraction of this term yields for the mutual electrostatic interaction energy between all pairs of protons

$$E_c = 0.6\frac{Z(Z-1)}{A^{1/3}}\cdot e^2 \text{ (MeV)}$$

The level diagrams shown later in this article are corrected for both Coulomb- and mass effects.

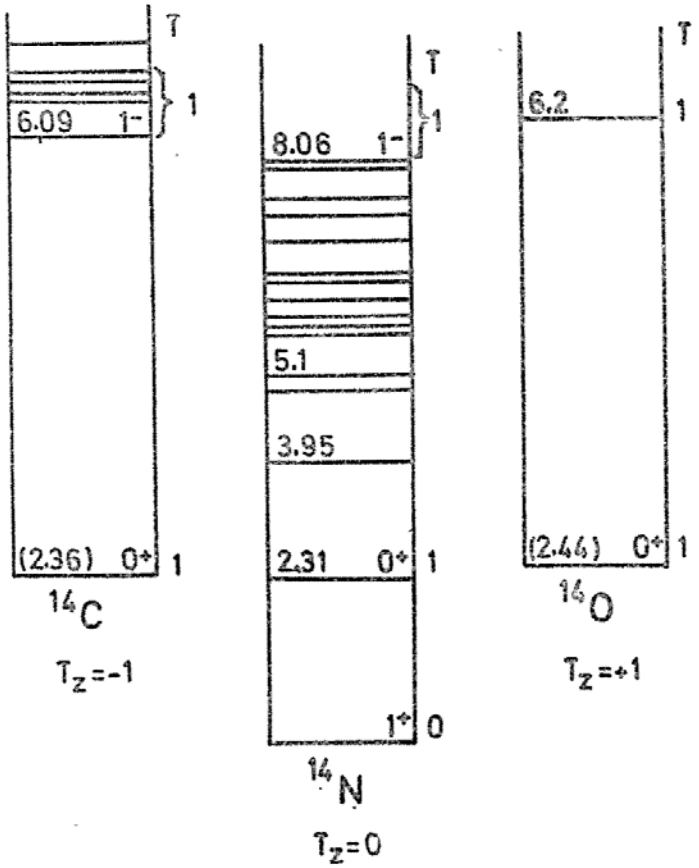

Fig. 2. Level diagram of the i-spin triplet of mass number $N+Z=14$ (From Ajzenberg-Selove and Lauritsen[2])

§2. ISOBARIC SPIN SELECTION RULES IN NUCLEAR REACTIONS

We know that the nuclear spin can be considered a good quantum number. But this is not equally true for the orbital angular momentum, because nuclear forces are not pure central forces. As an illustration we consider the ground state of the deuteron with $I=1$,

which contains wave functions with $l=0$ and $l=2$. Therefore, this state is made up of the two states $^3S_1$ and $^3D_1$, the latter of which makes a contribution of 4%. In a nuclear reaction the total spin of the interacting particles is conserved, which is expressed by the spin selection rules.

For interacting particles A, x with spin I_A, i_x, and mutual orbital angular momentum l, the total spin I of the whole system is given by the vector addition

$$\vec{I}_A+\vec{i}_x+\vec{l}=\vec{I}$$

This can also be written with the so called "triangle relation" (I_A, s, l), where $\vec{s}=\vec{I}_A+\vec{i}_x$ is the channel spin, which means the relation $|s-l|\leqq I\leqq s+l$ and two similar relations permutating s, l and I. If the colliding particles form a compound nucleus C, then the total spin I equals the spin I_c of the compound nucleus, otherwise I has only formal significance, defined by the equation of vector addition. In the following we consider a nuclear reaction $A(x,y)B$. Here the spin selection rule applies equally to the final stage of the reaction with interacting particles B, y.

Quite analogous selection rules are valid for the i-spin. With i-spin quantum numbers T_1, T_2, T_1', T_2', T for the particles A, x, B, y, C respectively, the i-spin conservation is expressed by the relations (T_1, T_2, T) and (T_1', T_2', T) or by the vector equation

$$\vec{T}_1+\vec{T}_2=\vec{T}_1'+\vec{T}_2'$$

This holds as far as nuclear forces are charge-independent. In this case the i-spin of each nuclear state is uniquely defined.

However, the Coulomb interaction cannot be neglected, as it makes the nuclear potential unsymmetric with respect to protons and neutrons. The Coulomb interaction vanishes except in the case of $p-p$ interaction.

This asymmetry of nucleon potential violates the condition that the i-spin T is a good quantum number. In terms of isobaric spin notation the Coulomb interaction may be written as

$$H_c=e^2\sum_{i<j}\left(\frac{1}{2}-\tau_{3i}\right)\left(\frac{1}{2}-\tau_{3i}\right)r_{ij}^{-1}$$

This can be decomposed into three terms $C=T^{(0)}+T^{(1)}+T^{(2)}$

where

$$T^{(0)}=e^2\sum_{i<j}\left(\frac{1}{4}+\frac{1}{3}\vec{t}_i\cdot\vec{t}_j\right)r_{ij}^{-1}$$

$$T^{(1)}=-\frac{1}{2}e^2\sum_{i<j}(t_{3i}+t_{3j})r_{ij}^{-1}$$

$$T^{(2)}=e\sum_{i<j}(t_{3i}+t_{3j}-\frac{1}{3}\vec{t}_i\cdot\vec{t}_j)r_{ij}^{-1}$$

The first term is an isobaric spin scalar and commutes with $\vec{T}^2$. It can be included in the nuclear Hamiltonian. $T^{(1)}+T^{(2)}$ does not commute with $\vec{T}^2$. It is that part of H_c which produces a mixing of different i-spin states in H_c, that is to mix into a state with i-spin T and amplitude $\alpha(T')$ of a state which has the same other quantum numbers (spin and parity) but different i-spin T'. From perturbation theory we have

$$\psi_0=\sum_\nu\alpha_\nu(T')\,|a_\nu,T>$$

where $\alpha_\nu(T')=<a_\nu,T'|H_c|a_0,T>\cdot(E_0-E)^{-1}$, and a_ν are the quantum numbers beside T, T', specifying the state ψ_0. $|\alpha_\nu(T')|^2$ is the probability of the occurrence of the state $|a_\nu,T'>$ within the actual state ψ_0.

Radicati[5] has made a theoretical estimate of mixing amplitudes for two or four nucleons outside the closed shells. McDonald[6] showed that contribution of impurity from states described by excitations of closed shell nucleons is still greater, and that the total impurity $|\alpha_\nu(T')|^2$ of a nuclear ground state is proportional to the number $\frac{1}{2}A(A-1)$ of interacting pairs. From the jj coupling shell model the total i-spin impurities of ground states are calculated to be 10^{-5} for ^{4}He, 10^{-3} for ^{12}C, and 10^{-2} for ^{34}Cl. The order of magnitude of these values is expected to be the same for low lying excited states. Experimental evidence for non-conservation of i-spin in nuclear reactions is mainly gained from (d,α) reactions, e. g. the $^{16}O(d,x)^{14}N$ reaction investigated by Brown[7]. The yield functions for the different transitions leaving ^{14}N in various excited states have been measured. The transition leading to the 0^+, $T=1$ first excited state of ^{14}N at 2.13 MeV is forbidden by the i-spin selection rule because the ground states of ^{16}O, deuteron and α-particle are all $T=0$

states. But nevertheless the cross section of this reaction is different from zero (although only a few percent of the allowed ground state reaction). Therefore there must be an i-spin impurity in the final state or in the excited states of the compound nucleus, provided the reaction proceeds in that way. Similar investigations are found in other papers[8-11].

The *i*-spin impurity increases with increasing mass number and with increasing excitation energy. This becomes most serious for the high excited states of a compound nucleus, where the excitation energy is in a region of closely spaced energy levels. The Coulomb energy may then be strong enough to mix the *i*-spins of neighboring levels. In this case we see *i*-spin conservation to be violated although in the initial system the particles have pure *i*-spin states.

Lane and Thomas[2] have considered the conditions under which *i*-spin conservation in nuclear reactions may be expected to be valid. A compound nucleus being formed, it depends upon its structure. The level structure of a compound nucleus can be characterized by the following quantities:

i) The average level spacing $<D^I>$ between states of equal spin I and parity.
ii) The average total width of these levels $<T^I>$.
iii) The average matrix element $<H_c>$ of the Coulomb forces between such states.

One may think of the following conditions for *i*-spin conservation:

(A) The "static" condition $<H_c> \ll <D^I>$ means that the Coulomb forces are considered too weak to mix the *i*-spins of neighboring states appreciably.

(B) The "dynamic" condition $<H_c> \ll <T^I>$ was first formulated by Morinaga[13]. In order to understand this condition, we consider the time of Coulomb interaction, whose order of magnitude is given by $\hbar/<H_c>$. The lifetime of a typical compound nucleus state is given by $\hbar/<T^I>$. If now the former one is much smaller than the latter, then there is not enough time for the Coulomb forces to act, and therefore the *i*-spin of the initial stage system will be conserved. In the limit of very small interaction times we get just the time required for the incident

particle x to pass the dimension of the target nucleus A. (This time is about 10^{-22} sec, but the lifetime of a compound nucleus is of the order 10^{-16} to 10^{-19} sec). In this case we are dealing with a "direct" nuclear reaction in which the nucleons within the particles A and x interact directly. These types of reactions are well known as "knock out"-, "stripping"- and "pick up"-reactions. They are characterized as two-step processes, not proceeding via an intermediate stage of a compound nucleus. It is clear then, that in this kind of reactions the i-spin should be expected to be conserved as long as i-spin purity is assured in the initial and final states.

§3. CROSS SECTIONS OF CHARGE-SYMMETRIC DIRECT NUCLEAR REACTIONS

In order to investigate the i-spin conservation in direct nuclear reactions we consider especially those reactions whose initial and final state particles are charge symmetric and for which the final state transitions lead to residual states which are members of an i-spin multiplet. The situation is illustrated in the schematic diagram of Fig. 3.

The reactions shown are of the type $A(x,y)B(T_z)$ and $A(x,y)B'(T_z+1)$, with at least one of the particles A, x being selfconjugate. Under this condition the i-spin in each stage of the reaction is uniquely defined. The matrix element of each transition is completely determined by wave functions of the initial and final state. In our case we compare the transitions indicated by y_0 and y_0', y_1 and y_1' etc. The corresponding residual states E_0 and E_0', E_1 and E_1' etc. of $B(T_z)$ and $B'(T_z+1)$, being isobaric analogue states, do have the same configuration (and therefore the same wave functions). This is also true for the initial states (the ground states of A and x) the wave functions of which are the same in both reactions. Thus the cross sections of both reactions differ from each other solely by the i-spin coupling coefficients C which are uniquely defined under the preassumptions stated above. The cross section for the nuclear transition $\alpha \rightarrow \beta$ can be written as

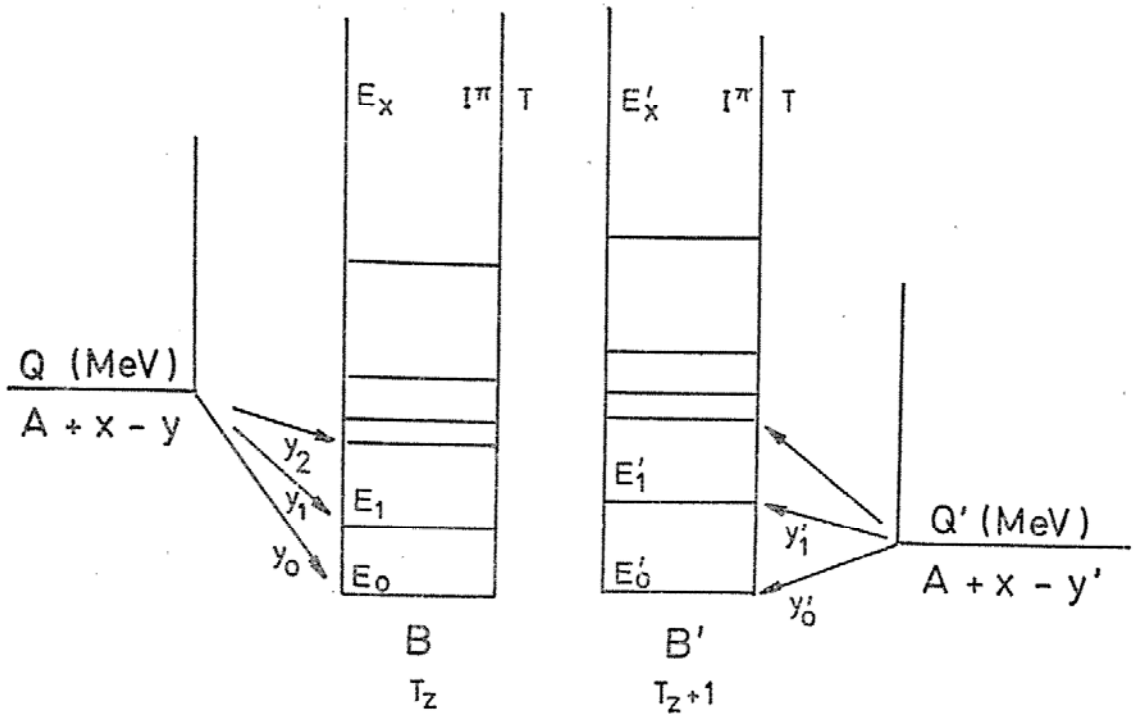

Fig. 3. Schematic level diagram for the reactions $A(x, y)B$ and $A(x, y')B'$ leading to the isobaric analogue states of B and B'.
Denoting the transfered particles by $(x-y)$ and $(x-y')$, their i-spin quantum numbers by T_1, T_{1z} and T'_1, T'_{1z}, it is assumed that $T'_{1z}-T_{1z}=1$. Then, also $T'_z-T_z=1$ for the residual states. This applies to reactions of the type (x, n), (x, p) and $(x, {}^3\mathrm{He})$, $(x, {}^3\mathrm{H})$, where x stands for any kind of incident particle like p, d, ^{3}He, etc.

$$\sigma_{\alpha\beta}=\sum_{l,j}<T_0T_{0z}T_1T_{1z}|T_0T_1TT_z>^2\cdot g|A_{\alpha\beta}|^2\cdot\theta^2_{\alpha\beta} \tag{1}$$

where α, β indicate the quantum numbers beside T, T_z which are needed to characterize the transitions. The quantity $\theta^2_{\alpha\beta}$ denotes the reduced width of a single particle, g is the statistical spin factor, and $A_{\alpha\beta}$ contains all information concerning the nuclear structure and the geometry of the reaction mechanism. (See[14]).

The i-spin coupling coefficients are the well known Clebsch-Gordan coefficients (see e. g. Condon and Shortley[15]). Let us denote by $(x-y)$, $(x-y')$ the nucleon (or nucleons) transferred to or taken from the target nucleus. Let T_0, T_{0z} be the i-spin and its third component of the target nucleus ground state, T_1, T_{1z} and T'_1, T'_{1z} be the corresponding quantum numbers for the particles $(x-y)$, $(x-y')$ respectively. Then we have the selection rules

$$(T_0,\ T_1,\ T), \qquad T_{0z}+T_{1z}=T_z,$$

$$(T_0,\ T_1',\ T), \qquad T_{0z}+T_{1z}'=T_z'$$

where T, T_z and T, T_z' are the quantum numbers of the isobaric analogue states of the residual nuclei B and B'.

In the case of a (d,n)- and (d,p) reaction we have

$$C^2=<T_0T_{0z},\ \frac{1}{2},\ -\frac{1}{2}|T_0\frac{1}{2}T_0+\frac{1}{2},\ T_{0z}-\frac{1}{2}>^2=\frac{T_0-T_z+\frac{1}{2}}{2T_0+1}$$

$$C'^2=<T_0T_{0z},\ \frac{1}{2},\ +\frac{1}{2}|T_0\frac{1}{2}T_0+\frac{1}{2},\ T_{0z}+\frac{1}{2}>^2=\frac{T_0+T_z'+\frac{1}{2}}{2T_0+1}$$

where $T_z=T_{0z}-\frac{1}{2}$ for a (d,n) reaction, and $T_z'=T_{0z}+\frac{1}{2}$ for a (d,p) reaction.

But it is $T_{0z}=T_0$ for the ground state of A, and therefore we get

$$\left|\frac{C}{C'}\right|^2=(2T_0+1)^{-1} \tag{2}$$

In the case of a direct reaction leading to a well defined shell model residual state, only one of the terms of the sum in equation (1) occurs and $|A_{\alpha\beta}|^2$ may be factorized in the usual way as

$$|A_{\alpha\beta}|^2=S_{\alpha\beta}\cdot\sigma^*_{\alpha\beta} \tag{3}$$

where $S_{\alpha\beta}$ is the spectroscopic factor which in the case of a stripping reaction is related to the particle capture into the state β. Comparing the cross sections of transitions leading to isobaric analogue states with T_z and T_z' we write for the branching ratio

$$q(y,y')=\frac{\sigma_{\alpha\beta}(T,T_z)}{\sigma_{\alpha\beta'}(T,T_z')}=\left|\frac{<T_0T_{0z}T_1T_{1z}|T_0T_1TT_z>}{<T_0T_{0z}T_1T_{1z}'|T_0T_1TT_z'>}\right|^2\cdot\frac{\sigma^*_{\alpha\beta}}{\sigma^*_{\alpha\beta'}}\cdot\frac{S_{\alpha\beta}}{S_{\alpha\beta'}}\cdot\frac{\theta^2_{\alpha\beta}}{\theta^2_{\alpha\beta'}}. \tag{4}$$

σ^* can be calculated from a reaction model and, in case of a stripping reaction, is the cross section obtained by the plane wave Born approximation or better the distorted wave Born approximation (DWBA). β, β' indicate the analogue states. For these states the spectroscopic factors as well as the reduced widths of single particles are expected to be equal and, canceling in equation (4) we get

$$q(y, y') = \left|\frac{C}{C'}\right|^2 \cdot \frac{\sigma^*_{\alpha\beta}}{\sigma^*_{\alpha\beta'}} \tag{5}$$

where C, C' are abbreviations for the i-spin coupling coefficients. The value of $q(y, y')$ predicted by this expression can be compared with experimental data.

A second way of investigation of charge symmetry in nuclear reactions is to consider the ratio of cross sections $q(y_i, y_k)$ with $i>k$, (where we have transitions to two different excited states of the same residual nucleus $B(T_z)$) and $q(y'_i, y'_k)$ which is the cross section ratio for the transitions to the corresponding isobaric analogue states. By similar arguments as before we expect

$$q(y_i, y_k) = q(y'_i, y'_k) \tag{6}$$

This can easily be tested by experiments measuring the particle yield functions of the corresponding reactions and comparing the relative intensity of the different particle groups. Instead of this, one can measure also the relative intensities of the deexciting γ-rays from the excited states of the residual nucleus.

The branching ratio $q(y_i, y_k)$ is obviously not very much affected by the disturbing Coulomb interaction because for transitions to residual states of the same T_z the cross sections will be affected to nearly the same extent and therefore in the cross section ratio the Coulomb effects are expected to cancel.

On the other side, this is not so in the predicted cross section ratio $q(y, y')$ of equation (5), because the Coulomb effects are different for the transitions β, β'. Equation (5) may be considered a good approximation only as far as the Coulomb effects are taken into account by the theoretical cross section σ^*. Obviously, besides the kinetic factor, also σ^* depends on the reaction mechanism and may differ appreciably for different reaction models. In the case of stripping type reactions, PWBA calculations fail in many cases to predict the experimental results correctly, as will be shown later.

A third evidence of charge symmetry in nuclear reactions is offered by comparing the angular distributions of the corresponding reactions. The cross section ratios of these reactions have been

considered in equation (4). The angular distribution is determined by the reaction mechanism which itself depends on the kind of reacting particles, the energy of the incident particle, the Q-value of the reaction and on the nuclear structure of the residual states. As pointed out above, the structure of isobaric analogue states is the same and therefore, provided the Q-values do not differ too much, the angular distribution of the reactions considered should have similar shapes.

§4. COMPARISON WITH EXPERIMENTAL DATA

In the following, some experimental date are selected in order to prove the agreement with the theoretical predictions. The number of examples could be enlarged but, as the present article is not intended to make a systematic study on this subject, the results represented here may suffice.

1) The reactions ^{6}Li$(d,n)^7$Be and ^{6}Li$(d,p)^7$Li. (see Fig. 4a-c)

Cross sections and angular distributions of these reactions have been measured by Birk et al.[16] and by Cranberg et al[17] for incident

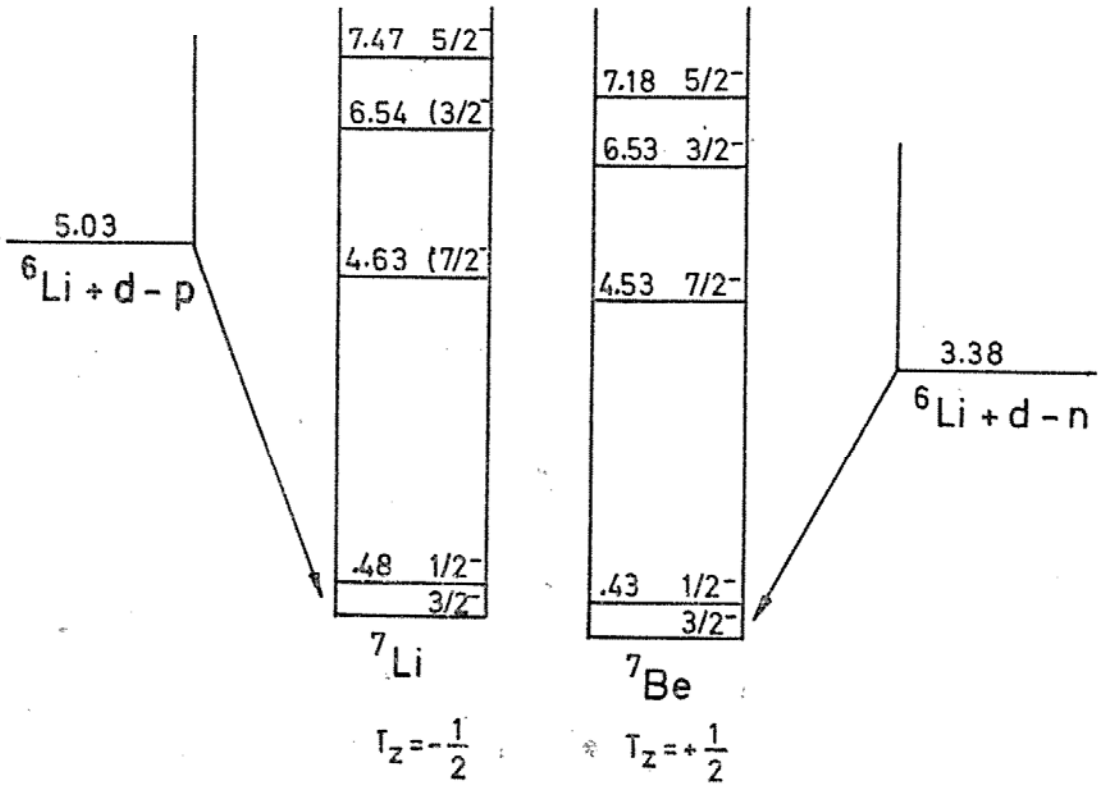

Fig. 4. The reactions ^{6}Li$(d,n)^7$Be(0) and ^{6}Li$(d,p)^7$Li(0)
a) Level diagram

deuteron energies between 0.4 and 3.2 MeV. The ratios of integrated cross sections $q(p_1, p_0)$ and $q(n_1, n_0)$ are plotted in Fig. 4b for comparison and show excellent agreement. The increase of q with decreasing incident deuteron energy is to be explained by a change in the reaction mechanism. The angular distributions of both particle groups in each reaction are displayed in Fig. 4c on an arbitrary scale for visual comparison. The similarity is evident.

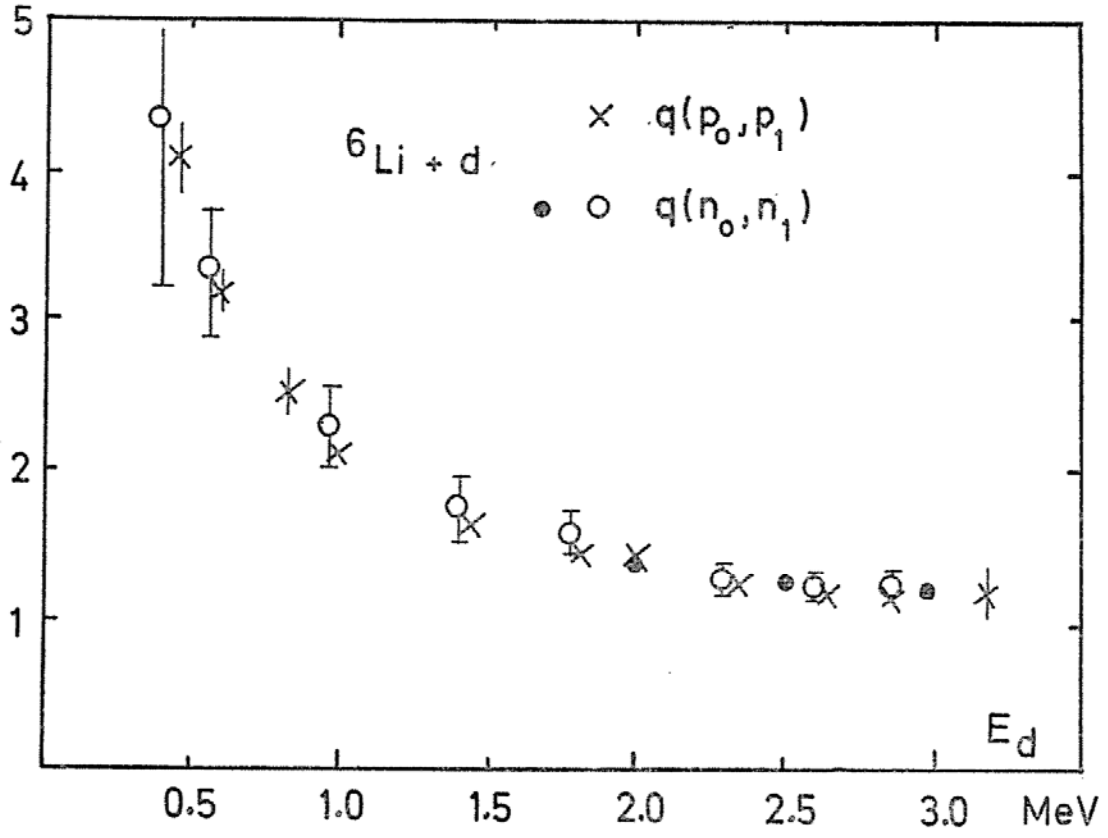

Fig. 4. b) Cross section ratios $q(p_1, p_0)$ and $q(n_1, n_0)$

The authors also give the cross section ratios $q(p_0, n_0)$ and $q(p_1, n_1)$. The ratio of i-spin coupling coefficients in this reaction is $|C/C'|^2=1$ since the target nucleus has $T_0=0$ (see equation (2)). The values of q measured are indeed approximately=1 within the experimental error (see Table I). The large errors are mainly due to the unknown target thickness in both the (d, p)- and (d, n)-experiments which have been performed separately. The indicated values of q are not corrected for Coulomb- or phase-space-effects.

2) The reactions $^{10}B(d, n)^{11}C$ and $^{10}B(d, p)^{11}B$. (see Fig. 5a-c)

Cross sections and angular distributions for the particle groups

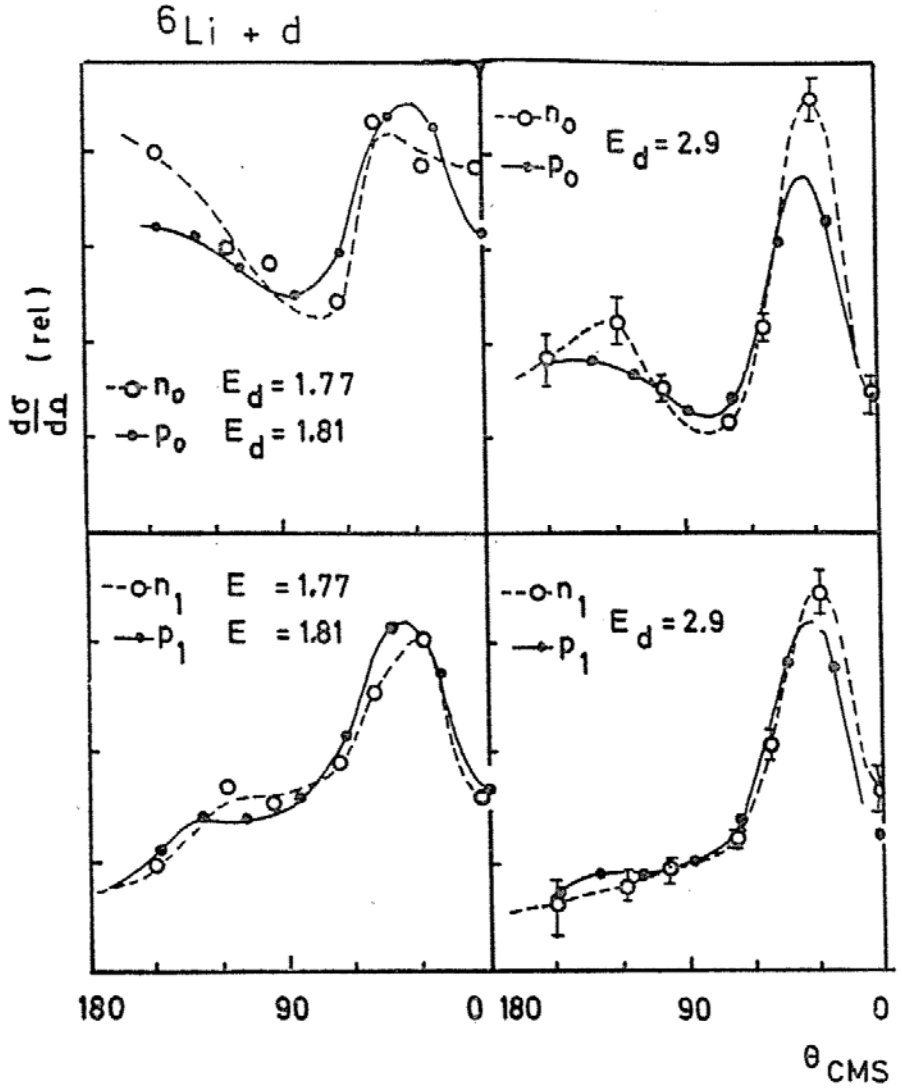

Fig. 4. c) Angular distributions of the particle groups p_0, p_1, n_0, n_1 Measurements are from Birk et al.[16] and Cranberg et al.[17]

Table I

E_d (MeV)	$q(p_0, n_0)$	$q(p_1, n_1)$
0.56	1.00±0.25	1.05±0.25
0.96	0.78±0.2	0.83±0.2
1.38	1.23±0.2	1.25±0.2
1.77	1.35±0.35	1.45±0.45
2.28	1.20±0.25	1.21±0.25
2.58	1.15±0.25	1.21±0.25
2.90	0.93±0.15	1.00±0.15

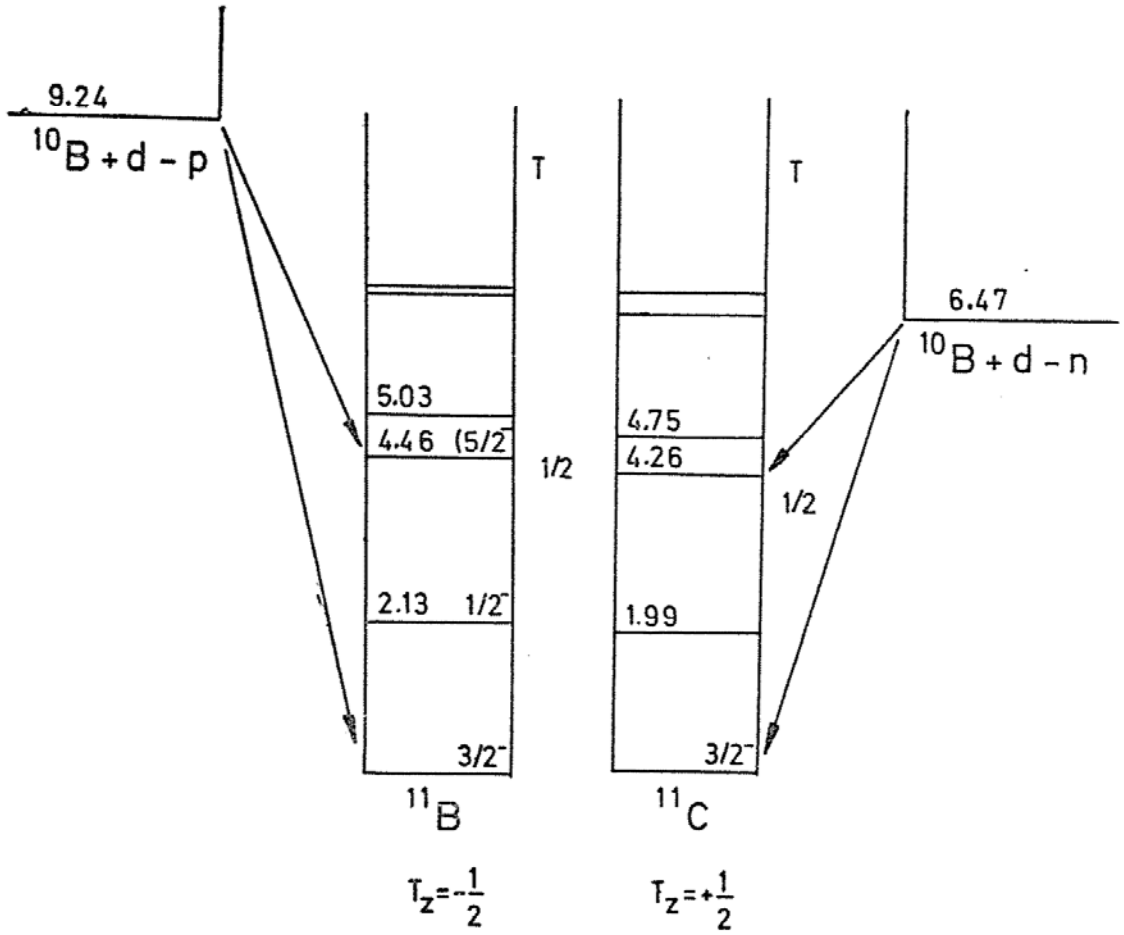

Fig. 5. The reactions $^{10}B(d,n)^{11}C$ and $^{10}B(d,p)^{11}B$
a) Level diagram

p_0, p_2, p_3 have been measured by Breuer[18] for incident deuteron energies E_d=1.4 to 3.3 MeV. These data can be compared with the corresponding measurements of the (d,n)-reaction made by Siemssen[19].

Fig. 5b shows some curves of the angular distribution for the particle groups p_0, n_0 and p_2, n_2 for several deuteron energies. In Fig. 5c a comparison is made for the cross section ratios $q(p_2,p_0)$ and $q(n_2,n_0)$ depending on the deuteron energy. The agreement may be considered sufficient, but could be better. The large errors are caused by poor counting statistics and error of neutron counter efficiency. Recently, high precision measurements of the cross section ratio $q(n_0,p_0)$ have been performed by Breuer[20]. In this experiment the proton- and neutron yield has been detected simultaneously from the same target. A neutron detector of the proton-recoil type was specially designed with a neutron efficiency accurate within 2%. The

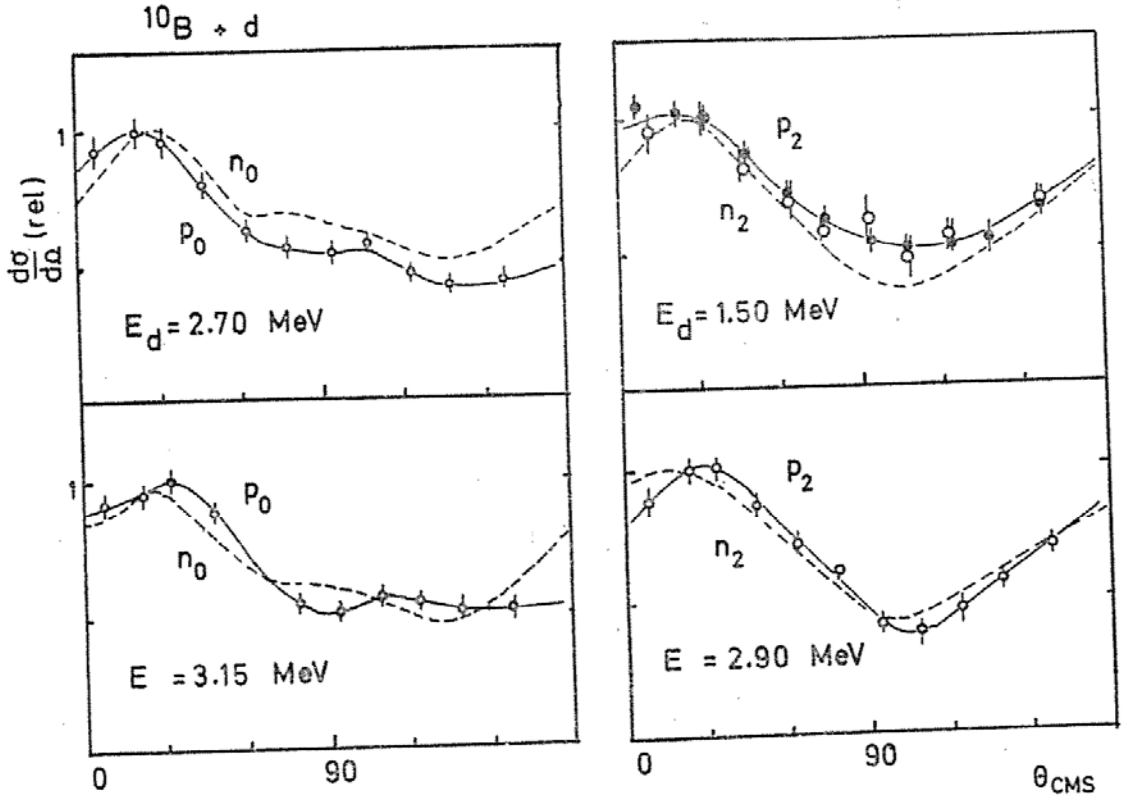

Fig. 5. b) Angular distributions of the particle group p_0, n_0, p_2, n_2 The points indicate the (d, p) measurements from Breuer[18]. The dotted curves represent the average experimental results of the (d, n) measurements from Siemssen et al.[19].

result is very satisfactory and agreement with the theoretical predictions is obtained.

3) The reactions $^{12}C(d,n)^{13}N$ and $^{12}C(d,p)^{13}C$. (see Fig. 6a-c)

The angular distributions for the ground state particle groups shown in Fig. 6b are from Gudehus et al.[21] and in Fig. 6c from Benenson and Jones[22]. The ratio of differential cross sections $q(n_0, p_0)$ at 30° measured by the latter authors at two different energies are given in Table II.

Table II

E_d	$q(n_0, p_0)$ (30°)
2.68	1.7±0.3
3.26	2.4±0.4

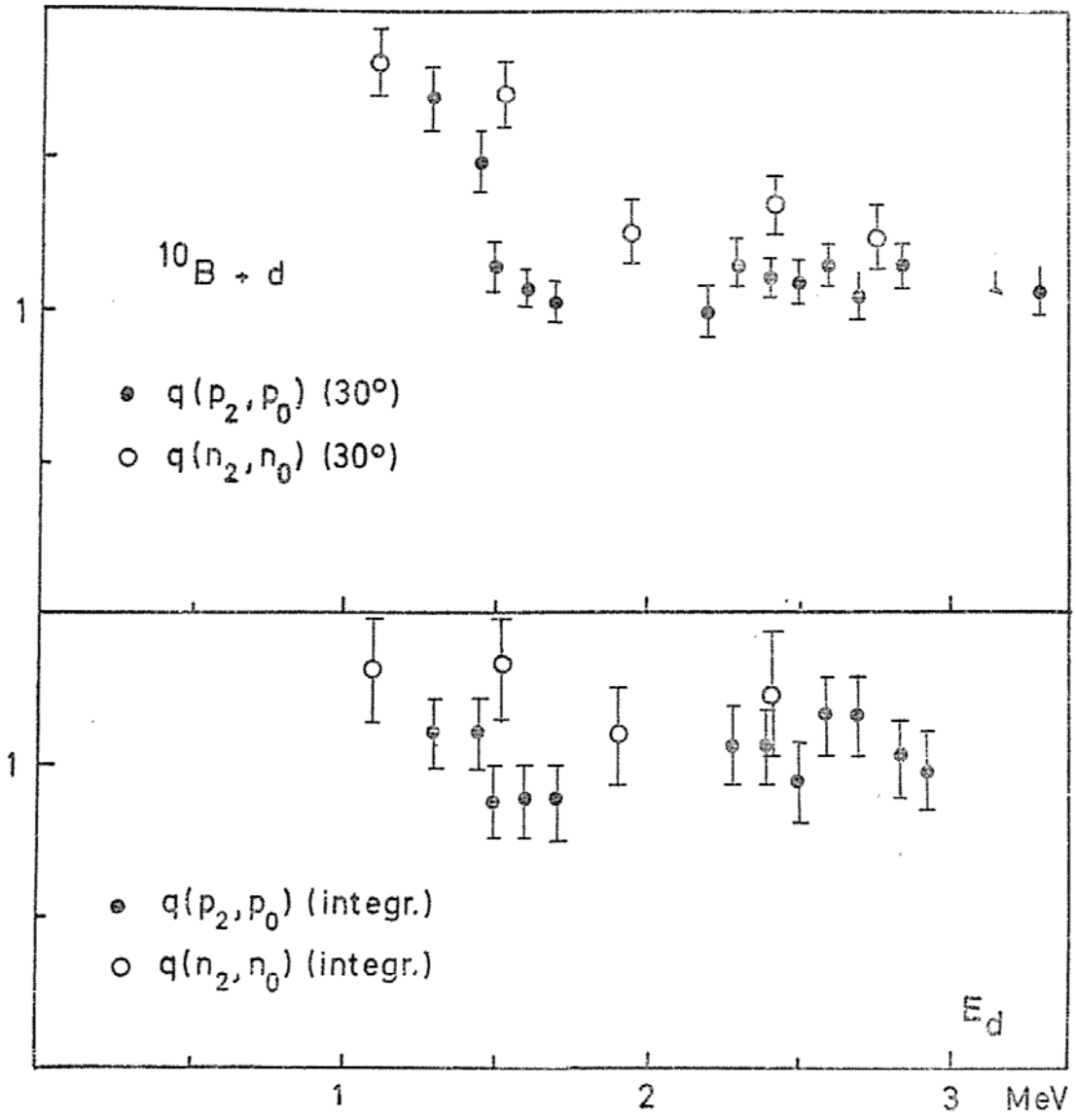

Fig. 5. c) Cross section ratios $q(p_2, p_0)$ and $q(n_2, n_0)$[18].

In this reaction again $|C/C'|^2=1$. The authors mention that the large deviation from this value is entirely explained by kinetic factors.

4) The reactions $^{12}C(^3He, n)^{14}O$ and $^{12}C(^3He, p)^{14}N$ (see Fig. 7a-b)

In this case the reactions studied are those leading to the isobaric analogue states ^{14}O (0) and ^{14}N (2.31) both of which are members of the i-spin triplet $A=14$ shown in the level diagram of Fig. 2.

The ratio of i-spin coupling coefficients, calculated in a similar way as described in §3 is $|C/C'|^2=2$.

Bromley et al.[23] have investigated the cross section ratio $q(n_0, p_1)$ (Fig. 7a) and the angular distributions (Fig. 7b) for ^{3}He-particle

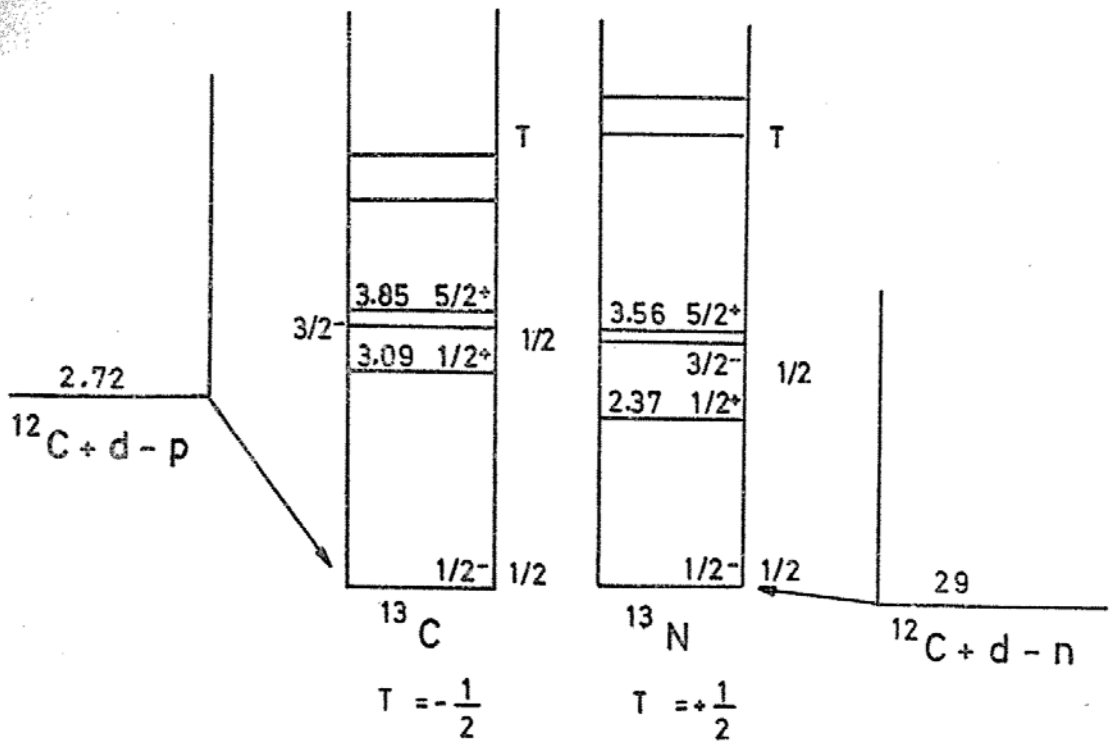

Fig. 6. The reactions $^{12}C(d, n)^{13}N$ and $^{12}C(d, p)^{13}C$
a) Level diagram

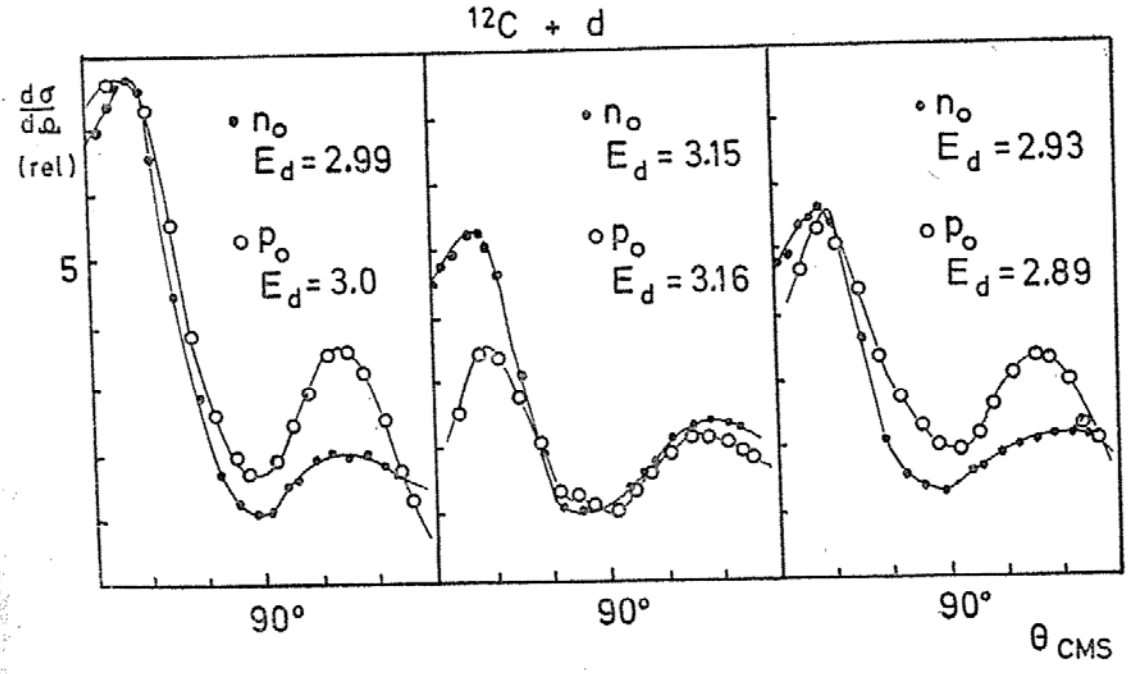

Fig. 6. b) Angular distributions of the ground state particle groups measured by Gudehus et al.[21]. The curves are displayed on a relative scale and are arbitrarily normalized to each other.

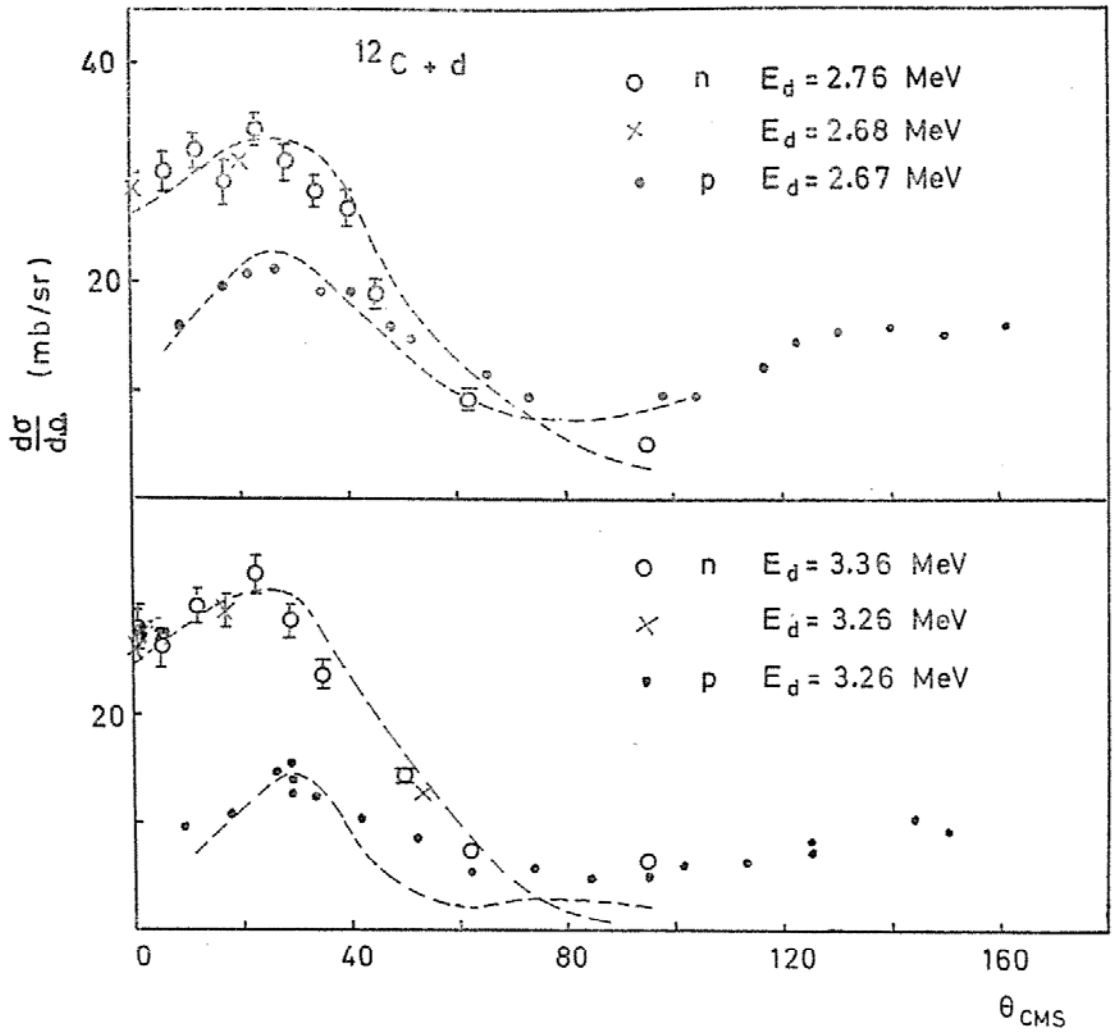

Fig. 6. c) Angular distributions of ground state particle groups measured by Benenson and Jones[22]. The curves represent PWBA fits.

energies between 1.3 and 2.6 MeV. We see that the value 2 is gradually approached by q for increasing energies. This energy dependence can be explained by barrier penetration effects and the negative Q-value of the (^{3}He, n)-reaction which has a threshold energy of $E(^3\mathrm{He})_{\mathrm{thr.}} = 1.44$ MeV. For higher indident particle energies further studies have been made by Fulbright et al.[24] For $E(^3\mathrm{He}) = 6.6$ to 10.6 MeV the result is that i) the angular distributions of the n_0 and p_1 groups, have very similar shape and ii) the ratio of differential cross sections $q(n_0, p_1)$ (10°) has an average value of 2 within the total energy interval, but fluctuates about ± 0.25 around this mean value, depending on the ^{3}He-energy. This fluctuation may be explained by the influence of compound nucleus formation and by interference

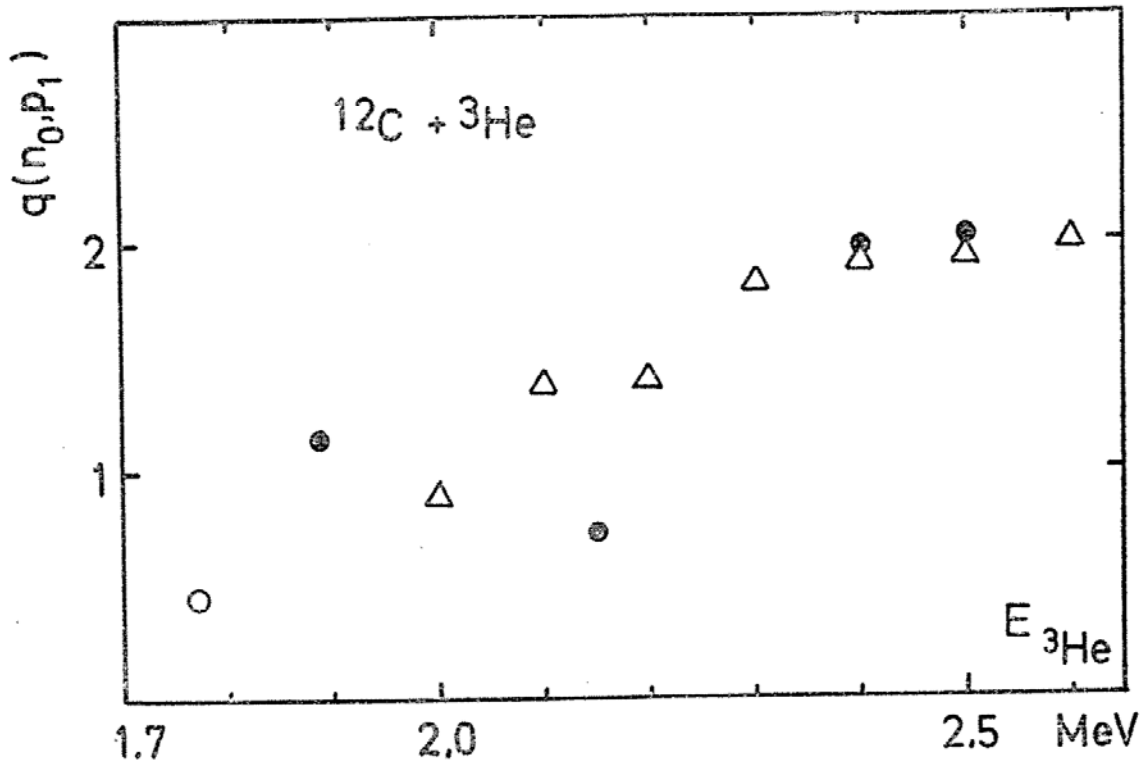

Fig. 7. The reactions $^{12}C(^3He, n)^{14}O$ and $^{12}C(^3He, p)^{14}N$
a) Cross section ratio $q(n_0, p_1)$, measured by Bromley et al.[23]. Triangles indicate differential cross sections at 90°, circles indicate integrated cross sections.

effects between compound nucleus- and direct interaction mode amplitudes.

5) The reactions $^{24}Mg(d, n)^{25}Al$ and $^{24}Mg(d, p)^{25}Mg$ (see Fig. 8a-b)

The results of the measurements of Goldberg[25] and Cox and Williamson[26] for the particle groups p_0, n_0, p_1, n_1, p_2, n_2 are shown in Fig. 8b and in Table III, which gives the peak cross sections for the three particle groups.

Table III

Residual State No.	σ peak (mb/sr)	
	$E_d = 4$ MeV (d, n)	$E_d = 8$ MeV (d, p)
0	3.0	17.0
1	57.0	230.0
2	2.5	9.3

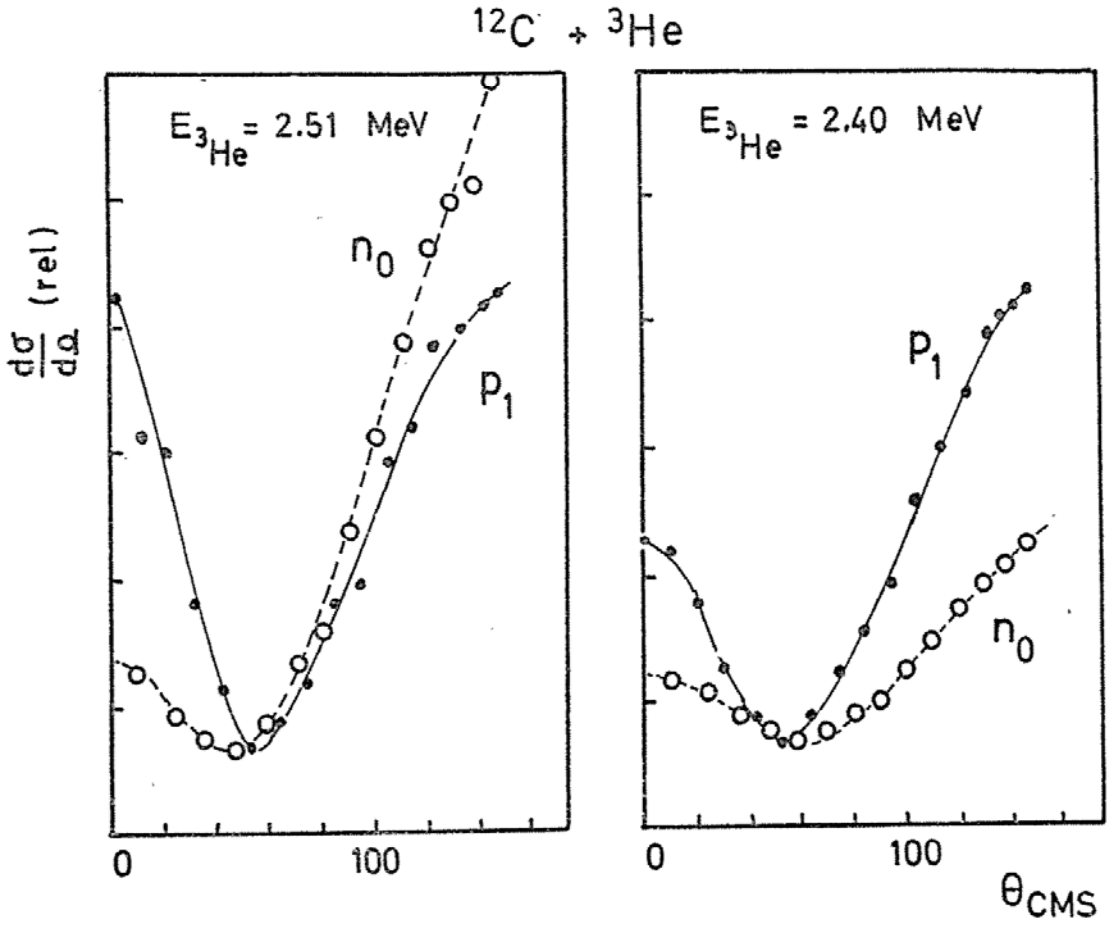

Fig. 7. b) Angular distributions of particle groups n_0, p_1[23]. The curves are normalized to their cross section minimum.

As in this investigation the incident deuteron energy in the (d,n)-reaction is much lower than in the (d,p)-reaction, the cross section values cannot be compared directly, but corrections due to kinetic factors should be made. Moreover the large difference of Q-values (Q_{n_0}=0.06 MeV, Q_{p_0}=8.9 MeV) will cause a large difference of the penetration factors of the transferred nucleon and thus has a strong effect upon the cross section. The authors do not account for these effects.

6) Finally we refer to the experiments of Calvert, Jaffe and Maslin[27] who measured the ratio of peak cross sections $q(p_0, n_0)$ for the (d,n)- and (d,p)-reaction on the target nuclei ^{12}C, ^{14}N, ^{16}O and ^{28}Si and the ratio $q(n_2, p_0)$ for the same reactions on ^{9}Be leading to the second excited state $^{10}B(1.74)$ and the ground state $^{10}Be(0)$, both of which are members of the i-spin triplet T=1 of the isobars A=10.

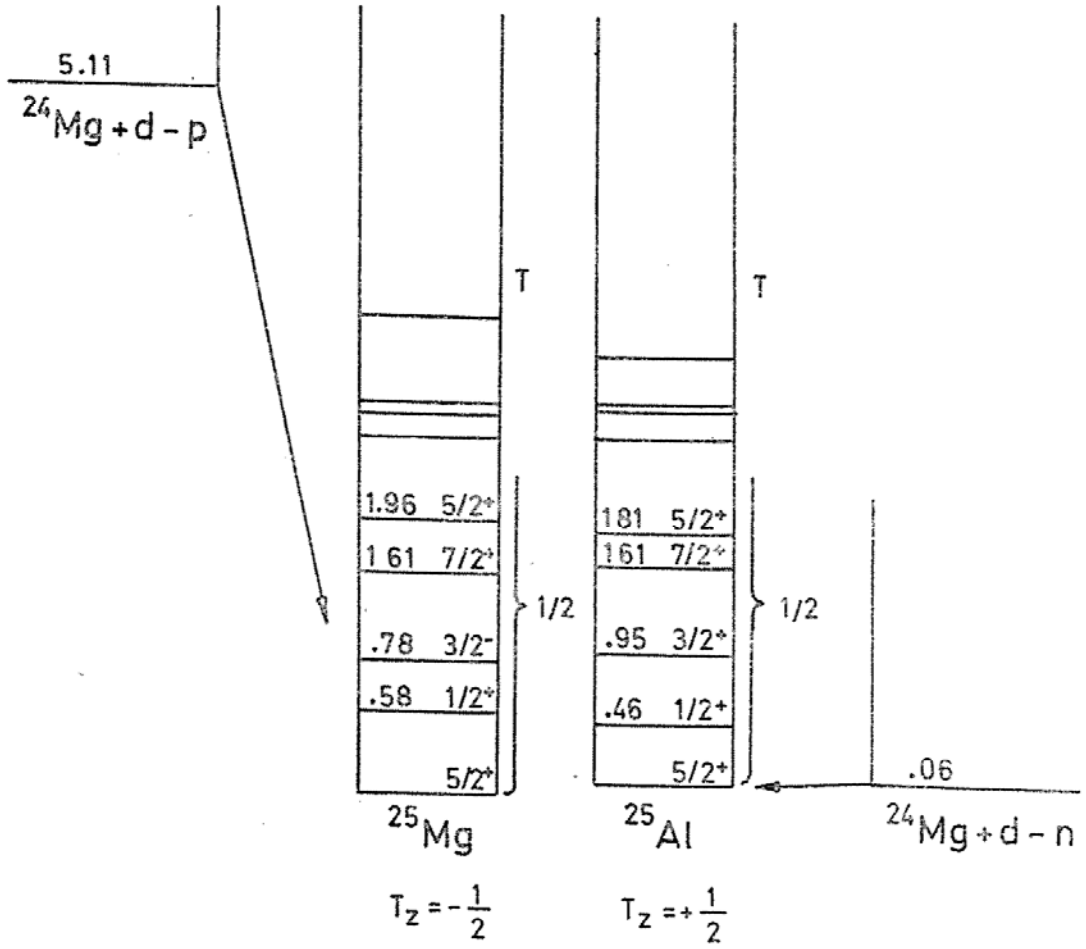

Fig. 8. The reactions $^{24}Mg(d,n)^{25}Al$ and $^{24}Mg(d,p)^{25}Mg$
a) Level diagram

The (d,n) and (d,p) measurements were performed simultaneously, using the same target, with an incident deuteron energy $E_d=$ 9 MeV. Table IV shows the results.

The third column gives the value of the i-spin coupling coefficients. The fourth column gives the cross section ratio corrected

Table IV

Target nucleus	(σ_p/σ_n) peak	$\left\|\frac{C'}{C}\right\|^2$	q corrected	Q_p (MeV)	Q_n
^{9}Be	1.64±0.25	2	2.16	4.46	2.62
^{12}C	0.50±0.05	1	0.86	2.72	−0.29
^{14}N	1.16±0.14	1	1.71	8.62	5.07
^{16}O	0.47±0.08	1	1.30	−1.92	−1.63
^{28}Si	1.02±0.15	1	0.58	6.25	0.50

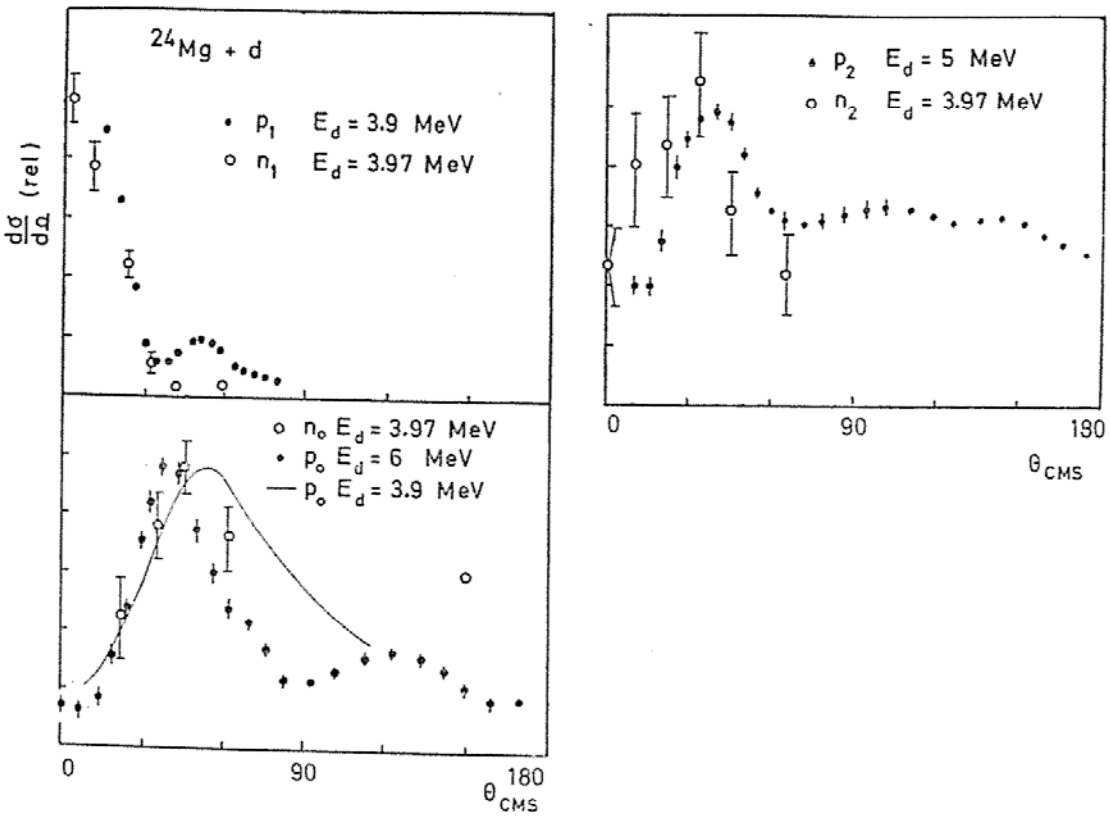

Fig. 8. b) Angular distributions of the first three particle groups. (d,n)-measurements are from Goldberg[25]. (d,p)-measurement are from Cox and Williamson[26]. The angular distributions are normalized to peak cross section.

for kinetic factors. The last column gives the Q-values of the (d,p)- and the (d,n)-reaction respectively.

It is seen that fair agreement is attained for the target nuclei ^{9}Be, ^{12}C and ^{16}O, but there are deviations of at least 50% for ^{14}N and ^{28}Si. In the case of ^{14}N, compound nucleus formation might be involved which probably accounts for the bad value of q corrected. In the case of ^{28}Si, the disagreement might possibly be explained by the large difference of Q-values.

It should be pointed out here that cross section measurements at a single incident particle energy may not always be very conclusive. This is because of strong cross section fluctuations depending on the incident particle energy which have been observed in many cases in the yield functions of differential cross sections. It is seen that these fluctuations predominate in the stripping maximum of the forward direction and is well explained by compound nucleus-direct amplitude

interferences. Therefore the cross section data presented in the foregoing examples are not necessarily very reliable for the purpose of the study of "charge symmetry", even in the case of small experimental error. Therefore it would be better to take the average cross section over a wide energy interval and, secondly, to take the integrated cross section instead of the differential cross section at some forward angle.

REFERENCES

(1) SCHINTLMEISTER: *"Der Isospin von Atomkernen"*. Verlag Kunst und Wissen, Berlin.
(2) F. AJZENBERG-SELOVE and T. LAURITSEN: *Nucl. Phys.* **11**, 1 (1959).
(3) M. A. PRESTON: *"Physics of the Nucleus"*. Addison Westley Publ. Co. (1962).
(4) W. E. MEYERHOF: *"Elements of Nuclear Physics"*. McGraw Hill Series in Fundamentals of Physics, (1967).
(5) L. A. RADICATI: *Phys. Rev.* **87** 521 (1952).
(6) W. M. MACDONALD: *Phys. Rev.* **100** 51 (1955).
(7) C. P. BROWN: *Phys Rev.* **104** 1958 (1956).
(8) C. P. BROWN: *Phys. Rev.* **114** 807 (1959).
(9) Y. HASHIMOTO and W. P. ALFORD: *Phys. Rev.* **116** 981 (1959).
(10) J. JANECKE: *Nucl. Phys.* **48** 129 (1963).
(11) P. G. BIZETTI and A. M. BIZETTI-SONA: *Nucl. Phys.* **A108** 274 (1968).
(12) A. M. LANE and R. G. THOMAS: *Rev. Mod. Phys.* **30** 257 (1958).
(13) H. MORINAGA: *Phys. Rev.* **97** 444 (1954).
(14) M. H. MACFARLANE and J. B. FRENCH: *Rev. Mod. Phys.* **32** 567 (1960).
(15) E. U. CONDON and G. H. SHORTLEY: *"The Theory of Atomic Spectra"* Cambridge University Press, London and New York (1953).
(16) M. BIRK, G. GOLDRING, P. HILLMAN and R. MOREH: *Nucl. Phys.* **41** 58 (1963).
(17) L. CRANBERG, A. JAQUOT, and H. LISKIEN, *Nucl. Phys.* **42** 608 (1963).
(18) G. BREUER: *Z. Phys.* **178** 268 (1964).
(19) R. H. SIEMSSEN, M. COSACK and R. FELST: *Nucl. Phys.* **69** 209 (1965).
(20) G. BREUER: to be published.
(21) T. GUDEHUS, M. COSACK, R. FELST and H. WAHL: *Nucl. Phys.* **80** 577 (1966).
(22) R. E. BENENSON, K. W. JONES and M. T. MCELLISTREM: *Phys. Rev.* **101** 308 (1956).
(23) D. A. BROMLEY, E. ALMQUIST, H. E. GOVE, A. E. LITHERLAND, E. B. PAUL and A. J. FERGUSON: *Phys. Rev.* **105** 957 (1957).
(24) H. W. FULBRIGHT, W. PARKER ALFORD, O. M. BILANIUK, V. K. DESHPANDE and J. W. VERBA: *Nucl. Phys.* **70** 553 (1965).
(25) E. GOLDBERG: *Phys. Rev.* **89** 760 (1953).
(26) S. A. COX and R. M. WILLIAMSON, *Phys. Rev.* **105** 1799 (1957).
(27) J. M. CALVERT, A. A. JAFFE and E. E. MASLIN: *Phys. Rev.* **101** 501 (1956).

PLANE DEFORMATION IN A SEMICIRCULAR PRISM

WOLFGANG KROLL

Abstract: We introduce a simple method which allows to find the stress distribution in a semicircular prism, when the deformation does not depend on the axial coordinate.

INTRODUCTION

The problems of plane deformation have been solved in a very elegant way with the methods of conformal mapping especially by Muskhelishvili, an account of which has been given in his Some Basic Problems of the Mathematical Theory of Elasticity. Here we intend to show how some elastic problems for the semicircular prism can be solved by elementary methods. We want to consider a semicircular prism under constant pressure on the plane part of the surface and also the problem in which a constant radial pressure works on the circular part of the surface. In treating these problems it becomes clear, that the solution must be written as a series of $\cos(2n+1)\vartheta$ resp. $\sin(2n+1)\vartheta$, when the polar angle ϑ takes on the circular surface values between $-\frac{\pi}{2}$ and $+\frac{\pi}{2}$. Then there arises the difficulty that one cannot use these functions for a Fourier-expansion. To avoid this difficulty one has to consider a circular cylinder for which ϑ takes values between $-\pi$ and $+\pi$ and to assume appropriate forces on its surface.

THE CIRCULAR CYLINDER UNDER RADIAL PRESSURE

We consider therefore a circular cylinder of radius a under the radial pressure p on one half of the surface which is held in equilibrium by tangential forces which work on the edge of a diametrical plane. Our surface-conditions in the usual notation are then

$$\sigma_{rr}|_{r=a} = \begin{cases} -p\,; & -\pi < \vartheta < -\frac{\pi}{2}\,; \quad \frac{\pi}{2} < \vartheta < \pi \\ 0\,; & -\frac{\pi}{2} < \vartheta < \frac{\pi}{2} \end{cases}$$

$$\sigma_{r\vartheta}|_{r=a} = C\left[\delta\left(\vartheta - \frac{\pi}{2}\right) - \delta\left(\vartheta + \frac{\pi}{2}\right)\right].$$

Here $\delta(x)$ is the Dirac δ-function and the value of C will be determined by the condition of equilibrium. When we expand these functions in Fourier-series, we obtain

$$\sigma_{rr}|_{r=a} = -\frac{p}{2} + \frac{2p}{\pi}\sum_{n=0}^{\infty}\frac{(-1)^n}{2n+1}\cos(2n+1)\vartheta$$

$$\sigma_{r\vartheta}|_{r=a} = \frac{2C}{\pi}\sum_{n=0}^{\infty}(-1)^n\sin(2n+1)\vartheta.$$

The stress components σ_{rr}, $\sigma_{\vartheta\vartheta}$, $\sigma_{r\vartheta}$ are obtained from the stress function χ by the relations

$$\sigma_{rr} = \frac{1}{r}\frac{\partial\chi}{\partial r} + \frac{1}{r^2}\frac{\partial^2\chi}{\partial\vartheta^2}, \qquad \sigma_{\vartheta\vartheta} = \frac{\partial^2\chi}{\partial r^2},$$

$$\sigma_{r\vartheta} = -\frac{\partial^2}{\partial r\,\partial\vartheta}\left(\frac{\chi}{r}\right),$$

where the stress-function χ satisfies the biharmonic equation

$$\Delta\Delta\chi = 0.$$

The boundary-conditions suggest that the stress-function has the form

$$\chi = Ar^2 + \sum_{n=0}^{\infty}\left[a_n r^{2n+3} + c_n r^{2n+1}\right]\cos(2n+1)\vartheta.$$

From it we obtain

$$\sigma_{rr} = 2A - 2\sum_{n=0}^{\infty}\left[a_n(2n-1)(n+1)r^{2n+1} + c_n(2n+1)n r^{2n-1}\right]\cos(2n+1)\vartheta$$

$$\sigma_{r\vartheta} = 2\sum_{n=0}^{\infty}(2n+1)\left[a_n(n+1)r^{2n+1} + c_n n r^{2n-1}\right]\sin(2n+1)\vartheta.$$

From the boundary-conditions we obtain the equations for the determination of the coefficients a_n and c_n

$$2A = -\frac{p}{2}, \qquad 2a_0 a = \frac{2p}{\pi}, \qquad 2a_0 a = \frac{2C}{\pi}$$

we find therefore

$$C = p.$$

In general we have to do with the equations

$$a_n(2n-1)(n+1)a^{2n+1} + c_n(2n+1)\,n\,a^{2n-1} = -\frac{p}{\pi}\frac{(-1)^n}{2n+1}$$

$$(n+1)\,n\,a^{2n+1} + n\,c_n\,a^{2n-1} = \frac{p}{\pi}\frac{(-1)^n}{2n+1}.$$

From them we find

$$a_n = \frac{p}{\pi}\frac{(-1)^n}{2n+1}a^{-(2n+1)}; \qquad c_n = \frac{(-1)^n p}{\pi}\frac{a^{-(2n-1)}}{2n+1}.$$

Our stress-function is therefore

$$\chi = -\frac{p}{4}r^2 + \frac{pa^2}{\pi}\sum\frac{(-1)^n}{2n+1}\left[\left(\frac{r}{a}\right)^{2n+3} - \left(\frac{r}{a}\right)^{2n+1}\right]\cos(2n+1)\,\vartheta.$$

We can write it in closed form.

We have

$$\sum\frac{(-1)^n}{2n+1}\left[\left(\frac{r}{a}\right)^{2n+1} - \left(\frac{r}{a}\right)^{2n+1}\right]\cos(2n+1)\,\vartheta = Re\,\frac{r^2-a^2}{a^2}\sum\frac{(-1)^n}{2n+1}\left(\frac{r}{a}\right)^{2n+1}e^{i(2n+1)\vartheta},$$

where *Re* means the real part.

Now we have with $z = \frac{r}{a}e^{i\vartheta}$

$$\sum\frac{(-1)^n}{2n+1}z^{2n+1} = \frac{1}{2i}\ln\frac{1+iz}{1-iz}.$$

The real part of this sum is with $z^* = \frac{r}{a}e^{-i\vartheta}$

$$\frac{1}{2}\operatorname{arctg}\frac{1-zz^*}{z+z^*} = \frac{1}{2}\operatorname{arctg}\frac{2ar\cos\vartheta}{a^2-r^2}.$$

We find therefore

$$\chi = -\frac{p}{4}r^2 + \frac{p}{2\pi}(r^2-a^2)\operatorname{arctg}\frac{2ar\cos\vartheta}{a^2-r^2}$$

Now we see that for $\vartheta = \pm \frac{\pi}{2}$ the stress-function reduces to

$$\chi|_{\vartheta=\pm\frac{\pi}{2}} = -\frac{p}{4} r^2,$$

so that

$$\sigma_{\vartheta\vartheta}|_{\vartheta=\pm\frac{\pi}{2}} = \frac{\partial^2\chi}{\partial r^2}\Big|_{\vartheta=\pm\frac{\pi}{2}} = -\frac{p}{2}$$

Also $\sigma_{r\vartheta}$ vanishes for $\vartheta = \pm \frac{\pi}{2}$ because

$$\frac{\partial}{\partial\vartheta}\,\frac{r^2-a^2}{r}\,\operatorname{actg}\,\frac{2ar\cos\vartheta}{a^2-r^2} = -\frac{2a\sin\vartheta\,(a^2-r^2)}{(a^2-r^2)+(2ar\cos\vartheta)^2}$$

for $\vartheta = \pm \frac{\pi}{2}$ reduces to $-2a\sin\vartheta$ and therefore does not depend on r. Therefore

$$\sigma_{r\vartheta}|_{\vartheta=\pm\frac{\pi}{2}} = -\frac{\partial^2}{\partial r\,\partial\vartheta}\left(\frac{\chi}{r}\right)\Big|_{\vartheta=\pm\frac{\pi}{2}} = 0$$

THE SEMICIRCULAR PRISM

The results we have obtained for the circular cylinder include the solution for the semicircular prism which stays under constant pressure on the plane surface. We have only to restrict the polar angle to the region between $-\frac{\pi}{2}$ and $+\frac{\pi}{2}$. When we further replace $\frac{p}{2}$ by p, the resulting stress-function

$$\chi = -\frac{p}{2} r^2 + \frac{p}{\pi}(r^2-a^2)\operatorname{arctg}\frac{2ar\cos\vartheta}{a^2-r^2}$$

describes the stress distribution in the semicircular prism $\left(0 \leqslant r \leqslant a;\ -\frac{\pi}{2} \leqslant \vartheta \leqslant \frac{\pi}{2}\right)$ completely for the case that the constant pressure p works on the plane surface and equilibrium is established by tangential forces on the edges. The circular surface is force-free in this case.

From our results we can also obtain the stress-distribution in the semicircular prism for the case that the plane surface is force-

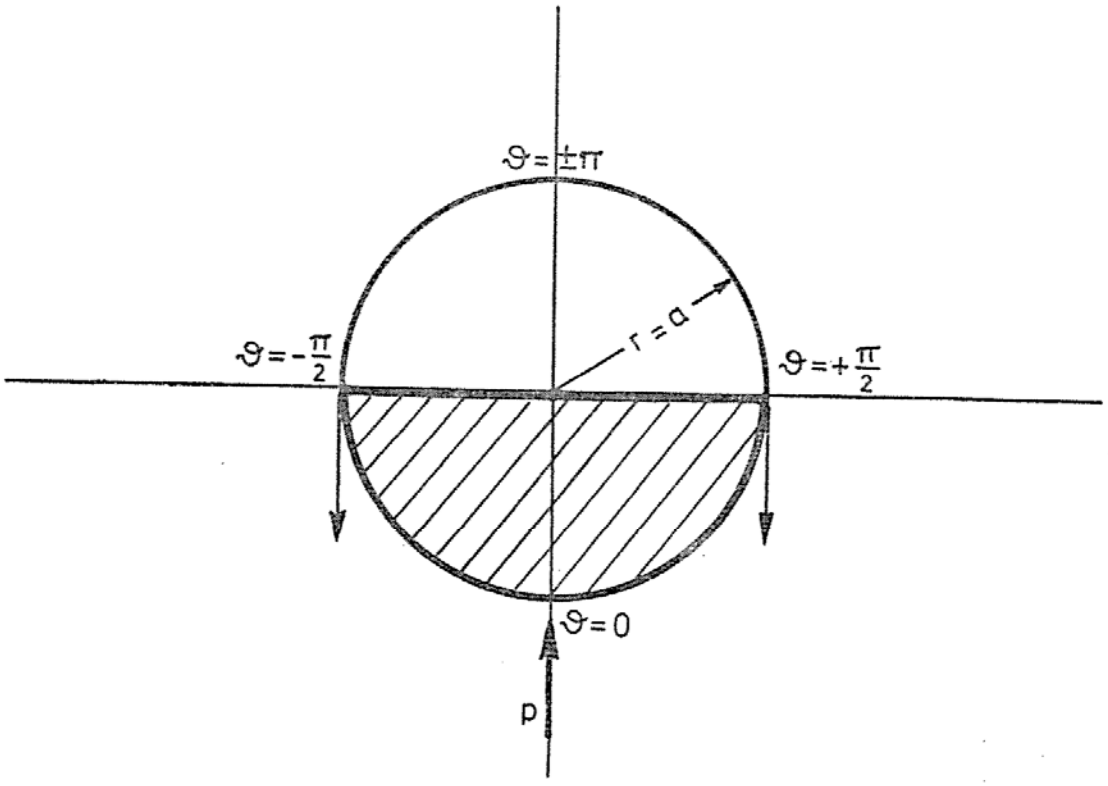

Figure. The shaded part represents the semicircular prism. The arrows indicate that the prism is in elastic equilibrium under a radial and a tangential pressure on the cylindrical surface.

free and a constant radial pressure works on the circular surface. We have only to omit the first term in the last expressions and to replace p by $-p$. Therefore the stress-function

$$\chi = -\frac{p}{\pi}(r^2 - a^2)\,\mathrm{arctg}\,\frac{2ar\cos\vartheta}{a^2 - r^2}$$

satisfies the boundary-conditions

$$\sigma_{rr}|_{r=a} = -p\,, \qquad \sigma_{\vartheta\vartheta}|_{\vartheta=\pm\frac{\pi}{2}} = 0\,, \qquad \sigma_{r\vartheta}|_{\vartheta=\pm\frac{\pi}{2}} = 0,$$

and

$$\sigma_{r\vartheta}|_{r=a} = -2p\left[\delta\left(\vartheta - \frac{\pi}{2}\right) - \delta\left(\vartheta + \frac{\pi}{2}\right)\right].$$

"The first process, therefore, in the effectual study of the sciences, must be one of simplification and reduction of the results of previous investigations to a form in which the mind can grasp them."

J. C. MAXWELL

THERMAL ANALYSIS STUDIES: MEASUREMENT OF VISCOSITY OF GLASS

URBAN E. SCHNAUS, O. S. B.

Some research work on vitreous and plastic materials has begun in the Physics Department of Fu Jen University with a simple beam-bending apparatus to determine the viscosity of small glass rods and bars under suitably chosen loads and temperatures. The specimens used are about 6 centimeters long and have circular or rectangular cross-section, from 10 square millimeters to 60 square millimeters in area.

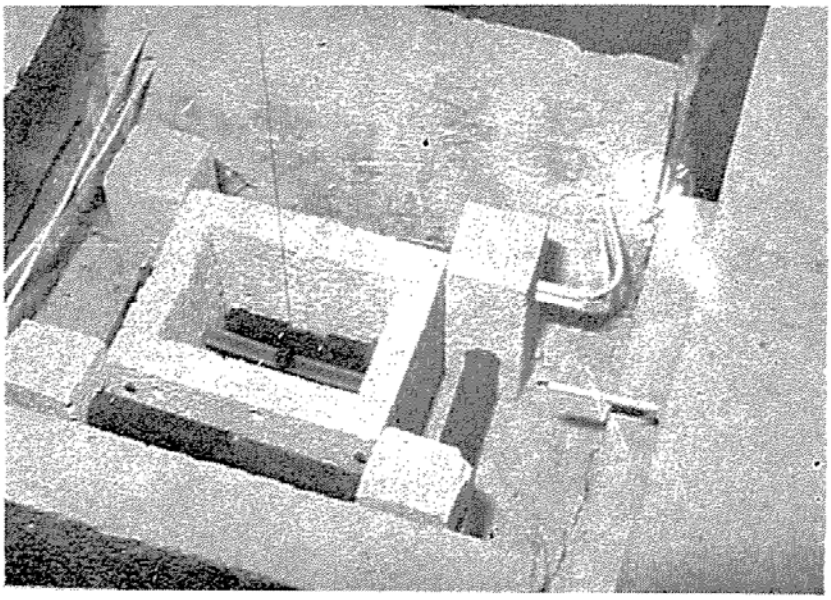

Plate 1. Close-up Top View: Glass Bar in Beam-Bending Device.

One of the small beams is shown in place after bending in Plate 1. The temperature-control thermocouple is seen extending into the oven space at the right. A second thermocouple, not visible in the photograph, extends upward directly under the left end of the glass bar. Cartridge heating elements are in place on ceramic supports around the ceramic muffle enclosing the metal beam support.

The loading weight can be seen in place in Plate 2, above the vertically supported linear variable deflection transformer (LVDT) which supplies a voltage output proportional to the deflection of the

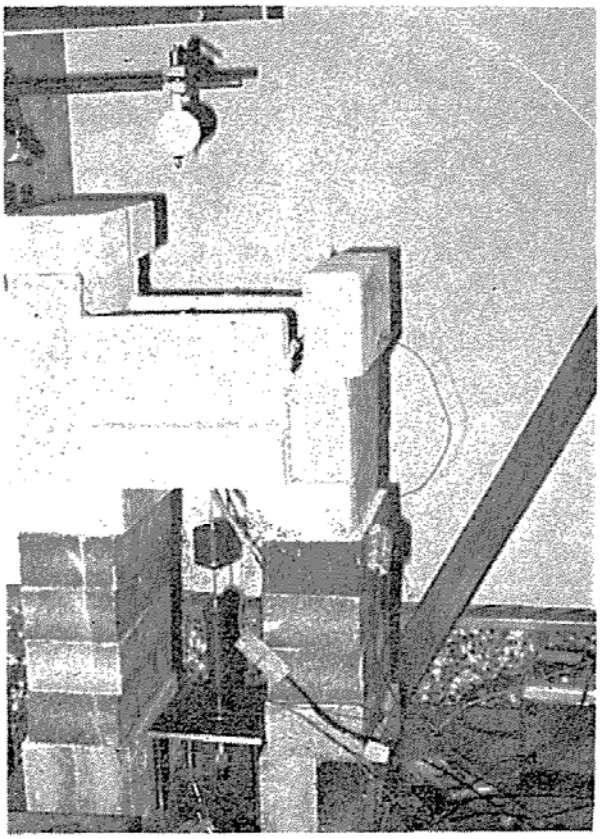

Plate 2. Side view: Beam-Bending Device for measuring Viscosity of Glass.

beam. The micrometer adjustment for the position of the LVDT is visible at the lower end of the support.

Auxiliary equipment includes a two-pen potentiometric recorder; one pen is used to record the temperature measured by the platinum-rhodium thermocouple near the glass beam; the other pen records the deflection measured by the LVDT. In parallel connection with the temperature input to the strip-chart recorder is an accurate DC potentiometer which monitors the temperature reading and enables the temperature to be read to a thousandth of a millivolt; one-hundredth of a millivolt corresponds to about one °C in the range around 600°C with this thermocouple. An electronic temperature control device regulates the current to the cartridge heaters and is the third main item of auxiliary equipment.

The deflection rate of a beam in this device is a convenient indirect means of measuring the viscosity of glass in the temperature range from 300°C to 900°C and viscosity range 10^{10} to 10^{14}

poise.[1] A parallel-plate viscometer has been added to our equipment in the current school year, and is capable of viscosity measurements from 10^6 to 10^{11} poise. Direct measurements of specific heat and heats of fusion and transformation of vitreous and plastic materials by differential scanning calorimetry will also be possible with new equipment recently made available in our laboratory.

I. INTRODUCTION

There are about 700 different glass compositions now in commercial use. Although about 90 percent of all glass tonnage produced throughout the world is oxide glass of the soda-lime type so widely used for windows and bottles, new types of glass are constantly being developed and new uses are being found to increase the thousand or so essentially different applications of the versatile material we call glass.[2]

Glass is one of man's oldest materials; a common natural glass, obsidian, was widely used in the Stone Age for arrowheads, spear heads, and knives. The earliest artificial glass was produced about

(1) Viscosity is the property of a fluid to withstand a velocity-dependent shear: real liquids will not support a very slow shear, a tangential stress between two surfaces separated by some finite distance. But they will support a rapid shear. The coefficient of viscosity, η, is defined by the equation

$$\frac{F}{A}=\eta\frac{dv}{dy}$$

where dv is the difference in velocity between top and bottom surfaces separated a distance dy; η has units dynes sec/cm^2 in the c. g. s. system, and is called a *poise* after Poiseulle, an early investigator. For glass and most liquids, η decreases as the temperature increases, while for gases η increases with temperature. Our concern here is with the important molecular properties of materials that can be deduced from this temperature variation.

(2) There are many general treatments of glass in the literature of science. One of the best is *Glass* by G. O. Jones (Second Edition, 1971, available as a 128-page Science Paperback, distributed in the U. S. A. by Barnes & Noble, Inc., New York City). The article on 'Glass' by J. R. Hutchins, III and R. V. Harrington of the Corning Glass Works, Corning, N. Y. in Vol. 10, p. 533-604 of Kirk-Othmer: *Encyclopedia of Chemical Technology*, 2nd Edition, John Wiley & Sone, Inc. New York (1966), contains more technological and industrial information. Both these references have good bibliographies and have been useful sources for this article.

14 thousand years ago when stone beads were glazed to make them more attractive. The earliest articles made completely of glass date back to about 7000 B. C.

Though some advances were made in glass technology in applications to optics during the 17th and 18th centuries, there has been more advance in scientific knowledge of glass in the past 40 years than in all history before. Extensive data is now available on glass composition ranges and on the physical and chemical relationships which determine the usefulness of glass for many applications. But many gaps remain in this knowledge. In particular, no adequate theory is yet available to explain the viscosity of glass. Nor is there an adequate theory to explain the practical strength of glass or its atomic structure, though a good beginning has been made with the "random network" theory.

II. THE NATURE OF GLASS

Glass is a non-crystalline solid; it is a material having suitable rigidity at ordinary temperatures and made from arrays of atoms in which there is no long-range order in their structure. Many plastics, and some metals and organic compounds will fit this definition. But ordinarily the term 'glass' is restricted to inorganic materials formed by melting processes. The American Society for Testing and Materials (ASTM) defines glass as "an inorganic product of fusion which has cooled to a rigid condition without crystallizing".

Though glass is often described as a supercooled liquid, this description is not accurate when applied to glass. A volume-temperature diagram, Figure 1, shows the difference in a substance that can exist in the liquid, glass, and crystal state; without going into the details of the rates and the processes involved, it can be said that the upward deviation from the metastable equilibrium curve of a supercooled liquid is the mark of a glass, as also is the presence of a transformation range around T_g, the glass transformation temperature, which is different from T_f, the normal freezing temperature.

A corresponding marked change in specific heat is observed around T_g. This is shown in Figure 2, where heat capacity values for the chalcogenide glasses, As_2S_3 and As_2Se_3, are recorded.

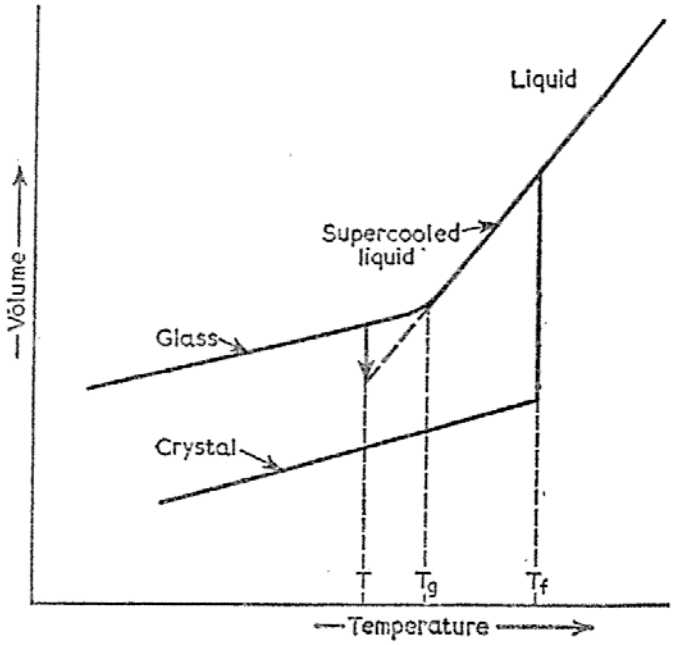

Fig. 1. Relation between the glassy, liquid and solid states

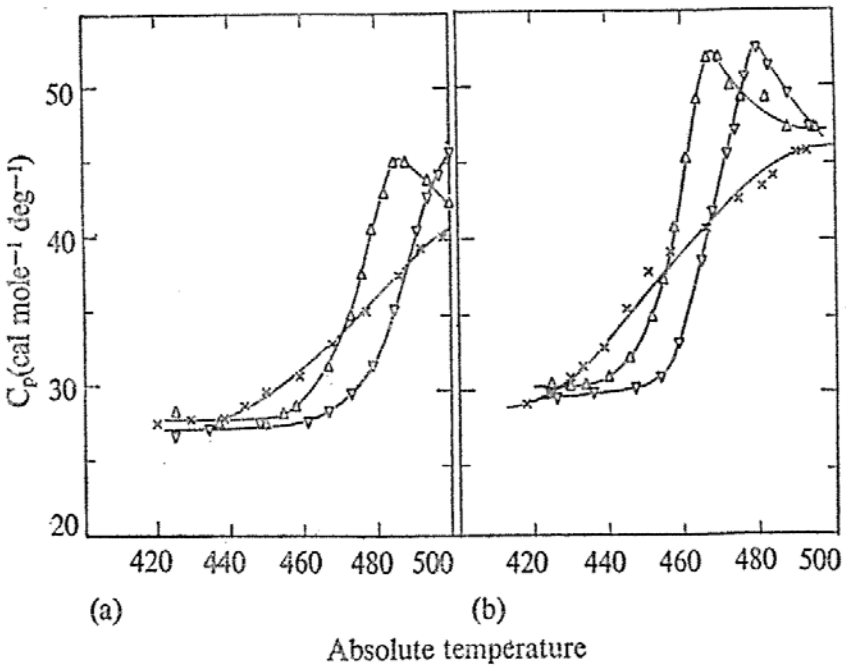

Fig. 2. Heat capacity scans in the glass transformation range
(a) As_2S_3
(b) As_2Se_3
△ Upscan 5 deg/min
▽ Upscan 20 deg/min
× Downscan 5 deg/min

The break in these diagrams around T_g is considered to be due entirely to kinetic factors; it indicates when the viscosity of the supercooled liquid becomes so great that the atomic adjustments are too slow to be shown on an ordinary graph. A structural configuration becomes frozen in, and this glass configuration persists practically unchanged at all lower temperatures. That the glass is really not in equilibrium in the same way that ordinary crystals are is shown by the fact that all glassy materials will "devitrify" and crystallize under certain conditions.

III. STRUCTURE OF GLASS

A prominent theory proposed since 1930 is that of Zachariasen: the atoms in a glass form a three-dimensional network in which the energy content is comparable to the corresponding crystal network, although the glass lacks the crystal symmetry. According to this theory four requirments are postulated for an oxide to be a glass former: 1) each O atom must be linked to no more than two cations; 2) the number of O atoms around a cation must be small, i. e. three or four; 3) the O polyhedra must share corners, not faces or edges, to form a three-dimensional network; and 4) at least three corners must be shared. This is the basis of the "random network" theory of glass structure, shown schematically in Figure 3 for oxide glasses, as contrasted with the regular structure of crystalline silica. X-ray diffraction studies tend to support Zachariasen's theory, but many questions remain to be answered clearly before a complete understanding of the structure of glass is achieved.

A study of the elements (not oxides) has shown that elements of Group VI in the periodic table: O, S, Se, and Te, form glasses by themselves. Experimental work with S and Se indicates that liquid Se is an equilibrium structure of Se_8 rings and long polymeric chains. This structure is frozen into Se glass when the liquid is quenched below T_g; heat capacity studies[3] give strong support for this theory. Studies of other properties such as density, thermal expansion,

(3) Moynihan, C. T. and Schnaus, U. E. *Heat capacity and equilibrium polymerization of Vitreous Se*; *J. Amer. Ceram. Soc.* 54 136-140 (1971).

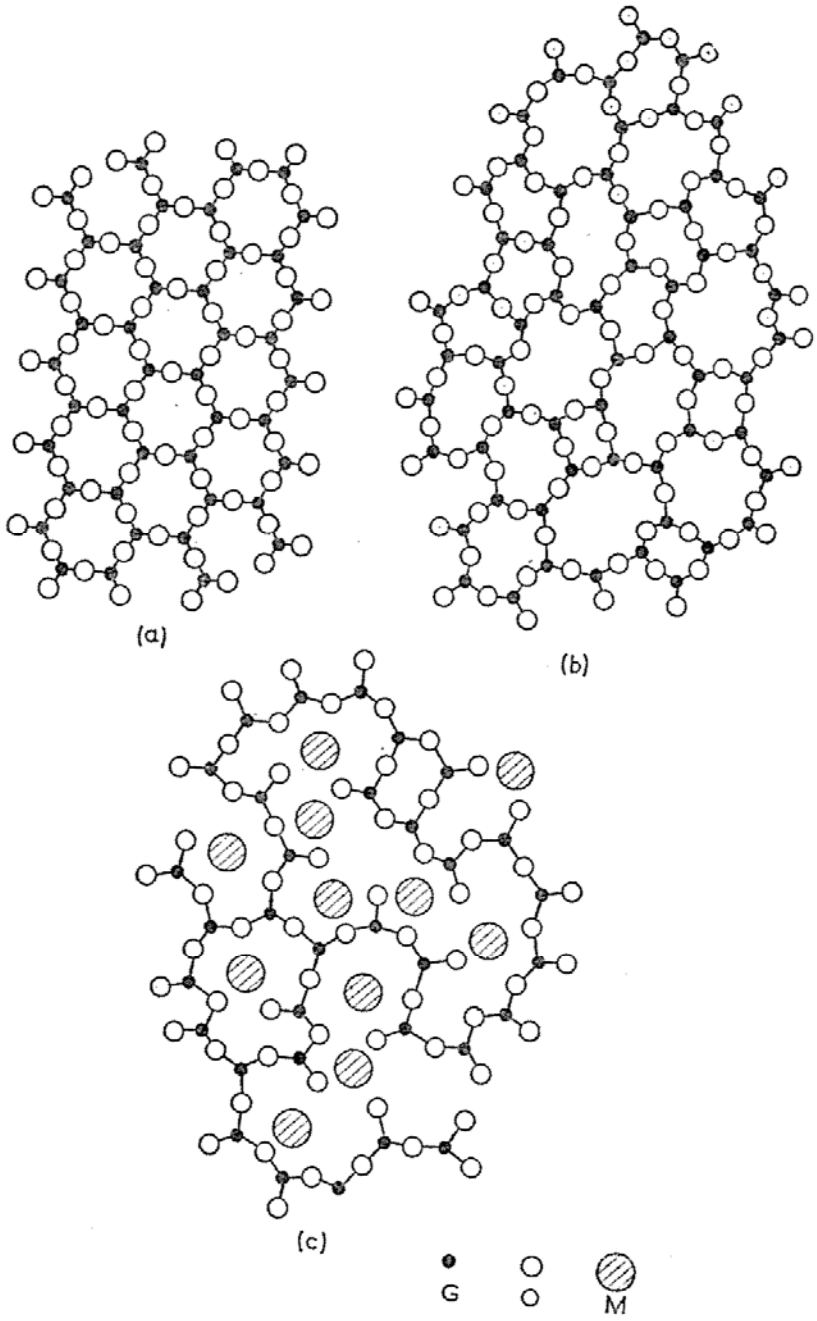

Fig. 3. Structures of an imaginary two-dimensional oxide (G_2O_3)
(After Warren and Zachiararasen)
(a) As crystal
(b) As glass
(c) In a mixed glass of G_2O_3 and M_2O where M is a singly charged metallic ion

dielectric constants, infra-red and Raman spectra, and color, are contributing toward a final picture.

Since oxide glasses are of most commercial importance they have been most thoroughly studied. Oxide substances are classified

as glass-formers, intermediates, and modifiers according to their single-bond strength, cation to oxygen; glass-formers like B-, Si-, and Ge-oxide have highest bond strength and can form three dimensional glass networks without requiring other substances. Modifiers like Pb-, Mg-, Ca-, and K-oxides have lower bond strengths; they tend to bond ionically with the anions in the glassy network; hence they are used to change specific properties like viscosity, electrical conductivity, and thermal expansion. An intermediate oxide, though not capable of forming a glass alone, may enter in the glass structure in a glass-forming and/or in a modifying position.

A somewhat more useful classification divides the common oxides that are not glass-formers into two groups, stabilizers and fluxes. The fluxes lower melting and working temperatures by decreasing viscosity; Na_2O, K_2O, and B_2O_3 are the most important examples. Stabilizers like CaO, MgO, and Al_2O_3 improve chemical durability and/or help to prevent crystallization.

In all, some 66 glass-forming systems have been identified among the elements, but only a few of them are of commercial interest, and of these few SiO_2, silica or quartz, is by far the most important. Extensive tables of compositions and properties of silicate systems are available. Pure silica glass is difficult to make because of its high viscocity at temperatures that can be maintained in ordinary glass furnaces. There are two commercial silica glasses, both about 99.9% pure SiO_2, now available and sold as fused quartz and fused silica, respectively. These are excellent glasses, with highly cross-linked three-dimensional structure, high use temperature and low coefficient of thermal expansion; they have low ultrasonic absorption and excellent transmission of radiation down to about 1800 Å in the ultraviolet; few ordinary glasses transmit light below wavelength 4000 angstroms.

The function of fluxes in glass manufacture has been extensively studied. As mentioned above, these oxides are added to silica in commercial production to reduce the high viscosity of the silica glass and thus to bring large-scale glass manufacture into the range of industrially accessible temperatures and refractory materials used

for making furnaces. Soda, Na_2O, is the flux used most extensively. It "softens" the glass by breaking the SiO_2 bonds, as indicated in Figure 4(b). But the addition of the soda alkali increases the solubility of the glassy product. Hence stabilizing oxides like lime, CaO, are added to make chemically durable glasses. The optimum glass, considering cost, durability, and ease of manufacture, is soda-lime glass containing 72% silica, 15% soda, 10% lime and magnesia, 2% alumina, and 1% miscellaneous oxides. The NBS (National Bureau of Standards, U. S. A.) No. 710 Standard Glass is near to this composition, though it contains no magnesia or alumina.

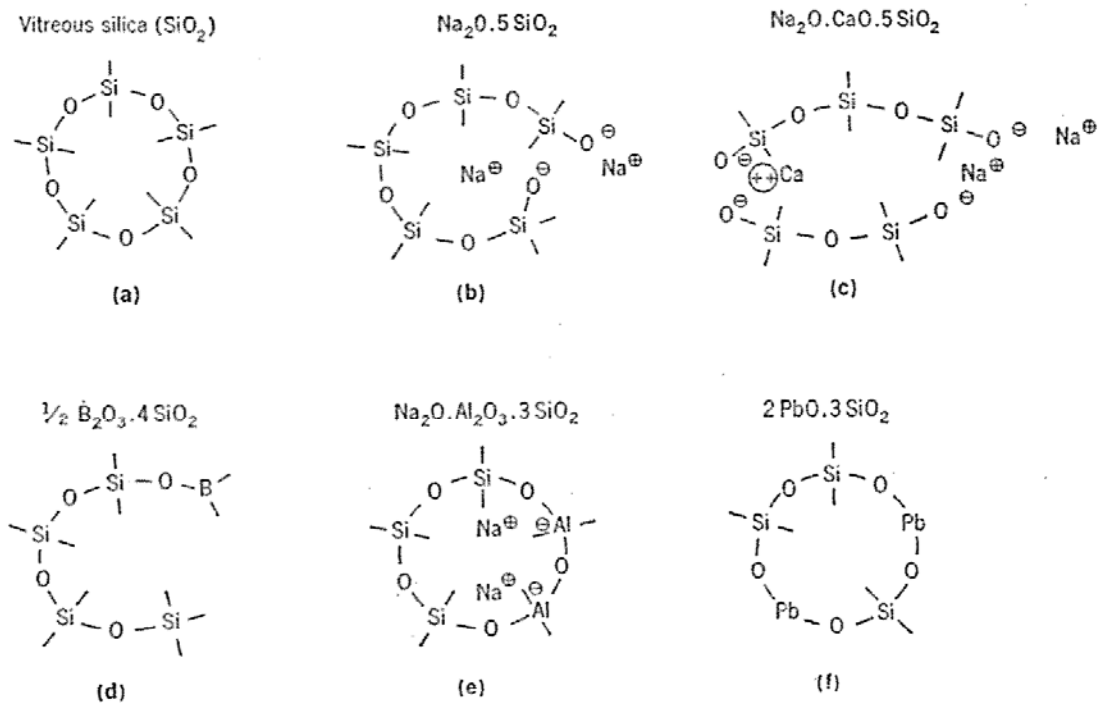

Fig. 4. Schematic representations of glass structures. Si-indicates bending through bridging oxygens common to two SiO_4 tetrahedra.

Alumina (Al_2O_3) is present with silica in many types of sand used for making glass; it acts to "harden" the melt, i. e. to increase chemical durability and resistance to devitrification. It also acts to increase dielectric strength: glasses with a high percentage of alumina are used for electron tubes, for stove ware, and for glass ceramics. The use of boric oxide in place of some of the soda results in a glass of much lower expansion coefficient and greater mechanical strength. Glasses marketed under trade names like Pyrex, Hysil,

Kimax, etc., and much used for laboratory and stove ware, are usually of this borosilicate type.

Lead oxide is a flux that yields glasses with high refractive index and high density. but with low softening temperature. Glasses used in optical and electrical applications often have a considerable amount of PbO in them.

Practically every element in the periodic table has been used intentionally in the manufacture of glass. Non-silicate systems using elements of low atomic weight have been developed for x-ray transmission. Phosphate glasses have been found to be highly resistant to hydrofluoric acid, while compositions containing FeO are strongly absorbant in the infra-red part of the spectrum and are the most efficient heat-absorbing glasses made. For transmitting infra-red radiation chalcogenide glasses formed from components of high atomic weight, particularly Se, Ge, As, and Sb have been found best[4]. Minor constituents like colloidal gold or silver and oxides like MnO affect the color of glasses. Small amounts of Ce are added in glass melts to make photosensitive glasses; ions like Cu, Sn, or Pb in a glass will cause it to fluoresce.

Other effects can be achieved by controlled crystal growth inside the glass: opal glasses are made in this way, and the new field of glass ceramics has developed from this technique.

IV. GLASS MANUFACTURE

Converting materials like sand, feldspar, borax, soda ash, and limestone into glass is basically a melting process requiring large amounts of heat energy. Natural gas is least expensive for this purpose, and hence most frequently used. On the island of Taiwan, where a considerable amount of glass is manufactured for export, the industry is centered where a good supply of natural gas is available; stand-by burners using fuel oil are often installed in glass plants using natural gas as primary fuel. Electric heating is now coming into use, since molten glass is an electrolyte and the melt

(4) Schnaus, U. E. and Moynihan, C. T. *Heat capacities of infrared transmitting glasses* Ge_{28} Sb_{12} Se_{60} *aud* Ge_{33} As_{12} Se_{55}; *Mater. Sci. Eng.* 7 268-271 (1971).

can be heated by passing current through it. In some large plants in the U. S. A. electric heating is being used to supplement that of the gas or oil fuel, at the same time helping to achieve uniform temperature in the batch. Continuous tanks are used in large-scale production: capacities of 1000 tons and daily outputs of 150 tons are fairly common. About 9 kilocalories of heat are required to make a kilogram of glass; in the U. S. A. the fuel cost per kilogram of glass is between 1/2¢ and 1¢.

Making glass means that the materials mentioned: sand, soda ash, limestone, etc. are converted into a homogeneous liquid free of crystalline matter. Many of the oxides used: silica (1710°C), CaO (2580°C), and MgO (2800°C), have melting points in excess of any temperature found in ordinary glass furnaces. Hence there must be reaction and dissolution processes that cannot be considered as ordinary mixing and fusion. Sodium carbonate and silica yield sodium silicates which melt at a temperature less than 1100°C. Studies of reactions among glass batch materials like SiO_2, Na_2CO_3, and $CaCO_3$ show that the two carbonates form a low melting-point eutectic before either component decomposes. After these liquids begin to form the excess refractory oxides become a part of the melt by dissolution.

Two other processes, fining and conditioning, are required before the melted glass comes to proper working condition. Fining removes gaseous inclusions; conditioning achieves the necessary uniformity required before the glass is ready to be formed, pressed, cast, rolled, or drawn to some useful shape. And after the flat or formed glass has been produced, annealing is required in order to bring the heated mass to room temperature without setting up internal stresses and causing corresponding irregularities in density, index of refraction, etc. Annealing schedules in which the temperature is reduced over a period of weeks or even months in order to obtain the extremely small internal stress and high uniformity of index of refraction are required for many optical applications. But in the production lines of commercial flat glass and containers no such lengthy processes are used.

In recent years a great variety of secondary operations and treatments have been developed: finishing operations such as cutting, grinding, engraving, etching, glazing, and sealing have been perfected, along with secondary forming operations to produce foam glass and glass fibers. A considerable tonnage of glass is used in railway carriages and automobiles. Windshields and windows for cars have been made of laminated safety glass, having two thin sheets of polished plate glass laminated with a thinner layer of polyvinyl butyrate, shaped by bending over a metal frame at a temperature around 580°C. Tempering is a simpler strengthening process that produces a high compressive stress on the surface of flat or curved sheet glass through rapid cooling from temperatures near the softening point, where the viscosity is about $10^{7.6}$ poise.

V. THERMAL PROPERTIES OF GLASS

Measurement of selected physical properties is a convenient way to classify and control glass compositions and their manufacture. Among these physical properties there are optical and electrical ones like index of refraction, spectral absorption, dielectric strength, and electric resistivity. The mechanical properties most frequently studied are density, tensile and compressive strength, and hardness. Between these properties and thermal ones like coefficient of expansion, specific heat, and viscosity there are often significant relationships.

Viscosity is the property most used in describing glasses, for the melting, forming, annealing, sealing, and upper temperature use of glass is determined by its viscosity. The standard temperature points for glasses, the strain point, the annealing point, and the softening point, refer to viscosities of $10^{14.5}$, 10^{13}, and $10^{7.6}$ poise, respectively. The annealing point is the temperature at which internal stresses are relieved in a matter of minutes.

Glass is melted and fined at viscosities between 50 and 500 poise; it is pressed to form bottles, tumblers, etc. around 10^3 poise. It can be drawn into rods and fibers between 10^4 and 10^5 poise. The working point, the temperature at which glass is soft enough for hot-working

by most of the common processes corresponds to about 10^4 poise viscosity. Soda-lime silica glass has working point about 1000°C. The softening point for this common commercial glass, the point at which the glass will rapidly deform under its own weight, is about 700°C, and the annealing point is about 540°C. Pyrex, one of the most common borosilicate glasses, has annealing point about 580°C, softening point about 840°C, and working point about 1230°C. Fused silica has annealing point over 1100°C and softening point near 1500°C.

In research dealing with optical and electrical properties of vitreous materials it is often helpful to have data on basic thermal properties like specific heat and viscosity, which are in many cases related to the structural properties involved in absorption and transmission of electromagnetic radiation and in passage of electric current. A device of fairly recent invention for measuring specific heat and heat of transformation with considerable accuracy and speed is the differential scanning calorimeter. In this device the power required to raise the temperature of a small sample, of mass between 5 and 200 milligrams, can be measured over a considerable range of temperature, and a number of different rates of heating; the heat evolved in cooling processes can also be measured. The upper temperature limit for instruments thus far developed is 725°C, and hence the use of the DSC has thus far been limited to rather "soft" glasses.

Viscosity measurements between 10^0 and 10^7 poise, and over a temperature range between 900°C and 1500°C are usually made with rotating concentric cylinder devices similar to those used for ordinary liquids at much lower temperatures. For higher viscosities the fiber elongation method is often used; this requires much skill, even for glasses which form satisfactory fibers; a considerable number of glass compositions do not form fibers at all. Hence other methods have been sought.

VI. THE BEAM-BENDING METHOD FOR DETERMINING VISCOCITY OF GLASS

The theory of the beam-bending method for determining the

viscosity of glass was established over 60 years ago when Trouton[5] gave the general formula

$$\eta=\frac{gL^3}{2.4I_c v}\left[M+\frac{\rho AL}{1.6}\right] \qquad (1)$$

where η=viscosity (poise), g=acceleration due to gravity (cm/sec^2), I_c=cross-section moment of inertia (cm^4), v=mid-point deflection rate of beam (cm/min), ρ=density of the glass (gm/cm^3) A=cross-sectional area of the beam (cm^2), L=support span (cm), and M=centrally applied load (gm). The second term in the brackets accounts for the weight of the beam contributing to its own bending, which is usually so small that it can be neglected. In order to keep strictly c. g. s. units we use the equation in the form: $\eta=\frac{gL^3M}{144I_c v}$. For our apparatus L^3=179 cm^3 and M has a minimum value 42 grams corresponding to the empty loading pan plus associated hooks and the LVDT core. To determine v the LVDT constant (14.848 volts/inch deflection for our model) is used along with the slope of the deflection trace on the recorder chart.

Early reports of experiments using this technique[6] showed serious disagreement with fiber elongation results for the same glass. The work of Hagy[7] at the Research Center of the Corning Glass Works at Corning, N. Y., U. S. A. has established the usefulness of this technique. The ASTM has approved this method and has issued a bulletin (C 598) establishing procedures for its use. Our apparatus is rather simpler and bulkier than that described in Hagy's paper. Probably the main source of error is the uncertainty in the thermal expansion background: the loading rod's expansion is different from that of the brick supports on which the support span for the glass beam rests. Since the ASTM procedure requires deflection measurements during "cooling at a rate of 4±1 °C/min" we have had to

(5) Trouton, F. T. *Coefficient of viscous traction and its relation to that of viscosity*; *Proc. Roy. Soc.* (*Londcn*) **77** 426 (1906).

(6) Jones, G. O. *Determination of elastic and viscous properties of glass at temperatures below annealing range*; *J. Soc. Glass Technol.* **28** 432-462 (1944).

(7) Hagy, H. E. *Experimental evaluation of beam-bending method of determining glass viscosities in the range 10^8 to 10^{15} poises*; *J. Amer.Ceram. Soc.* **46** 93-97 (1963).

determine correction constants by measuring the deflection recorded for a thick, non-bending beam of fused silica glass while the temperature decreases at the prescribed rate. Standardization runs using samples of NBS No. 710 glass give results within 2°C of the accepted 546°C value for the annealing point (10^{13} poise) of this glass.

Our apparatus is not able to go to the temperature of 1500°C claimed for Hagy's design. In fact, the beam-bending method is not suited for determining the softening point (about 700°C) of soda-lime glass, since the bending rate of beams of usable size is too rapid to be measured. Extrapolation from beam-bending results can be used to determine the value for viscosity $10^{7.6}$ poise, as mentioned in the Hagy reference.

But a more direct measurement of this important temperature seems preferable. A parallel-plate viscometer based on a design by Fontana[8], also of the Corning research staff, has been made for use here at Fu Jen University in the shop of the Physics Department of The Catholic University of America in Washington, D.C., U.S.A. This device uses cylindrical samples about 6 mm in diameter and 6 mm high; the LVDT records the rate of compression of this cylinder as the temperature is increased.

VII. CURRENT GLASS RESEARCH PROJECTS

Work with the beam-bending apparatus in our laboratory thus far has been on two projects: A) Alkali-silicate glass samples from the Vitreous State Laboratory at The Catholic University of America in Washington, D.C., U.S.A.; and B) Commercial glass samples from Taiwan Glass Corporation[9]

---

(8) Fontana, E.H. *A parallel-plate viscometer for glass viscosity measurements to 1000°C*; *Amer. Ceram. Soc. Bull.* **49** 594-597 (1970). The author here acknowledges with pleasure and gratitude the courtesy shown him on a visit to the Sullivan Park Research Center of the Corning Glass Works in September 1972. The generous cooperation of Raymond R. Barber of the Technical Information Center at Corning is also gratefully acknowledged.

A. Cooperative Work with Catholic University, Washington, D.C.

A program investigating properties of Na_2O–SiO_2 and K_2O–SiO_2 systems, without stabilizing additives, is under way in the Physics Department in Washington: reflection and transmission studies using laser beams, and electron microscopy of thin sections are techniques being used there. From them we have received two lots of samples for viscosity measurements and have sent detailed results to Washington. As mentioned above (pg. 83) soda and potash are frequently used as fluxes in glass mixes. But where alkali concentration is high chemical durability is poor; the research glass samples sent are hygroscopic and must be kept in dessicators. We give here a brief summary of our results.

1. *Soda and Soda-potash Compositions*

The first samples consisted of rectangular bars of four compositions: #1, $0.25Na_2O$–$0.75SiO_2$; #2, $0.33Na_2O$–$0.67SiO_2$; #3, $0125Na_2O$–$0.125K_2O$–$0.75SiO_2$; #4, $0.05Na_2O$–$0.245K_2O$–$0.74SiO_2$. For each composition a series of "runs" was made, begining with a constant temperature near the point where viscous flow begins and continuing measurements at constant temperatures increasingly higher to the point where the bending is too rapid to measure conveniently. After each series of constant-temperature runs one or two runs were made at decreasing temperature according to the procedure described in the ASTM bulletin mentioned above (pg. 88).

In using this procedure, equation (1), page 88, is modified to give a deflection rate corresponding to 10^{13} poise, which has been established as the annealing point for a glass:

$$\text{Deflection rate (cm/min)} = \frac{2.67(10^{-11})L^3M}{I_c}$$

where L, M, and I_c are the quantities specified above. Using this

(9) Through arrangements made by Mr. Rudi Yang of National Tsing Hua University, Hsinchu, Taiwan, and accompanied by him, Dr. H. Hesselfeld and the author visited the large Hsiang Shan Plant of the Taiwan Glass Corporation near Hsinchu in March 1972. We wish to express our gratitude here to Mr. Yang and to the management of the plant, especially Messrs. Lin Por-Fong, Lin Tsun-Lee, and H. W. Chang.

equation involves plotting the midpoint viscous deflection rates from the recorder chart as ordinates on a logarithmic scale against temperature as abscissae. Glass bending normally under load in the temperature span used for one of these plots will give a straight line on the graph; the annealing temperature is found by finding where the calculated value of the ordinate crosses this line, then reading below the corresponding temperature.

Over fifty such series of measurements were made for the four compositions of this group between April and June 1972. The constant-temperature runs for each composition were summarized on rectangular-coordinate graphs of log η vs 1/T°K. While the "scatter" was considerable on each of the four graphs, the consistency of the results was unmistakable and a good median line could be drawn to give acceptable values for viscosities from 10^{11} to 10^{14} poise. The agreement of the values for 10^{13} poise as determined by the two different methods was fairly satisfactory in all four cases, the values from the decreasing-temperature graphs corresponding quite well with those for bending at constant temperature.

The average values for the annealing point (10^{13} poise) as determined by the ASTM procedure were:

Glass #1 464°C	Glass #3 432°C
Glass #2 444°C	Glass #4 483°C

As expected, increasing soda content "softens" the glass noticeably. But substituting potash for soda in equal proportions in Glass #3 did not harden it: the annealing temperature is lower than for Glass #1, also a 75% silica glass. However, substituting potash for practically all the soda yields the "hardest" glass in the group.

2. *Potash-silica Compositions*

A second series of samples sent from Washington consisted of beams of four other compositions: #1, $0.25K_2O$–$0.75SiO_2$; #2, $033K_2O$–$0.67SiO_2$; #3, $0.38K_2O$–$0.62SiO_2$; and #4, SrO–K_2O–SiO_2. The relative amounts were not given for the #4 glass.

Viscosity measurements were made as for the first series and summarized results sent to Washington in the form of log vs 1/T°K plots for each composition as before. Agreement of the 10^{13} poise

temperature values as determined by the two different methods was not as good; especially for the #3 glass of this series there was considerable difference; this composition is the most hygroscopic of all those sent. The graphs, however, showed much the same uniformity as those of Series 1 above.

Average values for the annealing temperature as determined by the ASTM procedure were:

Glass #1 491°C[10]	Glass #3 463°C
Glass #2 484°C	Glass #4 596°C

The SrO–K_2O–SiO_2 glass is the hardest of any we have worked with thus far; it compares favorably with the commercial borosilicate glass Pyrex. Without some knowledge of the relative amounts of the three oxides in the mix little can be said.

B. Measurements of Samples from Taiwan Glass Corporation

1. *Flat Glass and Container Glass*

The first samples from Hsinchu came in March, in the form of rods drawn from the melt in the furnace. They were of three kinds, labeled Mountainside Flat, Seaside Flat, and Container, representing samples from the three production lines in continuous operation at this large commercial establishment. All were soda-lime glass, of fairly standard composition: chemical compositions were given for the two different varieties.

The principal test used in the Quality Control Division at the plant is one of density; a flame spectrometer is available, but not in regular use. Our hopes of being able to establish significant differences in the viscosity temperatures for the three different kinds of samples were not realized; in fact, we are still working to get a better picture of the difference between the two varieties, Flat and Container. The first samples were tapered, and had elliptical cross-sections. The critical value of I_c, which figures prominently in the

(10) This value agrees quite well with Glass #4 of Series 1 above, almost the same composition; apparently soda is a more effective "softener" than potash and has less effect on chemical durability. An explantion for the low value of the annealing temperature for Glass #3 of Series 1: $0.125K_2O$–$0.125Na_2O$–$0.75SiO_2$ remains to be given.

equation for viscosity, had a large percent of indeterminate error and the first results had little uniformity.

From the chemical composition, the most significant difference between the two glasses is in CaO and MgO content: Container glass has 10% CaO while the Flat glass in production at Hsinchu has about 7.75% CaO. However, the Flat glass has 4% magnesia, while the Container glass has only $\frac{1}{4}$% magnesia. The Container glass also has about $\frac{1}{2}$% borax, which is entirely absent in the Flat glass composition.

In May 1972 some better samples came from Hsinchu; Flat glass samples of 5 mm thickness were supplied from cut-offs in the regular production line. From these we have cut good rectangular beams with a Buehler "Isomet" diamond saw now available in our laboratory. The round rods of Container glass sent at the same time were considerably better, with less taper and flatness. Results from log η vs 1/T°C plots for a series of measurements on five samples of each glass were:

	Flat Glass	Container Glass
Strain Point ($10^{14.5}$p.)	500.5°C	504°C
Annealing Point	541°	543°
Softening Point ($10^{7.6}$p.)	723°	718°(11)

Work at present under way in the laboratory with additional samples of these two kinds of glass from Hsinchu has the purpose of better establishing the viscosity difference between these two production glasses.

VIII. CONCLUSIONS

Useful data concerning properties of glasses can be obtained with rather simple apparatus. It is gratifying to report that our application for cooperative research support from the National Science Council in Taiwan has received a favorable response, and we hope

(11) These values were obtained by extrapolation on the plots; such wide extrapolation is not recommended. A direct measurement of the softening temperature will be made when we are able to put our parallel-plate viscometer into service.

to enlarge the scope of our activity. At present there is little research activity in vitreous materials in Taiwan. The extensive production facilities in glass and plastics manufacture offer a good field for development of new products. We hope that thermal analysis work in our laboratory can be of service in this field.

Our project has also furnished some scope for undergraduate student work in the laboratory. Routine measurements and calculations are being done by students; one of them is now operating the beam-bending apparatus independently. More of them will be able to become acquainted with this work as new equipment is added; we feel that our project affords useful training for later activities in the laboratory.

THE AIR POLLUTION PROBLEM IN TAIWAN, REPUBLIC OF CHINA

YEONG FANG

INTRODUCTION

The major task of men nowadays is how to treat the by-products of modern science, the so called "pollution" problems, such as air water, land, noise and radiation pollutions. These have seriously annoyed and worried people all over the world.

Research on these problems has been carried on and is well established in many countries, especially in America, Russia, Sweden, Japan, Germany and Australia. However, Taiwan is still in her starting step. The pollution problems have become serious due to the acceleration of economic development and the fast increase of population in a small island. It seems urgent to study the problem and provide a positive scheme for applying corrective action to reduce the pollution.

This report is a survey of the air pollution problem in Taiwan. The first source of information is provided by "The Institute of the Environmental Sanitation Department (IESD)".[1] The 4th section of the institute is responsible for the air pollution control in all the cities and industrial areas except Taipei city. The second source of information is provided by "The Taipei Municipal Environmental Sanitation Department (MESD)" which controls the air quality of Taipei city and the near-by industrial areas.[2]

Air pollution control started in Taiwan under IESD in 1961. The two initial measurements were on dust fall and suspended particulates. Not until July 1969, when the "Taiwan Provincial Five Year Plan for Environmental Sanitation Improvement" was approved by the Provincial Government, had air pollution control become formally established. The major work of this plan on air pollution includes the following:

1. Setting up of air pollution monitoring stations in most large cities (excluding Taipei city) and industrial areas in the counties.

2. Supervision of and technical guidance for the factories.

3. Legislation-preparation of draft of clean air acts and regulations.

4. Public education on air pollution.

This plan is financially supported by the County Government with 100,000 NT/yr., by the Provincial Government with 1,000,000 NT/yr, and by the China-America Foundation with 1,000,000 NT/yr, (40 NT=1 US Dollar).

There is a total of 71 monitoring stations distributed in 13 different cities/counties, which include residential, commercial and industrial areas. These monitoring stations are listed below:

Cities/counties	Number of stations
Keelung city	5
Taichung city	6
Tainan city	4
Kaohsiung city	12
Ilan county	8
Taipei county	9
Taoyuan county	3
Hsinchu county	3
Changhua county	5
Chiayi county	4
Tainan county	5
Kaohsiung county	5
Taichung county	2

In addition to dust fall and suspended particulates, the smoke concentration, stack smoke emission, SO_2, H_2S, NO_2, Cl_2 and F_2 concentrations were analyzed. These are listed below:

Item	Unit	Sampling apparatus
Dust fall	tons/sq. mile/ month	Glass jar 6″ in diameter
Suspended particulates	$\mu g/m^3$ of air	Staplex High Volume Air Sampler
Smoke concentration	COHS/1000 ft	AISI Automatic Tape Sampler

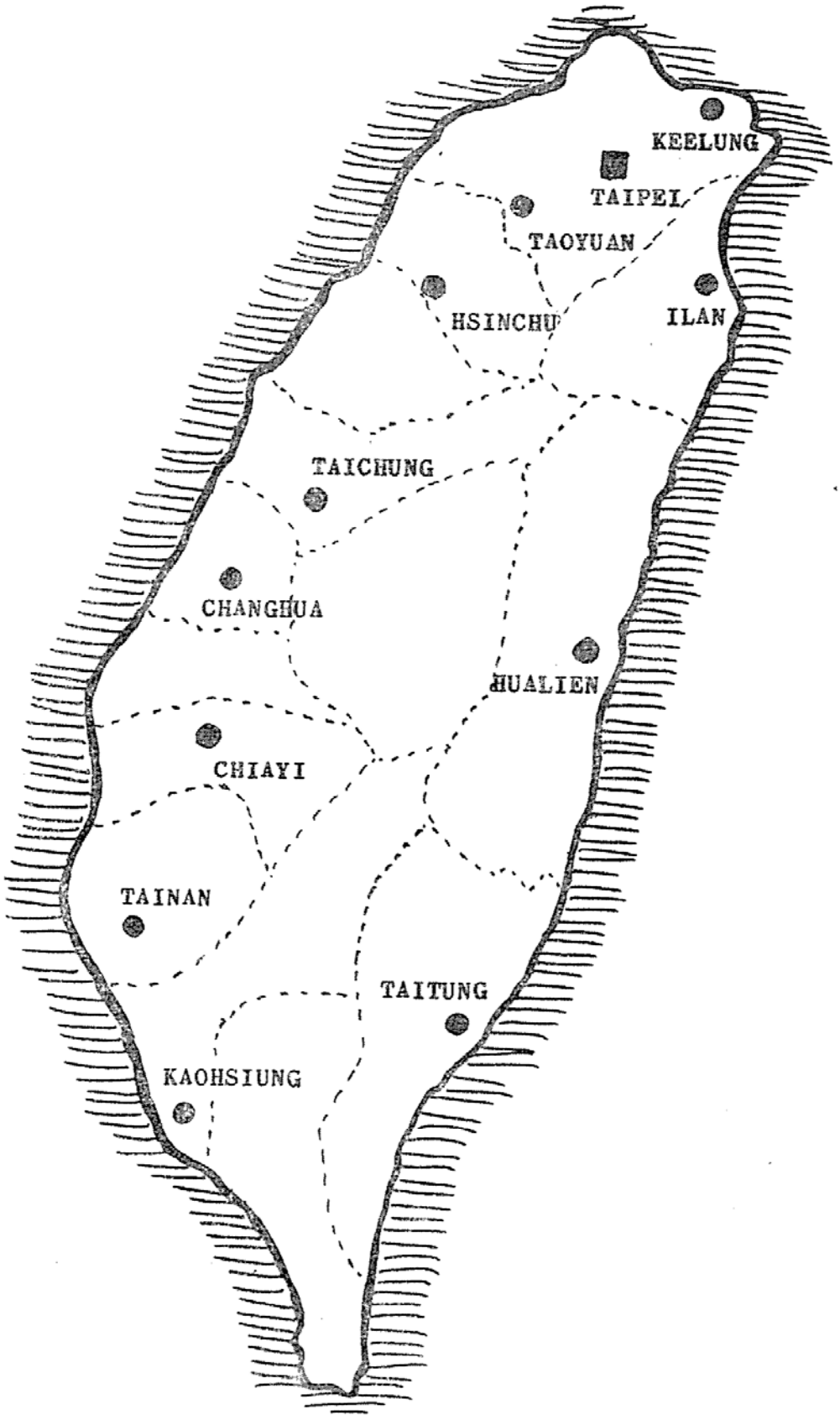

Fig. Map of Taiwan

Stack smoke emission	No. of Ringelmann	Ringelmann Chart
SO_2 concentration	ppm	S/I SO_2 Analyzer/Recorder
H_2S concentration	ppm	AISI Automatic H_2S Tape Sampler
NO_2 concentration	ppm	NO & NO_2 Analyzer/ Recorder
Cl_2 & F concentration	ppm	MAST Microcoulomb Recorder

The Taipei Municipal Environmental Sanitation Department joined the monitoring work in 1968. Up to 1971, twelve monitoring stations had been set up and one movable monitoring unit became available. The distribution of these 12 stations is listed below:

Code	Location	Kind of area
1	Kungting Road	Commercial
2	Tungyuan Primary School	Industrial
3	Mindsu Junior high-school	Industrial & residential
4	Chungshan	Industrial & residential
5	Nankang District Office	Industrial
6	Tachi Bus Station	Industrial & residential
7	Peitou	Residential
8	Shihlin	Commercial, industrial & residential
9	Yangmingshan	Residential
10	Kuting	Commercial & residential
11	Chingmei	Residential
12	Mucha	Residential

Items of sampling and analysis carried at MESD are: total particulates, dust fall, SO_2 concentration, stack smoke emission, lead content (using a Perkin Elmer Atomic Absorption Spectro-photometer), CO and NO_2 concentrations. In addition, the topographical, meteorological conditions and wind direction/velocity were also studied.

CLASSIFICATION OF AIR POLLUTION

Before going into the analysis of data, we look into the classification and source of different pollutants. These can be classified

into two categories:[7,8]

(1) Particulates including smoke, dust, fly ashes and fumes.

(2) Vapor and poisonous gases including SO_x, H_2S, NO_x, Cl_2, F, hydrocarbons, etc.

SOURCES OF AIR POLLUTANTS

1. Black *smoke* is caused mainly by incomplete combustion of soft coal which is used in factories, restaurants, hotels, residential buildings, steam engine locomotives, commercial and military ships. In the north section of Taiwan there are many coal mines; and coal is cheaper than other fuels. Black smoke becomes a serious problem in northern Taiwan. Heavy smoke also comes from heavy oil burners whenever the fuel/air ratio is too high. This happens in most kitchens in public schools, residential, or commercial areas. The heavy smoke emission is also due to open burning of garbage, agricultural waste and asphalt for road paving. Motor vehicle engines often emit smoke, especially when first started. Buses and trucks use diesel oil which is a lower quality fuel compared to gasoline. Improper driving technique, overloading, poor maintenance, and aging of vehicles are all factors which contribute to smoke from motor vehicles.

2. *Dust* is generally caused by building and road constructions, while fly ash comes from cement plants, lumber yards, calcium carbide plants, and the grinding of phosphate in fertilizer companies.

3. *Fumes* are emitted from iron and aluminum smelters or foundries. They contain iron oxide, zinc oxide, cupric oxide, etc.

4. *Poisonous gases* and vapors are emitted from different factories:

(i) The soft coal in Taiwan contains 1–3% sulfide and petroleum contains 3% sulfide. When they are burnt, SO_2 or SO_3 (to a lesser extent) are formed. SO_2 also leaks from sulfuric acid plants.

(ii) H_2S from oil refineries, coal gas works, other chemical factories, paper mills, and sewage plants.

(iii) NO_2 from fertilizer and nitric acid plants, and from motor vehicles.

(iv) CO due to the incomplete burning of gasoline through internal combustion engines of automobiles or from the combustion of coal.

PROPOSED STANDARD

At present there is only one local regulation to control air pollution—the "Air Pollution control measurement in Taipei city". A nation-wide air pollution control regulation was drafted four years ago, but is still waiting to be passed by the Executive Yuan.

The following standards are known as the "Stack Emission Standards", and are only effective in the Taipei area.

Poisonous gases	ppm	Poisonous gases	ppm
CH_3CHCHO	0.5	SO_2	1.5
CH_3CHO	50	NO_2	1.5
NH_3	30	CS_2	5
CO	30	H_2CO_3	1.5
$C_2H_5SO_4H$	15	HF	1.0
HCl	1.5	$C_6H_5CH_3$	50
Cl_2	0.3	photoxidant	0.3
PCl_3	0.2	PH_3	0.02
$C_6H_4(CH_3)_2$	50	HCHO	1.5
gasoline	150	$CH_3COC_2H_5$	50
HCN	3	H_2S	3
HI	0.02	$C_6H_5CH_3$	50
$CHClCCl_2$	30	C_6H_6	10

Dust, fly ashes, or fumes	$\mu g/m^3$ of air at 0°C. 1 atm
CRO_3	0.03
CN	1.5
F	1.5
Pb	0.05
PCl_5	0.3
H_2SO_4	0.3
dust	5

The smoke concentration is limited to No. 2 of the Ringelmann chart.

While starting the fire, the No. 3 Ringelmann is allowed, but no longer than 3 minutes.

Regulations for the exhaust gas from motor vehicles have not been established.

THE EFFECTS OF AIR POLLUTION

General effects on human health

It is our respiratory system, particularly our lungs, that are most sensitive to polluted air. The common diseases are emphysema, chronic bronchitis, chronic constructive ventilatory disease, bronchial asthma, common cold, acute infection of the upper respiratory tract, and lung cancer.[3] Research on the effects of air pollution on human health has not been done in Taiwan. However, analyzing the medical cases from the 1970 report of the Institute of Environmental Sanitation, Taiwan Provincial Health Department, it was discovered that the death rate from respiratory ailments, such as acute upper respiratory infections, lobar pneumonia, bronchopneumonia and acute bronchitis, are surprisingly high. The total death record due to these ailments shows 5754 persons in one year.[4] There may be a direct relation to the high degree of air pollution in Taiwan.

The diseases caused by different pollutants

The dimensions of the *particulates* can vary from 0.01 μ to 100 μ. The dust fall usually has sizes between 10 μ–20 μ and and will eventually settle down to the ground by gravity. The suspended particulates have sizes ranging from 0.1 μ to 1 μ. Particulates when combined with SO_2 mist will penetrate deep into the lungs and will cause more damage than particulates alone. Other poisonous particulates such as arsenic, given off by copper smelters, is suspected to cause cancer. Asbestors fibers have been associated with chronic lung diseases. Beryllium, used in rocket engines, appears to produce tumors. Cadmium is a respiratory poison and may contribute to high blood pressure and heart disease. Fluorides are discharged into the air during the manufacture of phosphate fertilizers and cause severe damage to cattle and to vegetation. The crippling skeletal disease

in cattle is called Fluorosis. Lead is a cumulative poison and is discharged into the air by motor vehicles due to the decomposition of tetraethyl lead used as the antiknock in gasoline. Lead can damage the brain of young children and impair the functioning of the nerve system in adults.

Carbon monoxide is discharged mainly from motor vehicles due to incomplete combustion of gasoline. Carbon monoxide combines with hemoglobin about 210 times faster than oxygen and effectively prevents the transport of oxygen from lung to tissue. Persons having chronic heart disease, lung disease, or anemia are the most susceptible and experience dizziness, headache and lassitude. Higher concentrations and longer exposure will cause death. The highest allowable concentration in the air is 100 ppm. Cigarette smoking subjects the lung to a constant poisoning equivalent to breathing air with 120 ppm of CO.[5]

Sulfuric acids, SO_2, and SO_3, combine with water to form acid mist in the air. This mist can scatter light, reduce visibility, corrode metals, and destroy sculptures. SO_2 alone will irritate the upper respiratory tract and, if absorbed on particulate matter, will penetrate deep into the lungs and damage the tissue. Prolonged exposure to relatively low levels of SO_2 has been associated with increased cardiovascular mortality in older people; prolonged exposure to higher concentration increases the respiratory death rate. The highest allowable concentration in air is 5 ppm.

Nitrogen dioxide (NO_2) is a brownish red, extremely poisonous gas. It reacts with water and forms nitric acid which is as corrosive as sulfuric acid. During the morning rush hours, the NO_2 discharged from motors reaches a peak. It absorbs light in the blue region of the spectrum and is responsible for the brownish haze that stains the sky. The NO_2 reacts with hydrocarbons (exhaust gas from motors) and forms the photoxidants. The oxidants combine with particulates to form the smog, known as the "Los Angeles Smog." The mechanism of photochemical smog has been proposed as follows:[6]

$$NO_2 + h\nu \longrightarrow NO + O$$

$$RH+O \longrightarrow R+OH$$
$$R+O_2 \longrightarrow RO_2$$
$$RO_2+O_2 \longrightarrow RO+O_3$$
$$O_3+RH \longrightarrow \text{Photochemical oxidants.}$$

The most common effects of oxidants on the human body are eye, nose, and throat irritations, When the concentration of smog reaches 0.1 ppm, it blurrs the visibility to less than 3 miles and causes airplane accidents.

Ozone (O_3) is a pale-blue poisonous gas which can severely irritate mucous membranes, nose and throat, if exposed to it for more than 30 minutes. At higher concentrations ozone will interfere with the lung diffusion capacity and will lead to bronchial irritation, slight coughing, soreness in the chest, difficulty in breathing and wheezing. The highest allowable concentration of ozone in air is 0.1 ppm.

The *hydrocarbons* are also dangerous. Most aromatic aldehydes and heterocyclics are known to be carcinogens, especially 3, 4–benzpyrene components. Formaldehyde stops ciliary movement in 150 seconds at 0.5 ppm. Ketone destroys alveolar tissue (an air cell of the lung) in 10 minutes at 17 ppm. Peroxyacyl nitrate (PAN) irritates the eye at 2 ppm within 5 min.

Hydrogen sulfide, (H_2S) is a colorless and poisonous gas which has the smell of rotton eggs. Exposure to H_2S can cause headache and vomiting and longer exposure can cause death. It tarnishes silver and copper and combines with heavy metals, discoloring their surfaces.

Chlorine gas (Cl_2) is a greenish yellow irritating gas. Cl_2 can cause eye, nose, and throat irritation and is highly corrosive to metals when it reacts with water to form hydrochloric acid. The highest concentration is 1 ppm.

In Taiwan, damage to crops and vegetation by air pollution has been observed in 14 cities/counties. Up to 1969, a total of 67 cases were reported by farmers and residents whose properties and crops were damaged. Since a nationwide air pollution control policy has not been passed, a public hearing is used to solve the problems

between the victim and the owner of the factory. This is a slow and less effective method. Kaohsiung Ammonium Sulfate Corporation formerly paid 6 million NT per year to farmers until their SO_2 recovery plant was set up in 1960.

Air pollution accelerates the deterioration of materials, buildings, and metals. This, in turn, greatly increases maintenance and replacement costs. Metal corrodes, fabric weakens and fades, leather softens, rubber cracks, paint is discolored, glass is etched, and paper becomes brittle. It has been estimated that in Taipei city alone, air pollution costs residents more than 30 million NT for laundry expenses in 1972.

The degree of air pollution in Taiwan

The air pollution condition of Taiwan in 1972 has been compared with a few cities of the United States in 1955 (this is the only data available at present).[1] This comparison is shown in Table 1.

The items of analysis are: total particulates, dust fall, and smoke concentration (expressed in terms of COHS/1000 ft value). The total particulate content was further analyzed for its organic matter, water soluble matter, and water insoluble matter. The constituents of the organic matter were not analyzed, but in the water soluble matter, chloride (expressed as NaCl), nitrate, and sulfate contents were examined. In the water insoluble matter, lead, iron, and calcium contents were analyzed.

Comparing the total particulates, it was found. that Detroit has the highest level (344 $\mu g/m^3$ of air), Kaohsiung city ranks second and has the value of 306.9 $\mu g/m^3$. Taipei county follows with 285.3 $\mu g/m^3$, a little higher than Chicago which has 280 $\mu g/m^3$. All these cities are considered seriously polluted according to the standard set by the U. S. and Australia. The average dust fall of Taiwan including 12 cities/counties is 229.21 $\mu g/m^3$.

The average organic matter in total particulates is 19.08 $\mu g/m^3$. St. Louis has the highest level and reaches the value of 31.2 $\mu g/m^3$. Taipei county ranks second (24.03 $\mu g/m^3$). Taichung city follows with 23.26 $\mu g/m^3$, then Changhua county with 23.21 $\mu g/m^3$. Both are slightly higher than New York which has 22 $\mu g/m^3$ and Detroit with 21 $\mu g/m^3$. The amount of organic matter is often used to estimate

Table 1. Comparison of the pollutants in suspended particulates ($\mu g/m^3$) between Taiwan (1972) and U. S. A. (1955)

Taiwan	total particulate	organic matter	water insoluble matter	water soluble matter	chloride	nitrate	sulfate	Pb	Fe	Ca
Keelung city	246.48	18.23	94.66	151.99	4.40	7.61	21.17	0.11	3.83	13.29
Taichung city	225.16	23.26	93.55	132.39	2.78	11.30	20.06	0.13	2.80	9.74
Tainan city	224.54	16.50	96.57	127.98	4.00	8.03	17.74	0.13	2.19	13.55
Kaohsiung city	306.90	18 71	105.66	199.43	5.40	9.15	25.19	0.19	3.87	18.39
Ilan county	223.32	18.52	90.04	132.44	3.43	9.23	17.00	0.09	1.70	17.81
Taipei county	285.30	24.03	85.39	191.58	3.52	9.78	19.23	0.15	3.85	14.34
Taoyuan county	193.63	20.63	84.15	110.44	3.32	9.45	17.14	0.17	2.42	11.00
Hsinchu county	200.96	16.63	81.92	128.76	2.75	7.42	18.59	0.10	3.12	14.54
Changhua county	245.77	23.21	89.68	155.98	2.99	9.05	18.27	0.09	2.40	10.62
Chiayi county	205.75	18.42	93.65	116.89	4.66	11 56	19.97	0.12	2.26	10.48
Tainan county	186.26	13.82	80.59	107.61	2.40	8.34	17.95	0.12	1.88	10.53
Kaohsiung county	217.36	16.98	84.89	132.47	3.44	8.92	19.70	0.13	1.65	15.49
total average	229.21	19.08	90.06	140.66	3.59	9.15	19.33	0.13	2.66	13.32
percentage %	100.00	8.33	39.29	61.37	1.57	3.99	8.43	0.06	1.16	5.80
U. S. A.										
Los Angeles	265				5.13	1.44	14.4	5.2	4.7	2.5
Philadelphia	188					1.6	15.6	9.5	6.5	
Chicago	280					1.7	9.4	2.8	7.9	
New York	244	22				0.8	14.8	2.8	5.2	
Kansas	146					0.6	1.5	1.0	4.1	
Houston	129					1.0	2.4	1.0	4.0	
San Francisco	104					3.4	1.8	2.4	2.4	
Cincinnati	176				71.7	1.0	5.6	1.6	4.5	65
St. Louis		31.2								
Windsor		7.8								13.88
Detroit	344	21				1.2	7.5	2.9	8.3	

the smoke concentration. Only four cities were examined for their smoke concentration: Taipei county is the highest and has 3.10 COHS/1000 ft; Keelung city has 2.1; Kaohsiung city 2.0; and Taichung city 1.9. The degree of pollution based on COHS/1000 ft, set by the New Jersey Department of Health, is given below:

COHS/1000 ft	degree of pollution
0–0.9	insignificant
1.0–1.9	slightly polluted
2.0–2.9	polluted
3.0–3.9	serious
4.0 and above	very serious

According to this standard, Taipei county is in a serious condition. Keelung and Kaohsiung cities are both considered polluted. Taichung city is slightly polluted. It is interesting to note that although Kaohsiung city has the highest amount of suspended particulates among all the cities on the island, the organic matter is not the highest, nor is the smoke concentration. Instead, Taipei county is the highest both in organic matter and smoke concentration. This is because of the fact that factories in Kaohsiung do not use coal as their major energy source, whereas in Taipei county they do.

Of the total particulates, 61.37% is water soluble matter. The sulfate content constitutes 8.43% of the total particulates; 3.99% is nitrate; and 1.57% is chloride. Kaohsiung has the highest sulfate content among all the cities, namely 25.19 $\mu g/m^3$. Next is Keelung 21.17 $\mu g/m^5$, and third is Taichung with 20.06 $\mu g/m^3$. The average value of sulfate content of Taiwan is 19.33 $\mu g/m^3$, which is higher than that of U. S. A. (8.11 $\mu g/m^3$). The chloride content is difficult to compare since information from only two cities in the U. S. is available. Cincinnati has 71.7 $\mu g/m^3$ and the highest value of Taiwan is 5.40 $\mu g/m^3$ (Kaohsiung city.)

The water insoluble matter constitutes 39.29% of the total particulates. The average lead content is relatively low when compared with the United States: 0.13 to 2.9 $\mu g/m^3$ respectively. This is because of the lower rate of traffic flow in Taiwan. Kaohsiung city

is the highest in iron content among all the cities, 3.87 $\mu g/m^3$. This is easy to understand as there are 450 iron smelters and 99 metal works in Kaohsiung city. The average iron content is 1.16 $\mu g/m^3$ which is lower than 5.29 $\mu g/m^3$ in the U. S. The calcium content is highest in Kaohsiung city with a value of 18.39 $\mu g/m^3$. When this value is compared with St. Louis with 65.0 $\mu g/m^3$, it is obviously much lower.

In discussing the dust fall, the following standard is used:

Dust fall (ton/m^2/month)	Degree of pollution
0– 10	insignificant
10– 25	slightly polluted
25– 50	polluted
50–100	serious
above 100	very serious

The average dust fall of Taiwan is 23.5 tons/m^2/month which shows a slight pollution. The highest is in Kaohsiung city with 34.6 tons/m^2/month. Taipei county ranks second and has 29 tons/m^2/month. All these cities are considered polluted.

As an overall conclusion, we can say that Taiwan is seriously polluted, especially because of black smoke, fly ash, and sulfate contents. Among all the cities or counties, Kaohsiung city, Keelung city, and Taipei county are the most polluted spots in Taiwan. Tainan county is the least polluted among 12 areas if we exclude the non-industrial areas of Hualien or Taitung. However when discussing the degree of pollution, the use of average values can be misleading.

Factors that influence the air pollution of Taiwan

The highest population density in the world (407 persons/sq. kilometer), the rapid development of industry on a small island, the lack of strong legislative control, the shortage of technicians are the main factors which make the elimination of air pollution in Taiwan a difficult task. The cities have different types of factories, and therefore different pollution problems. In the following discussion we will select the three worst-polluted cities as examples.

Keelung city: There are 24 machinery factories, 20 chemical & fertilizer plants, 14 ship building establishments, 12 soy sauce plants, 10 lumber mills, 10 food manufacturing companies, 9 textile plants, 9 refrigeration plants, 5 electronic plants and 6 other factories. All together there are 119 factories according to data recorded in 1968. The major pollutant is black smoke; next in order are fly ash and poisonous gases. As mentioned before, the northern section of Taiwan is rich in coal mines. Keelung city alone has 43 coal mines. The coal is used not only by most factories but also by commercial and residential areas. Other users are steam locomotives and commercial ships. The fly ash comes from the Taiwan Fertilizer Corporation and results from the process of grinding phosphate. The fumes and poisonous gases come from the smelter of the Fertilizer Corporation. The SO_2 and NO_2 gases originate in the sulfuric acid plant, while CO, NO_2, hydrocarbons and lead particles are exhausts of gasoline cars.

Keelung city is surrounded halfway by mountains which are unfavorable to the dispersion of pollutants. The lack of technicians and the shortage of funds from the city government have made the pollution control very ineffective.

Kaohsiung city: There are 450 iron works, 202 chemical plants, 99 metal works, 76 lumber yards, 65 cement & brick plants, 54 soy sauce plants, 43 food manufacturers, 37 bean-curd plants, 23 clothing factories, 22 leather and rubber companies, 21 oil refining plants, 15 paper mills, and 38 other factories. All together there were 1145 factories recorded in 1968. Kaohsiung city is considered a heavy industrial area. Black smoke comes from the lumber yards which use scrap wood for burning, and large amounts of dust and fly ash are discharged into the atmospere by the cement companies; dust pollution is also due to road construction and to the hot, dry, and windy weather. The fumes come from iron smelters. The poisonous gases are from the petroleum company, the fertilizer corporation, the sulfuric acid plant, the plastic plant, and the aluminum corporation which pollute the air with SO_x, H_2S, CS_2 NO_x, CO, HF, HCl, Cl_2, C_2H_2, C_2H_6 and HCHO.

Taipei county: There are 119 textile plants, 71 machinery factories, 58 iron works, 37 plastic plants, 32 electronics factories, 30 leather and rubber plants, 26 chemical companies, 26 pharmaceutics plants, 23 food corporations, 20 lumber mills, 13 papermills, 11 transportation companies, 12 detergent plants, 10 dye-factories, and 46 other plants. All together there were 534 factories recorded in 1968. The traffic flow rate is the highest on the island. The high density of population, the lack of city planning, and the coal used by factories, residents, hotels etc. make the air pollution control a difficult problem.

Result of sampling and analysis from 12 monitoring stations in Taipei City

The water soluble and insoluble materials (coal tar, combustible matter, and ashes), suspended particulates, SO_2 and Pb concentrations are listed in Table 2. These data were collected from 12 monitoring stations in 1971. Due to insufficient equipment, the CO and NO_2 concentrations were analyzed on only a few streets.

The dust fall is usually related to the condition of coal combustion. The average dust fall in Taipei city is 16.706 tons/km^2/month, and 56.81% is water soluble matter. The amount of water soluble matter is about the same in either industrial, commercial, or residential area. Since soft coal is forbidden in commercial and residential areas, the poisonous gases contained in water-soluble matter will be: SO_2 due to heavy oil, natural gas, CO from motor vehicles and NO_2/ hydrocarbons, photochemical smog etc. There are 2.20% of coal tar, 14.18% of combustible matter and 26.67% of ashes in dust fall. The combustible matter is highest in industrial areas and second highest in commercial areas. This fact indicates that most of the factories use coal without an automatic coal feeder or without using chemical additives. Incomplete combustion often results from manual feeding with overloading and disturbance of the coal bed while cleaning the ashes.

The content of ashes in insoluble matter is higher than combustible matter. The existence of such high value of fly ash is due to road and building construction. If we use the standard for dust fall given above, we can conclude that the dust fall of Taipei city

Table 2. Air Pollutants of dust fall, suspended particulates, SO_2 value (expressed in units of SO_3 mg/day/100 cm PbO_2) and lead content of Taipei city (1971)

Monitoring stations Code No.	Dust fall (ton/km²/month)					suspended particulates μg/m³	SO_2 value	lead content μg/m³
	water soluble matter	water in soluble matter			total amount			
		coal tar	combustible matter	ash				
1	9.140	0.377	1.875	4.921	16.315	274.57	1.026	1.19
2	8.704	0.314	3.146	7.850	19.865	324.99	0.852	1.34
3	10.863	0.336	1.825	3.313	16.523	216.54	0.696	0.22
4	10.531	0.457	3.021	6.094	20.102	413.14	0.879	1.69
5	14.912	0.855	6.439	5.529	27.686	458.62	1.318	2.05
6	10.544	0.343	2.429	4.469	17.815	281.05	0.895	2.72
7	7.047	0.330	1.880	3.297	12.397	208.64	0.771	0.73
8	7.878	0.294	2.224	3.631	14.027	260.58	1.000	0.48
9	4.673	0.256	0.979	2.392	8.348	77.05	1.499	1.11
10	10.160	0.262	1.252	4.274	15.948	157.38	0.562	1.28
11	11.612	0.364	1.572	3.982	17.530	164.88	0.621	0.29
12	7.830	0.226	1.782	3.717	13.916	208.18	0.511	1.28
average	9.491	0.368	2.369	4.456	16.706	253.80	0.886	1.20
%	56.81	2.20	14.18	26.67	100			

is moderate. The more serious problems are suspended particulates, poisonous gases and smog.

The average value of suspended particulates in Taipei is 253 $\mu g/m^3$, which matches with New York in 1955, and is twice that of the average for the U. S. A., (105 $\mu g/m^3$), recorded in 1965 from 291 monitoring stations. The highest recorded amount of suspended particulates (485 $\mu g/m^3$) is in Nankang, an industrial area. This is possibly the highest in the world. The lack of control is obvious. Yangmingshan, a residential area, is lowest in suspended particulates (77.05 $\mu g/m^3$). However, the SO_2 value, expressed as SO_3 mg/day/100 cm^2 PbO_2, is higher at Yangmingshan than at the other stations (1.499). This is not due to the burning of coal but to the many natural sulfide springs. The average SO_2 value in Taipei city is 0.886. The average lead content is 1.2 $\mu g/m^3$ and is the highest on the island. This is directly proportional to the traffic flow rate which has a value lower than that of New York in 1955 (2.8 $\mu g/m^3$).

The pollution from exhaust gases of motor vehicles has been examined on a few streets in Taipei. The traffic flow rate is highest at the intersection of Chungking N. Rd. and Mingcheng W. Rd. with 2500 automobiles/hr. (The ratio of cars to motorcycles at that intersection is 10:6. The exhaust gas from 15 motorcycles is equivalent to that of one car). This figure matches Kasu-Migaseki, Tokyo, Japan, in 1964. With reference to exhaust gases, the average CO concentration in Taipei is 10 ppm, which is within the acceptable safety limit, but the maximum level at Chungshan Police Station reaches 24.75 ppm, indicating slight pollution. (According to the standards of CO concentration set by Japan, the average hourly value for 24 hours continuous monitoring should be below 10 ppm; the average hourly value of 8 hours continuous monitoring should be below 20 ppm). When a car begins to accelerate and later maintains constant speed, the hydrocarbon emission is about 650–1300 ppm. So far no measurement of the hydrocarbon concentration was made. The oxidant value is 0.036 ppm, which is below the critical safety level of 0.05 ppm, recommended by Japan and the U. S. A. The average $\dot{NO}_2$ concentration is 0.039 ppm, also below the critical safety

level of 0.05 as recommended by Japan.

Factors influencing the pollution problem of Taipei city

Population:

The population of Taipei city recorded in 1970 was 1,689,723 which gives the highest population density in the world (6209 persons/sq. kilometer). Of the population growth from 1969 to 1970, 41.4% was due to immigration from other cities of the island.

Factories:

There are 2914 factories in Taipei according to the 1969 statistics. The type of factories are brick and cement plants, coke oven plants, steel mills, fertilizer corporations, chemical factories, and glass factories. Taipei comprises 20,540 registered manufacturing companies; when other trade companies are included, the total is about 25,928. Statistics show that 64% of these added companies are commercial. Taipei is both industrial and commercial.

Topography:

Taipei city has a topography similar to London, England; and Dorona, Pennsylvania. Both of these cities have experienced a recent pollution disaster. Taipei is within a basin surrounded by mountains and hills. A temperature inversion layer is created on top of the city like a lid on a pot which makes the diffusion of the pollutants difficult. In the morning, if the humidity increases above 85%, the SO_2 mist combines with the particulates to form the "London type" smog. At noon, if the humidity is below 75%, the ozone, nitrogen dioxide, and hydrocarbons result in a "Los Angeles type" smog. The average wind velocity is 3.23 miles/hr which is not too helpful for the dispersion. To the north of Taipei is the Keelung industrial area. On the south-west side are Sanchung, Hsinchuang, Chungho, and Panchiao, all of which are industrial towns. The wind direction is generally easterly (E 24.9%, ESE 18.6%, ENE 11.05%) and the high concentration of suspended particulates in Taipei is due to the pollutants flowing in from these nearby cities. The Central Mountains do not favor the dispersion either.

Traffic:

The high traffic flow rate, bad driving habits of most drivers,

over-loading, poor maintenance and aging of cars, are the factors that cause the high amount of exhaust gases in Taiwan's big cities.

Methods of control of air pollution used in Taiwan[1,8]

Smoke elimination recommendations:

1. Proper selection of fuel and banning the use of soft coal for residential areas restaurants, hotels or schools. Encouraging the use of electric heating and shifting to heavy oil for industries.

2. Use of correct type and proper installation of boilers, with complete combustion facilities; prohibiting overloading of coal. Chain stokers or screw type under-feed stokers are recommended; the proper oil/air ratio should be maintained. The stack height should be a minimum of 20 meters. Chemical additives in fuels must be used regularly. An example is Wei Chuan Food Manufacture Co. at Sanchung, which uses a chain stoker and supplies a chemical additive while burning the coal. Complete combustion is achieved and there is no smoke. They estimated that 150,000 NT/month is saved due to the complete combustion of coal. For manual coal feeding an example is the Tien Bian Pharmaceutical Company in Sanchung. They have shifted to high-quality coal and used chemical additives. The stack smoke emission was reduced below No. 1 of Ringelman. For wood burning boilers, the chipper and automatic feeder system should be used. Examples of this type of control are Taiwan Lumber Yard and Kuo Feng Lumber Yard in Kaohsiung. A complete combustion can be achieved without smoke. Factories which have shifted from coal to heavy oil and use an automatic fuel/air controler are Wan Chia Hsiang Soy-sauce Company and Ta Hwa Brick Yard in Kaohsiung. These have no further smoke problems; however, the SO_2 emission is increased.

Dust and fume elimination

1. Multiple cyclones, bag filters and electrostatic precipitators are recommended for cement and grinding workshops. Examples are the Chang Hsin Iron Smelter in Sungshan, which uses a filter-bag house, and the Taiwan Cement Company and South-East Cement Company in Kaohsiung; both of these use electrostatic precipitators to collect the fly ash. The effect is good and the cement collected

saves money for the company.

2. Wet scrubbers are recommended for metal fumes collection such as the scrap metal recovery works Tang Rung Iron Smelter Co. in Hsichi. When the wet scrubber method is used, the waste water should be precipitated and filtered before discharging back into the stream.

Vapor and poisonous gas elimination: Recommendations here are:

1. A change in the method of manufacturing, such as the adoption of a double conversion system for sulfuric acid manufacturing.

2. The recovering of emitted gases such as the use of NaOH, NH_4OH, or H_2O to absorb SO_2, SO_3, NO_2 and H_2S. Companies which use this method are Kaohsiung Ammonium Sulfate Corporation and Ting Yang Chemical Company in Kaohsiung.

3. The burning (at 900°–1400°F) of the exhaust gases to less dangerous gases, by methods such as the use of an after burner for motor vehicles to change carbon monoxide to carbon dioxide. One disadvantage is that the NO_2 content will increase upon heating exhaust gases to higher temperature.

REFERENCES

(1) C. P. HSU and V. H. WEI: "Air Pollution in Taiwan Province", Institute of Environmental Sanitation, Taiwan Provincial Health Department, Taipei, Taiwan; 1960 and 1971.
(2) C. Y. CHUANG: "Research of Air Pollution in Taipei City", Taipei, Republic of China; Jan. 1973.
(3) _____: "The Effect of Air Pollution", U. S. Department of Health, Education and Welfare, Public Health Service, Washington, D. C., National Center for Air Pollution Control; 1967.
(4) _____: "Health Statistical Abstract, Taiwan Province 1970", Dept. of Health, Taiwan Provincial Government, Rep. of China.
(5) B. S. CHANG, A. COMITO et al.: "An Analysis of the Air Pollution Problem in the Detroit Area", Engineering Design E501, E502, University of Detroit; April 1971.
(6) C. Y. CHUANG: "Environmental Quality", Taipei, Taiwan, Dec. 1971.
(7) W. STRAUSS: Air Pollution Control", Wiley-Interscienc, New York; 1971.
(8) _____: "Air Pollution Engineering Manual", U. S. Dept. of Health, Eduction and Welfare, Public Health Service; 1967.
(9) A. C. STERN: "Air Pollution", Academic Press, New York; 1962.

THE WORLD FOOD PROBLEM

SR. EVAMONICA JAMLANG, S.SP.S.

Abstract: The so called world food problem is in theory not a problem of the present but of the near future. Theoretically, the world's food production should still be able to support the world's population. In actual fact, however, around 65% of the world's population does not have enough to eat. We examine here the factors that make up the present situation and those which can contribute to the predicament of world food shortage.

THE CURRENT SITUATION

1. Food Consumption

The USDA World Food Budget–1970 divides the world into two categories according to diet adequacy:

a. Diet adequate group — includes those regions whose average diets are above the minimum reference standards for 1970 — United States, Canada, Mexico, Brazil, Argentina — Urguay, Northern, Southern, and Eastern Europe, USSR, South Africa, Japan, and Oceania — and constitutes 36% of the world population.

b. Diet deficient group — includes those regions whose average diets are in some way deficient — Central America, other South America, North Africa, West Central Africa, East Africa, West Asia, India, other South Asia, other East Asia and Communist Asia — and constitutes 64% of the world population.

A more common classification, especially as far as economic development is concerned, consists of the two categories: developed and developing countries. Regardless of the name, the countries are grouped more or less in the same way differing only in some centrally placed countries like the USSR, Eastern Europe, and some Central and South American countries.

A comparison of the average diets in different countries with regard to calorie and protein content (Table 1) shows concretely the difference between the diet adequate and diet deficient countries.

Table 1. Per Capita Food Energy Value and Protein Content of the National Diet in Selected Countries, 1966/67[a]

Country	Calories Per Day	Protein Content (Grams Per Day)		Country	Calories Per Day	Protein Content (Grams Per Day)	
		Protein Total	Animal Protein			Protein Total	Animal Protein
Far East				North America			
China (Taiwan)	2,400	62.2	19.3	Canada	3,180	95.9	64.2
India	1,810	45.4	5.4	United States	3,160	93.8	66.7
Japan	2,350	77.6	24.6				
Korea	2,390	70.5	11.5	Europe			
Pakistan	2,070	51.9	10.7	Denmark	3,290	91.9	56.4
Philippines	2,070	48.6	18.2	France	3,250	103.3	61.9
Latin America				West Germany	2,870	79.9	51.9
Argentina	2,960	88.0	58.7	Italy	2,860	85.4	35.5
Brazil	2,850	71.1	19.8	Netherlands	2,900	82.7	52.8
Mexico	2,680	74.5	23.7	Spain	2,860	85.1	36.7
Panama	2,280	60.7	24.7	United Kingdom	3,220	88.9	53.3
Africa							
Ethiopia	2,040*	68.8*	14.8*	Oceania			
Mauritius	2,370	48.2	13.5	Australia	3,190	91.9	60.8
Uganda	2,070*	50.1*	10.2*	New Zealand	3,470	109.4	74.8

* 1963-1965 figures

[a] Source: The State of Food and Agriculture, 1968, Food and Agriculture Organization of the United Nations, p. 176-179.

As a whole, the developing countries have diets that depend largely on grains and other starchy foods for calories with a low proportion of protein foods. Compare the North Americans, who derive only 24.4% of their caloric supply from grains and 30 6% from livestock products, and the Asians, who obtain 74.5% of their caloric supply from grains and only 3.8% from livestock products (Fig. 1). Actually, people in many developing countries would need more protein than those in developed countries because the former are exposed to more infections and contagious diseases than the latter.

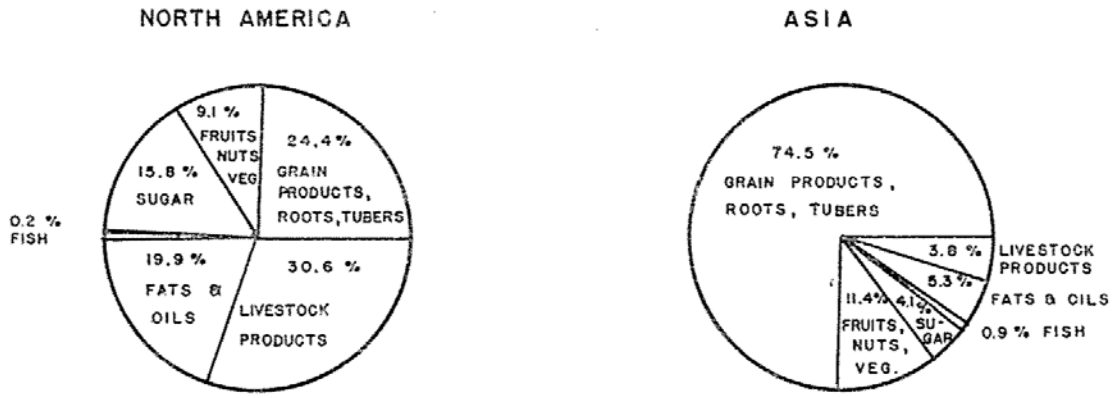

Fig. 1. Comparison of Average Diets—Borgstrom (1965)

The national diet of Taiwan has a better quality than most far eastern countries. It has improved steadily from an average caloric content of 2,233 in 1956 to 2,660 in 1970 and from a protein content of 53.9 g/day in 1956 to 72.2 g/day in 1970.(6)

Adequate calories do not necessarily mean adequate diet. The real problem of nutrition is the protein problem. Widespread protein deficiency diseases, like kwashiorkor, among children in developing countries attest to this fact. We have just began to realize the far reaching consequences of inadequate protein intake during the early years of life. Evidences are accumulating that protein deprivation, especially during the first two years of life, can permanently affect mental and physical development. What are the causes of low protein consumption in developing countries? First of all, animal protein is generally expensive since the feed conversion efficiency is low. The beef animal has the lowest efficiency, requiring 20 kg of feed to produce 1 kg of protein while the laying hen has the highest

efficiency, requiring only about 4 kg of feed to produce 1 kg of protein. In only a few countries can a majority of the people afford much animal protein in their diet. In Argentina, Australia, Canada, New Zealand, and the United States, meat is the main source of protein, providing 30–45% of the protein intake. In Ireland and Sweden, dairy products supply about 30% of the protein consumption. In all other countries, grain serves as the major source of protein. Fish is the main source of animal protein in many developing countries where there is a low supply of meat and dairy products.[1]

Another cause of a low intake of protein is lack of education regarding proper nutrition. Plant proteins, which are inexpensive, are not made better use of due to ignorance. In many developing countries, when mothers wean the child from the breast, they substitute a soft starchy diet which does not supply the protein needed for growth.

2. Food Production

For a stabilized food situation, food supply must at least equal food demand. Food production has depended largely on agriculture which supplies about 98% of the world's food. Agriculture needs land. At present, 3.5 billion acres of the world's 33 billion acres of land surface are under cultivation and 7.4 billion acres are pasture lands or meadows. Agriculture is therefore using roughly one-third of the world's land area.

North and Central America has 18% of the arable land and 14% of the total agricultural area whereas it constitutes only 8.8% of the world population. On the other hand, Asia has 31% of the arable land and 20% of the total agricultural land but constitutes 56.5% of the world population. Per capita production of food grains in 1968 was 136 kg for Asia and 819 kg for North and Central America. (Table 2) As of 1964, East Asians had already an average per capita grain consumption of 195 kg.[9] Asia, in general, is therefore not producing enough grain to feed its population.

It is estimated that the presently cultivated land can be expected to support a population of 3.8–15.9 billions depending upon the kind of diet. (Table 3) If we simply take into account the present human

Table 2. Per Capita Food Production by regions in 1968[a]

	World	Europe and U. S. S. R.	North and Central America	South America	Asia	Africa	Oceania
Mid-year population (millions)	3,483.0	693.0	309.0	180.0	1,946.0	336.0	18.5
Total food grains production (million tons)	1,179.5	192.9	253.1	45.0	264.8	59.4	19.7
Per capita food grains (kilograms)	338.0	278.0	819.0	250.0	136.0	176.0	1,064.0

[a] Source: FAO (1969) and United Nations (1969)

Table 3. Potentially Supportable Population in billions[a]

	European diet		Asian diet	
	3,000 calories per day	2,500 calories per day	3,000 calories per day	2,500 calories per day
European level of productivity				
In Asia				
(1 billion acres)	1.1	1.3	2.0	2.4
In rest of the world				
(2.5 billion acres)	2.7	3.2	5.0	6.0
Japanese level of productivity				
In Asia	2.0	2.4	3.8	4.5
In rest of the world	5.0	6.0	9.4	11.4

[a] Source: Brown et al. (1966)

population of 3.5 billions, we can be deceived into thinking that we will have enough food for decades to come. However, we have also to take into consideration the population equivalent of livestock. To fill the nutritional needs of 3.5 billion people adequately, a livestock population equivalent to about 15 billion people has to be maintained[2]. The world food production at present should therefore be supporting a population equivalent to 18.5 billions. The population equivalent of livestock is herein computed in terms of the protein requirements of an average man (70 g/day). Animal nutrition has established protein requirements for the different species of livestock and so the human equivalent of these species can be calculated. It is of course another matter whether the livestock are properly fed or not.

3. Food Distribution

As we have seen above, the world's food production can still be adequate to feed the world population. The fact is, however, that 65% of the population are not sufficiently nourished and starvation prevails in some parts of the world. The primary reason for this discrepancy is inefficient and unequal food distribution. As of 1963, half of the food produced in the world is consumed by one-fifth of its population. Diet adequate areas consume directly as food 25% of all crops utilized, whereas diet deficient areas consume directly as food 85% of the crops. For direct and indirect consumption, diet adequate areas consume 50% more crops, 44% more protein, 41% more calories than diet deficient areas[8,9].

4. Income

Surplus food in the developed countries do not automatically find their way into poorer countries. No food is usually the result of no money. The main reason for the unequal distribution of the world's food is lack of money on the part of the poor countries to buy the food they need from the countries which produce more food than they can use. Food aids to the needy countries have not solved the problem although these have helped to prevent full-scale starvation in many areas.

Income per capita as of 1959–61 was $1,074 in the developed countries excluding Eastern Europe and USSR and only $97 in the developing countries excluding Communist Asia. From this income $77 is spent per capita for food in the developed areas and $31, in the developing countries[9]. In the very poor countries, income elasticity of demand is about 0.5–0.7%, i. e., an increase of 1% in income may result in an increase of 0.5–0.7% in food consumption. In the rich countries, income elasticity of demand is only 0.1%[8].

Increasing the buying power of people in the diet deficient areas is a complex economic problem with a dim prospect of being solved in the near future.

PROJECTIONS INTO THE FUTURE

1. Population Increase

The world population was estimated at roughly 3.5 billions in 1968. Statistics are not very accurate since some countries have not taken any census or have not made it available for general information. The annual rate of population growth has an estimated average of 1.3% in the developed countries and 2.1% in the developing countries[9]. Decreased rates of mortality has also been brought about in almost all parts of the world through the advancements of medicine. The world population is therefore expected to double by the year 2000 as shown in Figure 2.[7]

2. Food Demand

Increase in population will naturally cause increase in food demand. An additional increase is to be expected also from changing age distribution. At present a great majority of the population, especially in the developing countries, are under the age of 15. Later the percentage of children can be expected to decrease due to birth control and since adults consume more food than children, food demand will increase.

Assuming that by the year 2050 the more developed countries will have a caloric consumption per capita equal to that of North America in 1960 (3,100 calories) except that animal protein consumption will be less due to substitution by plant protein which gives a

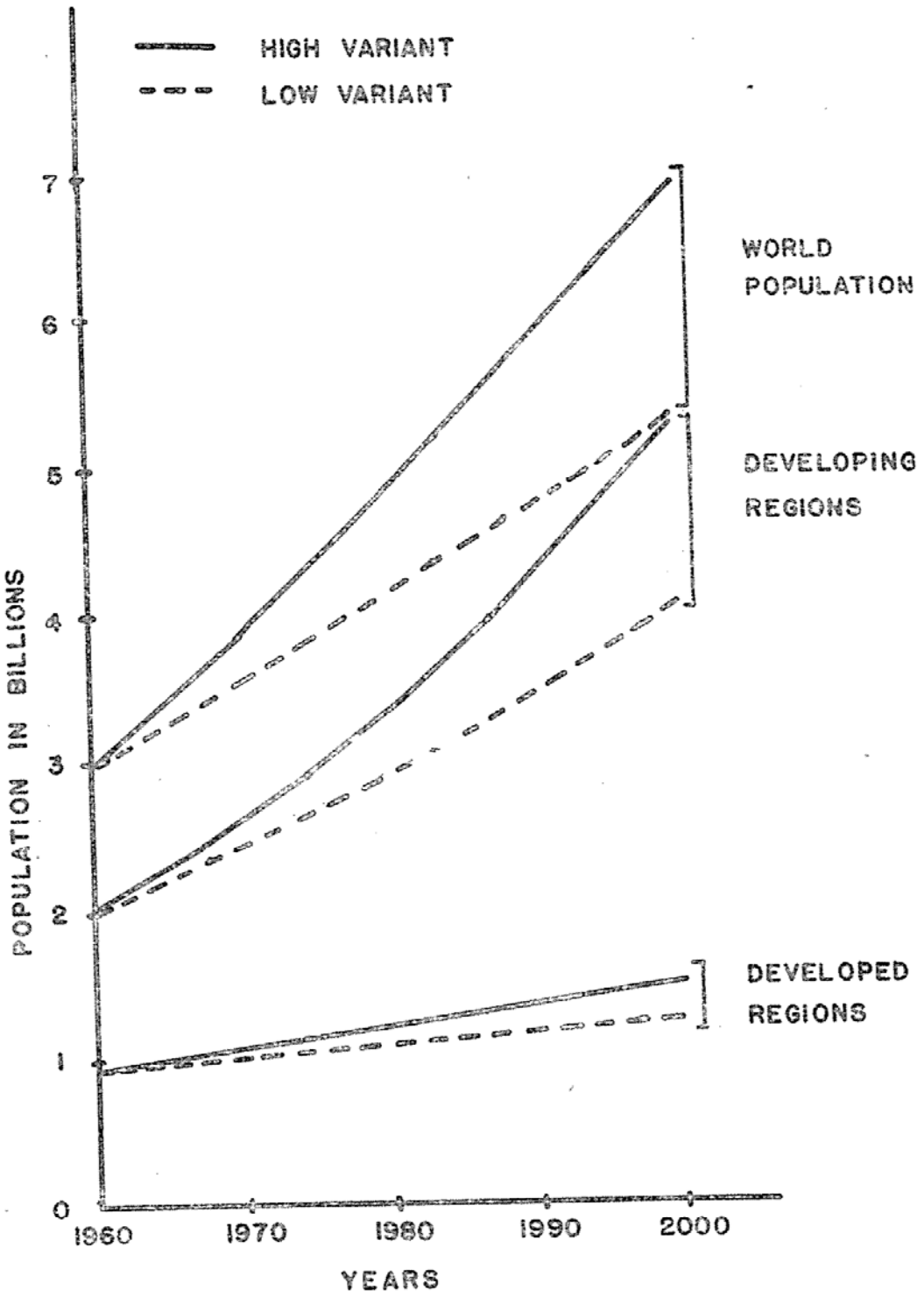

Fig. 2. Population Prospects –Kharbas & Salunkhe (1972)

final figure of 3,300 calories, and that the less developed countries will have reached the level of western Europe in 1960 (2,910 calories) except for less animal protein and more plant protein giving a final estimate of 3,100 calories per capita, we have the following picture of food demand in the year 2050:[8]

Table 4. Consumption of Primary Calories Per Day[a]

	1960	2050
LESS DEVELOPED REGIONS:		
Population (million)	2,022	9,000
Consumption per person:		
Calories	2,150	3,100
Animal protein, grams	9	30
Animal food, calories	180	600
Plant food, calories	1,970	2,500
Primary calories	3,230	6,100
Total Consumption:		
Primary calories (billion)	6,500	54,900
MORE DEVELOPED REGIONS:		
Population (million)	974	2,000
Consumption per person:		
Calories	3,050	3,300
Animal protein, grams	44	60
Animal food, calories	880	1,200
Plant food, calories	2,170	2,100
Primary calories	8,330	9,300
Total Consumption:		
Primary Calories (billion)	8,100	18,600
WORLD:		
Total consumption, primary calories (billion):		
Less developed regions	6,500	54,900
More developed regions	8,100	18,600
World Total	14,600	73,500

[a] Source: Thorkil (1968)

From the above figures, we can see that the developing countries will have a food demand 8–9 times that of 1960 and they will have to produce three times as much food as the developed countries. To meet this demand will be an immense task which will require exploring all possible sources of food and developing them to full capacity.

3. Present and Future Trends in Food Research and Development

a. *Increase of Production Yields*

Since most of the agricultural land is already under cultivation, future increase in land area will be less. Already now, efforts to produce more food are being channeled into increasing the productivity of the land by the use of high yielding strains of plant crops such as the "miracle rice" developed by the International Rice Research Institute and the high yielding wheat strain developed in Borlaug's "Green Revolution". In the future we can expect that agricultural research will produce high yielding strains of all plant crops, especially those used as staple foods.

More efficient agricultural methods are continuously being introduced in less developed areas in order that in the future, full productivity will be achieved in all parts of the world.

b. *Reduction of Food Losses*

Food losses due to pests and diseases, poor storage facilities, and inefficient handling of food should be eliminated. It was estimated that annual losses due to pests and fungi alone amount to 33 million tons, enough to feed the United States population for a year[7]. Farmers in the developing countries are being taught the proper use of pesticides to reduce and later eliminate the loss of crops in the field.

c. *New Sources of Food*

Non-traditional sources of food will be explored more and more in the future. Recent research efforts in this field have brought us the single cell protein (SCP) which is produced by growing single cell microorganisms (bacteria, yeast, fungi) in crude petroleum fractions or food plant waste products. Half a ton of Torula yeast can give 50 tons of protein. According to an estimate, microorganisms can produce the world's protein deficit (30 million tons/year) and use up only 1% of the world's annual production of crude paraffinic petroleum. Single cell protein is still in the stage of development and might take a few more years before it can be used for human consumption. At present, it is being used in a small scale for animal feed.

Our ocean resources have not been fully tapped. Fish species which have not been used for food are now being made use of in the form of fish protein concentrate (FPC), mainly for protein fortification of food items. At present, the cost is still too high to compete with cheaper sources of protein but with improved methods of production, cost will decrease. Different fish species are still being examined to find out which are non-toxic. The use of plankton, algae, and other marine plants as future sources of food is also under study.

Vegetable proteins are finding wider use and acceptability. With better methods of processing, textured soybean protein has gained better acceptance as "artificial meat". At present, it simulates such products as frankfurters, sausages, bacon, hamburger, chicken and beef cubes. In many developing countries, native protein sources like coconut, peanut, and legumes, are being used for baby food formulations.

d. *Formulated Foods*

Infant food formulas have been successful in the west as a first attempt at formulated foods. Developing countries are following suit using native sources of protein to fabricate weaning foods. In the past, mothers in developing countries have not been instructed with regard to infant nutrition so that children at the weaning stage were mostly given only soft starchy diets lacking in protein. Baby food formulas are being introduced to these mothers through nutrition programs conducted by FAO, WHO, and national health institutions in the different countries. Some of the better known weaning foods are: Incaparina, made in Guatemala from cotton seed and corn flours, torula yeast, and vitamins; Cerealinea, made in Brazil from soy flour, corn starch, milk powder, and vitamins; Duryea, which has constituents similar to Cerealinea, made in Colombia; and ProNutro, made in South Africa from soy, corn, and peanut flours, milk solids, and wheat germ. These products contain 20–30% protein.

Formulation of foods is now extending to adult foods, mostly in the form of reconstitutable beverages and cereal products. High

protein beverages and soy milk are being marketed not only in developing countries but also in the United States. We can expect to see more of these products in the future.

Fortification of foods through the addition of vitamins, amino acids, and proteins is not new but will receive more impetus in the future in the effort to do away with "empty calories". High protein noodles and wheat flour have been introduced in Taiwan.

e. *Food Processing and Preservation*

Food Science and Technology will continue to look for better ways of preserving food and preventing loss of nutrients and flavors during processing of foods. Freeze-drying will find more and more applications since it has been found to be superior to most methods of preservation as far as ease of handling and maintaining flavor, texture, and nutrients are concerned. The process is now being used in an industrial scale for eggs, mushrooms, asparagus, and instant coffee. It was employed for preparing food for the space exploration programs of NASA.

Food industry will try to minimize waste and pollution by developing ways of recycling and utilizing waste products.

CONCLUSION

We have presented here the problem of world food as seen by scientists and technologists in the field. The problem is imposing. Solutions have been proposed, but at present none of these seems to be a likely one to meet the problem on an equal footing. However, with the combined efforts of all: scientists, technologists, and laymen, in all fields, we can still hope that the problem might be averted.

REFERENCES

(1) ALTSCHUL, AARON M., and HORNSTEIN, IRWIN. 1972. Foods of the Future. *J. Agr. Food Chem.* **20**: 532.
(2) BORGSTROM, GEORG. 1965. "*The Hungry Planet,*" Macmillan, New York.
(3) BROWN, H., BRONNER, J., and WEIR, J. 1966. "*The Next Hundred Years,*" The Viking Press, New York.
(4) Food and Agriculture Organization. 1969. "*The State of Food and Agriculture,* 1968," United Nations, Rome.

(5) Food and Agriculture Organization. 1969. "*Production Yearbook*," Vol. 23. United Nations, Rome.
(6) Joint Commission on Rural Reconstruction. 1968-1970. "*Taiwan Food Balance Sheets.*" Taipei, Taiwan.
(7) KHARBAS, S. S. and SALUNKHE, D. K. 1972. World Food Population Problem. Some Possible Solutions. *Food Technol.* **26**: 148.
(8) KRISTENSEN, THORKIL. 1968. "*The Food Problem of Developing Countries*," Organization for Economic Cooperation and Development. (OECD).
(9) RASMUSSEN, C. L. 1969. Man and His Food: 2000 AD. *Food Technol.* **23**: 654.
(10) United Nations. 1969. "*Demographic Yearbook*," 21st issue. United Nations, New York.

CONTRIBUTORS TO THIS NUMBER

Michael Richartz, SVD 李嘉士 Ph. D. is the retired Dean of the College of Natural Sciences at Fu Jen University.

Yi-Ching Yen 顏一清 is professor of Mathematics at Fu Jen University.

Edward E. Fitchard, M. S., is a physicist at Texas A&M University, and is married to Shen-Sheng Chang 張申生, a graduate and former teaching assistant of Fu Jen University.

Philip Kwo-Lung Chang 張國龍 Ph. D. is associate professor at National Taiwan University and Fu Jen University.

Günter Breuer 包仁里 Ph. D., I. Institut für Experimentalphysik, Universität Hamburg, West Germany, is presently associate professor of Physics at Fu Jen University.

Wolfgang Kroll 克流 Ph. D. is professor of Physics at National Taiwan University and Fu Jen University.

Urban E. Schnaus, OSB 舒納思 M. S., Catholic University, Washington D. C., is associate professor of Physics at Fu Jen University.

Yeong Fang 方永 Ph. D. is associate professor of Chemistry at Fu Jen University.

Sister Evamonica Jamlang, SSpS 何木蘭 Ph. D. is head of the Department of Nutrition and Food Science at Fu Jen University.

PRINTED BY
CHING-HUA PRESS CO., LTD., TAIPEI